2017

Filomicelles Deliver A Chemo-Differentiative Therapy To Durably Control Carcinoma Cell Fate

Praful Raveendran Nair

University of Pennsylvania, prnair@seas.upenn.edu

Filomicelles Deliver A Chemo-Differentiative Therapy To Durably Control Carcinoma Cell Fate

Abstract

Current chemotherapy causes a host of side effects and better delivery of drugs to tumors is required to reduce this. Nanocarriers have been proven to not only deliver better to tumors but also solubilize more drugs in the core, with flexible 'filomicelles' being particularly effective. They are still open to improvements and one obvious way is to increase drug loading and hence drug dosage delivered to tumors. In the first part, the core of filomicelles was modified by the integration of aromatic groups into the hydrophobic block of a degradable di-block copolymer with the aim of improving delivery of aromatic drugs. Formed by self-assembly of amphiphilic di-block copolymer PEG-PBCL, flexible worm-like micelles with an aromatic core loaded more Paclitaxel than analogous aliphatic systems. The death of cancer cells and ploidy in surviving cells were higher followed by tumor shrinkage in vivo.

When cancer cells are treated with single drugs alone during chemotherapy, development of drug resistance has been commonly noted, eventually leading to relapse. Retinoic acid (RA) induces differentiation and proliferation arrest in many cell types. With carcinoma lines, we find dual drug treatment with RA and Paclitaxel increases ploidy and cell death beyond those achieved by either drug single-handedly, with effects being durable. A month after treatment, relapse rates are low for RA-TAX treated cells (15%), compared to almost all (92%) for cells treated with Paclitaxel alone. Reduction in levels of key cell cycle factor Cyclin-D1 and proliferation marker Ki-67 help clarify the basis for this synergy. These effects are greatly enhanced by loading the drugs into filomicelles. Co-loading the drugs into filomicelles lead to a more potent system compared to separate loading, with no loss in the integration efficiency of drugs. Notably, relapse rates were ~2% three months after treatment, highlighting the improvement offered by filomicelles. The combination retains its potency across multiple cell lines despite their varying responsiveness to RA alone. Drug loaded filomicelles are able to shrink subcutaneous lung and liver tumors in vivo. Tumor shrinkage was also observed with orthotopic liver tumors, leading to a survival benefit. These results highlight the irreversible synergy of killing cancerous cells while driving differentiation.

Degree Type
Dissertation

Degree Name
Doctor of Philosophy (PhD)

Graduate Group
Chemical and Biomolecular Engineering

First Advisor
Dennis E. Discher

Keywords
cancer, drug delivery, filomicelles, mouse models, paclitaxel, retinoic acid

Subject Categories
Chemical Engineering | Nanoscience and Nanotechnology | Oncology

FILOMICELLES DELIVER A CHEMO-DIFFERENTIATIVE THERAPY TO DURABLY CONTROL CARCINOMA CELL FATE

Praful Raveendran Nair

A DISSERTATION

in

Chemical and Biomolecular Engineering

Presented to the Faculties of the University of Pennsylvania in

Partial Fulfillment of the Requirement for the Degree of Doctor of Philosophy

2017

Supervisor of Dissertation

_____

Dennis E. Discher, Ph.D., Professor of Chemical and Biomolecular Engineering

Graduate Group Chairperson

_____

John Crocker, Ph.D., Professor of Chemical and Biomolecular Engineering

Dissertation Committee

Kathleen Stebe, Ph.D., Professor of Chemical and Biomolecular Engineering

Ravi Radhakrishnan, Ph.D., Professor of Chemical and Biomolecular Engineering

Vladimir Muzykantov, M.D./Ph.D., Professor of Pharmacology

FILOMICELLES DELIVER A CHEMO-DIFFERENTIATIVE THERAPY TO

DURABLY CONTROL CARCINOMA CELL FATE

COPYRIGHT

2017

Praful Raveendran Nair

ACKNOWLEDGEMENTS

I would like to thank all past and present members of the Discher lab, especially Prof. Dennis Discher, Dr. Manu, Amal, Karthick and Jerome. I am deeply indebted to my committee members: Prof. Vladimir Muzykantov, Prof. Kathleen Stebe, and Prof. Ravi Radhakrishnan for their suggestions. I would like to thank my previous committee members Dr. Matthew Lazzara and Prof. Raymond Gorte for attending my thesis proposal. I am extremely grateful to Dr. Marilyn Huff and Dr. Miriam Wattenbarger for their help and use of TECAN plate reader.

I would like to thank my family and friends for their support, especially my parents. Finally, I would like to acknowledge the beautiful game, SRT, Joel and Ellie for their roles throughout my PhD.

ABSTRACT

FILOMICELLES DELIVER A CHEMO-DIFFERENTIATIVE THERAPY TO DURABLY CONTROL CARCINOMA CELL FATE

Praful R. Nair

Dennis E. Discher

Current chemotherapy causes a host of side effects and better delivery of drugs to tumors is required to reduce this. Nanocarriers have been proven to not only deliver better to tumors but also solubilize more drugs in the core, with flexible 'filomicelles' being particularly effective. They are still open to improvements and one obvious way is to increase drug loading and hence drug dosage delivered to tumors. In the first part, the core of filomicelles was modified by the integration of aromatic groups into the hydrophobic block of a degradable di-block copolymer with the aim of improving delivery of aromatic drugs. Formed by self-assembly of amphiphilic di-block copolymer PEG-PBCL, flexible worm-like micelles with an aromatic core loaded more Paclitaxel than analogous aliphatic systems. The death of cancer cells and ploidy in surviving cells were higher followed by tumor shrinkage *in vivo*.

When cancer cells are treated with single drugs alone during chemotherapy, development of drug resistance has been commonly noted, eventually leading to relapse. Retinoic acid

(RA) induces differentiation and proliferation arrest in many cell types. With carcinoma lines, we find dual drug treatment with RA and Paclitaxel increases ploidy and cell death beyond those achieved by either drug single-handedly, with effects being durable. A month after treatment, relapse rates are low for RA-TAX treated cells (15%), compared to almost all (92%) for cells treated with Paclitaxel alone. Reduction in levels of key cell cycle factor Cyclin-D1 and proliferation marker Ki-67 help clarify the basis for this synergy. These effects are greatly enhanced by loading the drugs into filomicelles. Co-loading the drugs into filomicelles lead to a more potent system compared to separate loading, with no loss in the integration efficiency of drugs. Notably, relapse rates were ~2% three months after treatment, highlighting the improvement offered by filomicelles. The combination retains its potency across multiple cell lines despite their varying responsiveness to RA alone. Drug loaded filomicelles are able to shrink subcutaneous lung and liver tumors in vivo. Tumor shrinkage was also observed with orthotopic liver tumors, leading to a survival benefit. These results highlight the irreversible synergy of killing cancerous cells while driving differentiation.

TABLE OF CONTENTS

LIST OF TABLES

LIST OF FIGURES

LIST OF ABBREVIATIONS

AON: Antisense Oligonucleotides

AML: Acute myeloid leukemia

APL: Acute promyelocytic leukemia

ATCC: American Type Culture Collection

ATRA: All Trans Retinoic Acid, also referred to simply as RA

BBB: Blood brain barrier

BSA: Bovine Serum Albumin

CBP: CREB-binding protein

CR: Complete remission

CRABP: cellular retinoic acid binding protein

CRBP: cellular retinol binding protein

CREB: cAMP-response element-binding protein

CSC: Cancer Stem Cell

DMSO: Dimethyl Sulfoxide

DNA: Deoxyribonucleic acid

EPR: Enhanced Permeation and Retention

f: hydrophilic fraction

FBS: Fetal bovine serum

GPC: Gel permeation chromatography

GUV: Giant unilamellar vesicle

HAT: histone acetyl transferase

HDAC: histone deacetylase

HPLC: High performance liquid chromatography

IC50: Half maximal inhibitory concentration

l_p: persistence length

M_{CH2}: Hydrophobic block molecular weight

mg: Milligram

μl: Microliter

ml: Milliliter

μm: Micrometer

mm: Millimeter

μM: Micromolar

mM: Millimolar

MTD: Maximum tolerated dose

MTT: 3-(4,5-dimethylthiazol-2-yl)-2,5-diphenyltetrazolium bromide

MW: molecular weight

MWCO: Molecular Weight Cut-Off

NA: Numerical Aperture

NMR: Nuclear magnetic resonance

NO: Nitric Oxide

NOD-SCID: Non-obese diabetic Severe combined immunodeficiency

NSG: NOD-SCID-IL-2Rgc null

OB: polyethylene oxide polybutadiene

OBCL: polyethylene oxide poly(α)benzylcaprolactone

OCL: polyethylene oxide poly(ε-caprolactone)

OCLA: polyethylene oxide poly(ε-caprolactoneco-lactide)

OL: polyethylene oxide polylactic acid

P2VP: poly(2-vinylpyridine)

P4VPQI: poly(N-methyl-4-vinyl-pyridinium iodide)

PBCL: Poly(α)benzylcaprolactone

PBD: polybutadiene

PBD-P4VPQ: poly-(butadiene-*b*-*N*-methyl-4-vinyl pyridinium)

PBS: Phosphate buffered saline

PCL: poly(ε-caprolactone)

PCLA: poly(ε-caprolactoneco-lactide)

PDI: Poly dispersity index

PDMS: poly(dimethylsiloxane)

PEE: polyethylethylene

PEG: polyethylene glycol (same as PEO)

PEG-P2VP: PEG-poly(2-vinylpyridine)

PEG-PBD: polyethylene oxide polybutadiene

PEG-PCL: polyethylene oxide poly(ε-caprolactone)

PEG-PEE: polyethylene oxide polyethylethylene

PEG-PLA: polyethylene oxide polylactic acid

PEO: polyethylene oxide (same as PEG)

PEO-PBD: polyethylene oxide polybutadiene

PEO-PCL: polyethylene oxide poly(ε-caprolactone)

PEO-PCLA: polyethylene oxide poly(ε-caprolactoneco-lactide)

PEO-PLA: polyethylene oxide polylactic acid

PLA: poly-L-lactic acid

PLGA: poly(lactic-co-glycolic acid) polymer

PLL: poly-L-lysine

PML: Promyelocytic leukemia protein

PMOXA: poly-2-methyl-2-oxazoline

PPAR: peroxisome proliferator activator receptor

PPS: polypropylene sulfide

RA: All Trans Retinoic Acid

RAR: Retinoic Acid Receptor

RARE: Retinoic Acid Response Element

RBP: retinol binding protein

RTK: Receptor tyrosine kinase

RXR: Retinoid X Receptor

siRNA: Small interfering Ribonucleic Acid

SMRT: silencing mediator for retinoid or thyroid-hormone receptors

TAX: Paclitaxel

TR: thyroid hormone receptor

UV: Ultra violet rays

VDR: vitamin D receptor

VDRE: Vitamin D response element

VEGF: Vascular Endothelial Growth Factor

CHAPTER 1. INTRODUCTION

1.1. Current problems of cancer

Cancer is the uninhibited proliferation of once healthy cells, which hijack resources meant for healthy tissues (Figure 1.1). Eventually, they grow and displace nearby cells, compromising the proper functioning of the organ. Invasion of cells and metastasis to distant organs along the way leads to the development of more tumors, leading ultimately to death (Fidler, 2003). It ranks amongst the leading causes of mortality globally, with ~13 million new cases and 8 million deaths annually. In the United States, there were an estimated 1.7 million new cases in 2017 and 600 thousand mortalities (Siegel et al., 2017) and was the second leading cause of death, behind heart diseases. It has existed throughout the history of mankind, with the earliest recorded tumors dating back to 1600 BCE. More recently, over 500 billion dollars has been spent cumulatively since President Nixon declared the 'War on Cancer' in 1971. Not only is it a massive healthcare burden, but also a financial one, and the National Cancer Institute receives more than six billion dollars annually and has spent over 90 billion dollars since 1971 (Marshall, 2011). Despite all this financial input, the mortality rate has barely declined, unlike most other diseases whose death rate has plummeted with time, money, and research. While mortality rates have fallen 25% from its peak in 1991 (Siegel et al., 2017), this has been attributed largely to preventive measures rather than advances in treatment. Of the various subtypes of cancers, lung, colorectal, prostrate and breast dominate overall (Ries et al., 2006) (Ferlay et al., 2007). While prostrate, lung, and colorectal led to most cases

in men (~42% of all newly diagnosed cases), breast, lung, and colorectal was dominant in women (~30% of all new cases).

As mentioned above, preventive measures underlie the reason behind the drop in most cancer deaths. A rapid decline in the number of lung cancer cases followed (decades) after anti-smoking awareness campaigns. Routine Prostate Specific Antigen (PSA) screenings has led to a drop in new cases of prostate cancer (Schroder et al., 2009) (Andriole et al., 2009). In the same vein colorectal cancer rates have declined following colonoscopies to detect and remove polyps, abnormal growths that progress to cancers.

However, not all cancers are on the decline. Incidences of liver cancers, main focus of this thesis, along with certain types of leukemia, pancreas, tongue, small intestine, kidney and myeloma have increased in the last decade (Siegel et al., 2015). Another complicating factor comes from the fact that different ethnicities have different rates for each type of cancer. All the above factors contribute to complicate the treatment of a disease, which is already made complex by the fact that it's the patient's own cells that have run amok.

1.2. Chemotherapy and other current treatments

Cancer cells have mutations that enable it to survive in very difficult conditions and are, hence, a lot more resilient than normal cells (Greaves and Maley, 2012). As a result, the drugs developed for chemotherapy are extremely lethal. While chemotherapeutics encompass a large group of drugs (such as DNA damaging agents, anti-mitotics, anti-metabolites, topoisomerase inhibitors and cytotoxic antibiotics) (Marzo and Naval, 2013),

they rely on the rapid proliferation rate of neoplastic cells to take effect. Traditional cytotoxic chemotherapy (which includes these 'poisons') can be distinguished from targeted therapy in that the latter contains inhibition of growth promoting signals (such as RTK inhibitors, Leamon and Reddy, 2004) and antibody-drug conjugates (Zolot et al., 2013). Targeted therapies often target proteins that are mutated or overexpressed in cancers compared to normal cells, and in some cases, novel proteins that do not exist in healthy cells. The poster child of the latter case is Gleevec, which targeted the fusion protein of BCR-Abl in Chronic Myelogenous Leukemia (Drucker, 2002). The fusion protein tyrosine-kinase, when blocked, either induces apoptosis or reduces growth rate. Inhibitors of mutant B-raf are an example of this strategy (Flaherty et al., 2010). Gefitinib and Erlotinib, that target Epidermal Growth Factor Receptor (EGFR), are further examples (Feld et al., 2006). However, despite being 'targeted', side effects to this therapy exists in the form of anemia, thrombocytopenia, neutropenia, edema and increased risk of infection (Robert et al., 2005). It can be instantly noted that the side-effects are much less severe than conventional chemotherapy, and that cases of overdose are rare.

Other common modes of treatment include radiation, surgery and immunotherapy.

- Radiation therapy utilizes ionizing radiation to induce DNA damage (similar to some of the chemotherapeutics mentioned above) (Green et al., 2001). Superficial tumors such as melanomas can be treated by low energy X-rays, while for deeper tumors, higher energy rays are used.

- For localized solid tumors, surgical resection of the tumors along with its surrounding tissue may be an option (Simmonds et al., 2006). As lymph nodes one of the main destinations for metastases, in some cases, they are removed as well. This technique works best for earlier stage cancers, and as the first sentence implies, is incompatible with leukemias and lymphomas.

- Immunotherapy stimulates the immune cells (cytotoxic T cells, macrophages etc.) to eliminate malignant cells (Rosenberg et al., 2004). Common strategies involve use of antibodies that target overexpressed surface proteins (Mellman et al., 2011), checkpoint blockades (Pardoll, 2012), and modified T-cell transfers (Restifo et al., 2012).

Radiation therapy and surgery (which constitute local therapy) are often used in conjunction with each other, and frequently in combination with chemotherapy (Kaiser and Ellenberg, 1985) (Trotti et al., 2003) (Zitvogel et al., 2008). The principle here is similar to that behind combination chemotherapy (discussed below). Tissue of origin, stage of cancer and location (depth) of tumor form the key dictating factors in deciding which therapies are ultimately used. These can further be used in conjunction with hyperthermia Chua et al., 2009), which utilizes heat to either directly kill cells, or increase blood flow to tumors, which results in increased dose of chemotherapeutics to the tumors.

1.3. Limitations of chemotherapy and current problems

Both traditional and targeted therapies are injected intravenously. However, the body also contains healthy cells that have a rapid proliferation rate, that get affected by chemotherapeutics (particularly traditional chemotherapy). These include cells in the bone marrow (that undergo massive amounts of division to generate blood cells), digestive tract (which renews its epithelial cells rapidly, and hence divides rapidly) and hair follicles (that leads to apoptosis in keratinocytes). Hence, the same toxicity that anti-cancer agents depend on to take effect, limit the Maximum Tolerated Dose (MTD) (Chidambaram et al., 2012). Time scales for these side-effects to become apparent range from hours to years. The deleterious effects on cells in the bone marrow manifest itself in the form of immunosuppression and myelosuppression (Penn and Starzl, 1973). This drastically increases the chance of contracting an infection, which puts additional strain on a fatigued body. Severe myelosuppression might even require a bone marrow transplant. Immune suppression may also lead to anemia (Groopman and Itri, 1999) and neutropenic enterocolitis, which is an inflammation of the large intestine that may be associated with infection. Fatigue, nausea, vomiting, gastrointestinal distress, hair loss, and infertility are other common side-effects (Griffin et al., 1996). Finally, DNA damage induced and production of free radicals following chemotherapy often leads to toxicity in heart (Simbre et al., 2005), liver (King and Perry, 2001) and kidneys (Ries and Klastersky, 1986), eventually leading to organ failure.

This toxicity complicates the determination of optimal dosage. While higher doses lead to serious side-effects (as mentioned above), low dosages are ineffective (Frei and Canellos,

1980). Currently, dosage is calculated based on the patient's body surface area (Pinkel, 1958), which sacrifices precision for simplicity, and often leads to incorrect dosages. Adding to this complexity is the fact that free drugs have been plagued by problems such as poor tumor penetration and resistance (Trédan et al., 2007). The development of stiffer fibrotic tissues as well as the presence of barriers to delivery such as the blood brain barrier (BBB) reduces the final dose that is delivered (Deeken and Löscher, 2007).

However, after treatment with a single drug alone, over several periods of the normal cell cycle, cancer cell populations revert back to the original proliferative state, consistent with resistance and relapse commonly seen after conventional chemotherapy (Komarova and Wodarz, 2005). Further, development of a secondary neoplasm, often at the site of the first one has been frequently reported. Frequently, different chemotherapeutics are administered together (called combination chemotherapy) which have different modes of action and side-effects (Deng et al., 2015). This approach seeks to exploit two different pathways to minimize the survival of cancer cells. Combination Paclitaxel and Oxaliplatin, for example, have been administered to patients with germ-cell tumors (Bokemeyer et al., 2008). Anti-mitotics may be co-administered with alkylating agents (Frei and Eder, 2003). Actively diving cells are targeted by anti-mitotics, while cells in rest phase or G1 phase suffer DNA damage by alkylating agent, both eventually leading to apoptosis. Another strategy is to use a drug that synchronizes all populations of cells in the tumor (by controlling cell cycle or DNA synthesis), which are then vulnerable to the second drug (Lippman et al., 1984). This not only reduces the chances of resistance development, it also leads to lesser side effects as drugs can be used in lower doses. The

various mutations in cancer cells necessitates the use of combination chemotherapy, as the diversity caused by those mutations make it unlikely that one drug alone will be effective. On the flip side, more mutations lead to increased aberrations compared to healthy tissues, and hence more targeting opportunities and druggability.

Targeted therapies have not been completely spared from these side effects (Fang et al., 2011). Their clinical trials have been disappointing, and have provided little extension in patient survival. While some drugs (like Gleevec) have faced success, numerous cases of resistance after months of use have been reported. In the end, the cause for their failure is the same as that for conventional chemotherapy: genetic diversity between clones in the tumor. Additionally, cancer stem cells (CSCs) which are primarily responsible for tumor growth are relatively resistant to conventional chemotherapy, and hence all but guarantee the regrowth of tumors after treatment (Ginestier et al., 2009). Breast cancer stem cells were found to increase after chemotherapy (Li et al., 2008), which highlights the need for more specific therapies that target CSCs.

1.4. Increased angiogenesis in tumors and the EPR effect

Solid tumors have a higher vascular density than normal tissues and have blood vessels that are much altered structurally than those in the rest of the body (Fang et al., 2011). This is a result of the angiogenic signaling arising to sustain tumor growth (Folkman, 1971) (Folkman, 1995). The newly (and hastily) formed vasculature is structured poorly and is often leaky, with gaps in endothelial cells ranging from 200 nm to 2 µm. This is

caused by irregular vascular alignment, wider lumen and lack of smooth muscle layers (Suzuki et al., 1987). The defective architecture of tumoral blood vessels alter the permeability (and hence accumulation of larger molecules). As a result tumors see increased extravasation and accumulation of sub-micron sized particles (Torchilin, 2011) and some large molecules above 40 kDa in size. Proteins in this size range were retained 24 hours after injection, and increase in half-lives for polymeric micelles were 10-200 fold. An example of this effect is shown in Figure 1.2, where Evans blue dye was conjugated with albumin injected intravenously led to accumulation of the dye in tumors. Normal tissue did not exhibit significant dye accumulation. This constitutes the 'Enhanced Permeation' part of the EPR effect.

Additionally, tumors lack effective lymphatic drainage from the tissue. Hence, particles that penetrate the tumor get stuck and accumulate in the tumor, leading to the 'Retention' part of the EPR effect. Another critical role of lymphatic drainage in the context of tumor cells is that it is their main route of metastasis. Polymeric particles that accumulate in the tumor via EPR have also been reported to accumulate in the lymph nodes, potentially decreasing number of metastases (Maeda et al., 1979). Subcutaneously injected nanoparticles are especially suited for lymphatic targeting (Brigger et al., 2002).

First described in 1986 (Matsumara and Maeda, 1986), this effect has been an integral part of tumor targeting using larger molecules. Promoting selectivity to tumors, this effect is absent in normal tissues (Maeda et al., 2006) (Seki et al., 2009). The EPR effect has

accelerated the development of liposomal (Barenholz, 2012) and micellar drugs (Vincent et al., 2009). While polymeric formulations are in early phase of clinical trials (phase I or II), Doxil, which is a liposomal formulation is used in the treatment of Kaposi's sarcoma, breast and ovarian cancer. Accumulation in tumors not only increases the efficiency of delivery, but also increases the half-life of drugs in the tumor. Both these effects combine to increase the efficacy of the treatment and reduce side-effects.

Extending from chemotherapy, the EPR effect has been utilized in imaging and gene delivery as well (Torchilin, 2011). The EPR effect can be further enhanced by elevating blood pressure, causing increased circulation to the tumors. Methods of achieving this range from using Nitric Oxide (NO) releasing agents (Fukumura and Jain, 1998) or its generation in tumors (Yoshimura et al., 1996). Angiotensisn II has also been used that increases blood perfusion by contracting vessels and producing hypertensive conditions (Suzuki et al., 1981). The increased pressure pushes the blood (along with the drug) into the interstitial space. Additionally, as mentioned above, tumor blood vessels lack the smooth muscle layer which is needed for vessels to contract. This leads to lower pressure in tumor vessels and more blood flow towards it, and further increases accumulation.

EPR effect is most apparent in small tumors as larger tumors have a hypoxic core that contains necrotic parts. The hypoxia is a direct result of the lack of blood supply to these parts, and affects the delivery of drugs to the core. EPR effect is not spared from this, and the dependence of EPR effect on the vascularity is demonstrated by the fact that is more

dye accumulation in the periphery of the tumors (where angiogenic signals predominate), while the core does not see significant accumulation (Figure 1.2 B). Additionally, when drugs are delivered via conjugation to proteins, the accumulated proteins are susceptible to denaturation depending on their biocompatibility. This problem is partially resolved by PEGylating the protein (Sawa et al., 2000), a strategy used extensively with nanoparticles and will be described later. Finally, it has to be mentioned that while the hypervascularity of tumors augment drug delivery, their main function (which is to supply nutrients to tumor cells) is to sustain tumor growth. Hence, reducing angiogenesis can, in principle, starve the tumor of nutrients, and reduce growth. With this aim in mind, anti-angiogenic drugs and Vascular Endothelial Growth Factor (VEGF) inhibitors have been used in clinic (Ferrara et al., 2004)(Ferrara and Kerbel, 2005). These treatments however make it very difficult to penetrate and deliver drugs to the tumors again.

1.5. Nanoparticles for cancer drug delivery and other applications

Nanoparticles are sub-micron sized particles, which exhibit better tumor selectivity by exploiting the EPR effect. Their larger size permits them to accumulate in tumors via EPR effect described above (Figure 1.3). This kind of targeting is often called passive targeting to distinguish it from active targeting, which involves the 'active' recognition of targets by nanoparticles via ligands on its surface. Active targeting may be carried out via antibodies, antibody fragments (such as scFvs), DNA, and receptor ligands.

Dosage of chemotherapeutics through intravenous injections is often limited by the low

solubility of the compounds, as three-quarters of all chemotherapeutics are hydrophobic.

In nanocarriers, the drug is often 'loaded' into their core which is often hydrophobic as

well (although particles such as liposomes and polymersomes can have an aqueous pool

in the centre) (Figure 1.4). Hence, they solubilize more drugs in their core, which

increases the delivery of hydrophobic chemotherapeutics and allows them to act as drug

reservoir. Additional drugs that are prone to inactivation or degradation under

physiological conditions may be protected in the core. The final drug distribution is thus,

not just dictated by properties of the drug (molecular weight, hydrophobicity, charge etc.)

but also by those of the polymer and the assembled nanoparticle: weight (and hence,

size), hydrophobicity and hydrophilicity, degradation rate. Increasing number of

parameters make it hard to more precisely control every aspect of the delivery. However,

kinetic analysis suggests that endocytosis dominates over degradative drug release.

Nanoparticle formulations are often injected intravenously. The submicron size range

makes it a prime target for the immune system. Particles of smaller size don't take full

advantage of the immune system and get cleared via the kidneys. Larger particles (>5

μm) get stuck in the capillaries and may result in suffocation and death. Clearance by the

mononuclear phagocytic system (MPS) causes the drugs to get opsonized and cleared by

the macrophages. These drugs eventually end up in the liver and spleen, contributing to

off-target toxicity. On the flip side, the task of delivery to hepatic tumors is made much

easier and increased efficiency has been demonstrated in these cases using nanoparticles

(Chiannilkulchai et al., 1989). In delivery to liver tumors, loaded drug (Doxorubicin) was

first transferred from nanoparticles to Kupffer cells, which are macrophages in the liver. The drug was then transferred from the Kupffer cells to the malignant tissue (Chiannilkulchai et al., 1990), and no nanoparticles were detected in tumor cells. This mode of delivery in the case of hepatic tumors is one that is intimately connected with this manuscript and will be revisited in Chapters 4, 5, and 6 where delivery of Retinoic Acid and Paclitaxel will be discussed. At sufficiently high dosage, loaded chemotherapeutics can cause apoptosis of Kupffer cells and decrease in efficiency in the above mentioned process as well reduced immune surveillance. However, the side-effects experienced are much lower than with conventional chemotherapy (Brigger et al., 2002). Cardiotoxicity and hepatotoxicity, in particular, is highly reduced.

Addition of stealth coatings to the particle or increasing the curvature helps it circulate a lot longer. Decreased curvature leads to reduced size, which might be unsuitable for some applications. These coatings reduce the opsonization on the nanoparticles and make them invisible to macrophages and prolong the half-life of injected particles (Stolnik et al., 1995), increasing the circulation time, probability that the particle will accumulate in the tumors and increasing the efficacy of the treatment. These particles are suitable for treatment of tumors outside those in the MPS regions (Moghimi et al., 2001). Providing a coating of polyethylene glycol (PEG) on the surface is the most common method of imparting the stealth coating (Storm et al., 1995). This can either be done by adsorption of PEG or surfactants or using polymers with a PEG block at the hydrophilic end (Stolnik et al., 1995).

The use of active targeting increases the efficacy by delivering drugs to the target selectively. Most commonly, surface receptors that are overexpressed in cancer cells are the target of these nanoparticles. For example, folate receptors are overexpressed in cancer cells and they were targeted by folate-conjugated nanoparticles (Stella et al., 2000). These nanoparticles were selectively taken up by folate-receptor-bearing cells compared to passively targeted nanoparticles. Similar to folate receptor, transferrin (an iron binding glycoprotein) receptor has been targeted by paclitaxel loaded PLGA particles (Sahoo and Labhasetwar, 2005) and liposomes for transfection of p53 (Xu et al., 1999). Nanoparticles have also been used to target lectins in colon cancers (Minko, 2004)

Nanoparticles can also be loaded with contrast agents for imaging and diagnostic purposes. Superparamagnetic nanoparticles have been used as contrast agents in magnetic resonance imaging (MRI) (Bonnemain, 1998). Delivery by nanoparticles is not restricted to drugs or imaging agents, but can be extended to antisense oligonucleotides (Juliano et al., 1999) (Fattal et al., 1998). Application of polymeric systems for this application will be described in the next chapter.

1.6. Different types of Nanoparticles

Nanoparticles can be constructed from a host of materials including lipids, polymers, metals, metal oxides, silica, carbon nanotubes and other macromolecules (Figure 1.5).

1.6.1. Polymers

These can include both synthetic (polyethylene glycol polybutadiene and polyethylene glycol polyethylethylene) and natural (albumin, heparin etc.) polymers (Figure 1.5, A). Conjugate of paclitaxel (an anti-mitotic) to albumin called Abraxane has been successful in the treatment of breast cancer, non-small cell lung cancer and advanced hematologic malignancies (Gradishar et al., 2005). Polyethylene glycol (PEG) poly-L-glutamic acid is a synthetic polymer that has been conjugated to traditional chemotherapeutics such as Doxorubicin, Paclitaxel, Camptothecin, and Mitomycin C (Li, 2002). Conjugate of *N*-(2-hydroxypropyl)-methacrylamide copolymer (HPMA) with doxorubicin has been evaluated in a phase I clinical trial (Vasey, 1999). However, drugs don't necessarily have to be conjugated to the polymer. Amphiphilic diblock copolymers (polymers in which the hydrophobic block is attached to the hydrophilic one) self-assemble in water to generate micelles (Figure 1.5, B) and polymersome. Loading of these assemblies with drugs and their applications are discussed in depth in the next chapter. Dendrimers are polymers with branches emerging radially from the centre (Figure 1.5, C). They have been used as scaffolds as well as drug delivery, after conjugation with drugs like cisplatin (Svenson and Tomalia, 2012) (Malik et al., 1999).

1.6.2. Lipid and lipid based

Liposomes are vesicles self-assembled from lipids. They are spherical and have an aqueous pool in the centre (Figure 1.5, D) which can load aqueous drugs. Hydrophobic

dugs intercalate between the lipid bilayer, several of which are currently in clinic and in clinical trials (Hofheinz et al., 2005). Modified viruses with targeting molecules (Figure 1.5, E) have been used for specific tumor targeting (Manchester and Singh, 2006) Carbon nanotubes are cylinders composed of benzene rings (Figure 1.5, F). The efficacy of delivery of anticancer agents such as methotrexate has been improved by conjugating them to the walls of the nanotube (Pastorin et al., 2006).

In addition to the material of construction, the nanoparticle can also be tailored to response to a particular stimulus (Cho et al., 2008). This includes conditions that exist inside the tumor, but are different from those in physiological conditions. Altered metabolism in tumor cells lead to lower pH (6.5) existing in tumors compared to a physiological pH of 7.4. pH sensitive liposomes can be tailored to be stable in circulation but to release drugs at this lower pH (Yatvin et al., 1980). The altered metabolism also results in a much more reductive environment and the presence of unique or overexpressed enzymes (like matrix metalloproteinase-2), which have also been exploited similar to pH (Mansour et al., 2003).

Healthy tissue

Nucleus

Normal cell

Evolution of an early malignant cell

Early malignant cell

Cancerous cell

Necrotic cell

Rapid proliferation of cancer cells allow it to slowly displace normal ones

All normal cells have been eliminated from the vicinity, followed by loss of organ function

Cancer cells continue to divide at a rate faster than the availability of nutrients, resulting in a necrotic core

Figure 1.1. Cancer cells proliferate at a rapid rate, hijack the resources meant for healthy cells, and displace its nearby cells, compromising the proper functioning of the organ.
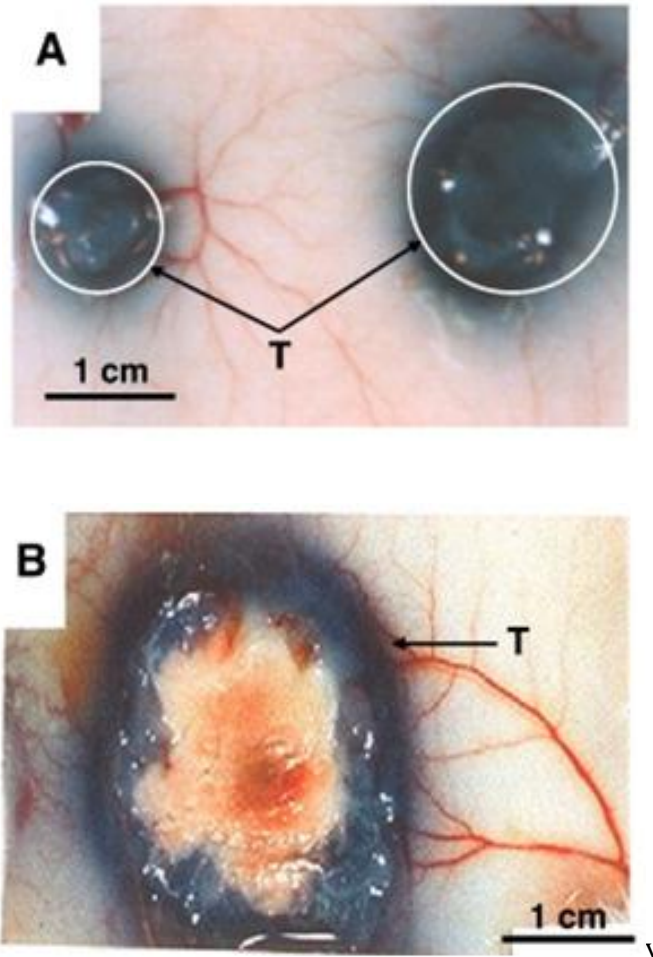
Figure 1.2. Illustration of the Enhanced Permeation and Retention (EPR) effect in tumors. Evans blue dye was conjugated with albumin and injected at 10 mg/kg. A) Tumors (white circles) showed preferential accumulation of the dye 24h after injection. Normal tissue does not exhibit dye accumulation. B) The dependence of EPR effect on the vascularity is demonstrated by the fact that periphery of the tumors (where angiogenesis predominates) see more dye accumulation, while the hypoxic (and partly necrotic) core does not see significant accumulation. Reference: Fang et al., 2011
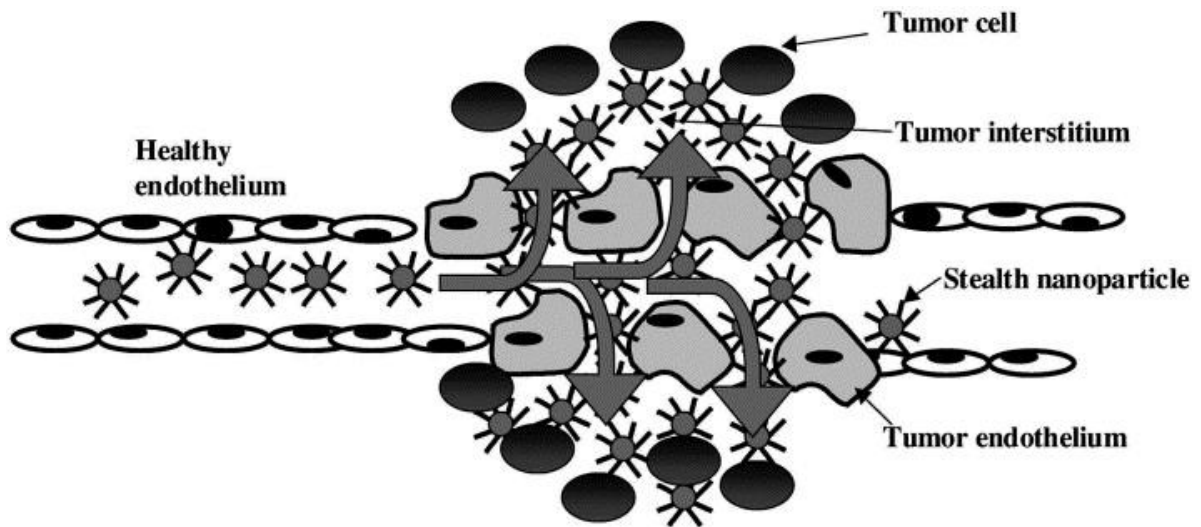
Figure 1.3. Accumulation of nanoparticles in tumors via EPR effect. Nanoparticles do not penetrate normal endothelium, but do so in leaky vasculature found in tumors. Combined with poor drainage, they accumulate in the tumor interstitium, where they are either endocytosed by cells or release their payload by nanoparticle degradation. Reference: Brigger et al., 2002
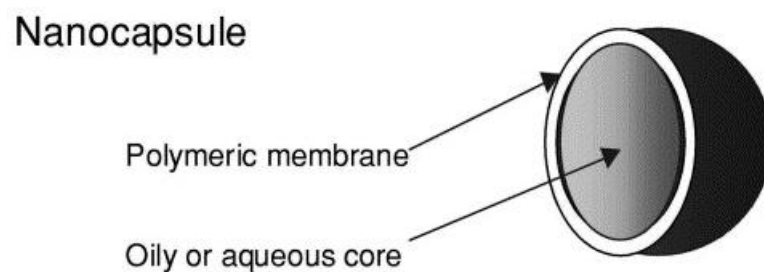
Figure 1.4. General structure of a nanoparticle. They have a shell with a hydrophilic exterior and a hydrophobic/aqueous core. Reference: Brigger et al., 2002
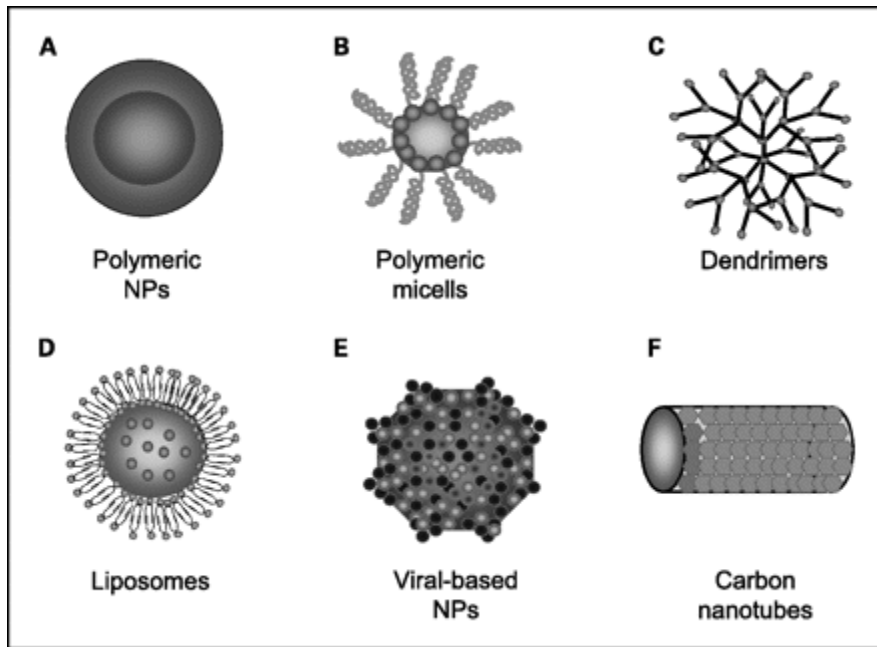
Figure 1.5. Different types of nanoparticles for drug delivery. Reference: Cho et al., 2008

CHAPTER 2. POLYMERIC DRUG DELIVERY

(Parts of this chapter will be published as Nair, P. R., Christian D.A., and Discher, D. E. Polymersomes. The Giant Vesicle Book)

2.1. Introduction to polymers

Phospholipids are the defining component of a cell's outermost plasma membrane, its nuclear 'double' membrane, and many other vesicular bodies in cells such as endosomes and lysosomes. Liposomes assembled from purified lipids have been utilized for several decades to encapsulate drugs in their lumen for drug delivery. However, a lack of stability for many types of liposomes results in poor control over payload retention. This, in addition to other vesicle properties, provided some practical motivation nearly 20 years ago for the development of polymersomes, a family of liposome structures self-assembled from block copolymers with lipid-like amphiphilicity (Discher and Eisenberg, 2002). They have since, not only provided a platform to study the physical properties of the polymer bilayers, but also developed as a new class of low permeability, mechanically tough cell-sized vesicles that cannot be made from standard lipids.

The great variety in types and sizes of polymers provides mechanisms for tuning membrane properties for applications in fields that range from drug delivery to devices. For example, in drug delivery to tumors, the high toxicity of most chemotherapeutics can often be better controlled with nano-carriers such as polymer vesicles (polymersomes) by

tuning the kinetics of drug release such that less of a toxic drug is delivered to healthy tissue (Chidambaram et al., 2011). Slow drug release from a nano-carrier will delay release into the bloodstream or to a disease site and limit drug excretion into urine, whereas very slow release will lead to drug accumulation in immune cells that generally clear nanoparticles from the bloodstream. Such design criteria are merely illustrative of properties that might be tuned with polymer based nano-carriers such as polymersomes and micelles.

2.2. Block copolymer amphiphiles and assemblies

A hydrophobic polymer linked covalently to a hydrophilic polymer yields an amphiphilic diblock copolymer and, like lipids, the polymers will tend to self-assemble in aqueous solutions in order to minimize exposure of the hydrophobic block to water. The morphology of these assemblies includes among others spherical micelles, cylindrical micelles, and vesicles – all of which have received substantial attention for drug delivery. Spherical micelles have long been used for delivery of hydrophobic drugs integrated into the hydrophobic block to solid tumors (Kwon and Okano, 1996). Cylindrical micelles have been used for similar applications, and will be discussed in detail in chapter 3. Polymer vesicles are more recent and have been loaded not only with hydrophobic drugs into the hydrophobic core of the membrane, but also with hydrophilic drugs into the vesicle lumen in order to deliver two anti-cancer drugs simultaneously to tumors (Ahmed et al., 2006a, Ahmed et al., 2006b). Vesicles have also been used for the co-delivery of siRNA and antisense (AON) oligonucleotides to treat genetic diseases (Kim et al., 2009a).

Unlike acyl chains in lipids, a sufficiently long hydrophobic block can also contain oxygen among other polar or water-soluble groups. Polyesters are one type of oxygen-containing, medically approved polymers that are particularly useful as they degrade via hydrolysis. Controlled release from biodegradable materials has formed the basis for many types of drug delivery systems (Leong et. al., 1985) among other applications (Middleton and Tipton, 2000). Polyester-based, rate-controlled release from degradable polymersomes have already been used to shrink tumors and treat genetic diseases (Ahmed et al., 2006a, Ahmed et al., 2006b, Kim et al., 2009a).

2.3. General background of structures

The self-directed assembly of amphiphilic molecules into a highly curved spherical micelle, a less curved cylindrical micelle, or relatively flat vesicle morphology is primarily dictated by the ratio of the hydrophilic and hydrophobic fractions (Blanazs et al., 2009). In contrast with lipids, the structure of polymeric amphiphiles can be tuned across a wide range of properties including molecular weight, polydispersity, charge, and crystallinity. Therefore, understanding the fundamental basis by which these block copolymers self assemble into different morphologies is crucial.

2.3.1. Microphase structures: polymersomes, worms, and spheres

A simple calculation of amphiphile geometry sheds light into its tendency to assemble into different morphologies. This is often obtained in terms of a 'packing parameter', that

indicates the curvature of the molecular structure (Figure 2.1) per (Discher and

Eisenberg, 2002). Mathematically, the packing parameter p is expressed as:

$$p = \frac{v}{al_c} \qquad \text{(2-1)}$$

where v is the volume of the hydrophobic chain, a is the cross-sectional area of the

hydrophilic chain at the interface, and l_c is the hydrophobic chain length (Israelachvili,

1991). The difference in structure from lipids leads to key differences in the calculation

of p. The value of a is taken as the area of the chain at energetic minimum, while l_c is

the average chain length over all conformations. These differences and have been the

subject of extensive simulation and theoretical research (Smart et. al., 2008). For

spherical micelles $p < 1/3$, whereas cylindrical micelles (or worms) have a p value

between 1/3 and 1/2, and vesicles (or polymersomes) result from a value of p between

1/2 and 1. While p values above 1 exist, their utilization in drug delivery systems has

been limited. Differences in the shapes and sizes of assemblies or aggregates influence

their properties as nano-carriers *in vitro* as well as *in vivo*, including properties such as

drug loading capacity, mode of clearance from bloodstream, etc.

Spherical micelles can be created with a wide distribution of polymer weights and block

ratios since a suitable packing parameter allows for very large hydrophilic blocks.

Spherical micelles are also kinetically trapped states of the larger cylindrical micelle or

vesicles assemblies if the latter are disrupted by excess energy (such as from ultrasound,

shearing, heat, electrical fields) (Discher and Ahmed, 2006). For these reasons and more,

spherical micelles are the most widely studied polymer assembly for drug delivery

(Kwon and Okano, 1996). However, they load only hydrophobic drugs and have lower drug loading capacity per particle compared to other morphologies.

Cylindrical micelles exist only in a narrow range of the packing parameter, and it is challenging to synthesize block copolymers that generate such micelles. Synthesis needs to be precisely controlled, and strong shear (among other physical perturbations) needs to be avoided to obtain cylindrical micelles. These factors make it difficult to make this shape, and hence, they are less commonly studied. However, benefits of this elongated shape for drug delivery (Geng et al., 2007) have led to significant interest in these nano-carriers of unusual shape, as reviewed in (Oltra et al., 2013). Higher drug loading capacity and evasion of uptake by phagocytes (cells that eat foreign substances) of these particles are particularly interesting properties in the context of drug delivery, and their applications are discussed in the next chapter.

Polymersomes have attracted considerable attention for their potential in drug delivery (Ahmed et al., 2006b, Xu et. al., 2005, Onaca et. al., 2009, Kim and Lee, 2010) among other applications. Unlike their micellar counterparts, polymersomes allow hydrophobic drugs to be loaded in the highly stable membrane core while hydrophilic therapeutics can be encapsulated in the aqueous lumen.

Dual drug loading in one carrier allows the co-delivery of drugs that simultaneously target two different pathways (Ahmed et al., 2006a). Polymersomes have been used also as nanoreactors (Vriezema et al., 2007) among other diverse applications. Importantly, giant polymersomes (pGUVs) have been essential to measuring and understanding the properties of these novel polymer membranes (Discher et al. 1999, Aranda-Espinoza et

al. 2001, Bermudez et al., 2002, Bermudez et al., 2003, Bermudez et al., 2004, Dimova et al. 2002, Itel et. al., 2014).

2.3.2 Other parameters that affect shape

Whereas packing parameter is the most important factor intrinsic to the constituent block, physical factors such as shear force and temperature also contribute to the final shape. Shear force, for example, applied via sonication can fragment cylindrical micelles to spherical ones irreversibly. In certain cases, the method of formation also influences the final shape.

2.3.3. Simulations on a small scale

The chemical simplicity of block copolymers has allowed the use of simulation studies to lend insight into the properties of block copolymer assemblies – including bilayer membranes. Block copolymer simulations have been performed using parameter sets that have been optimized for biological systems around 300 K. Coarse-grained models (that group a certain number of atoms together as one sphere) sacrifice atomistic detail for computational efficiency and have become more complex and realistic with time. The first coarse-grained molecular dynamics simulations of PEG-PEE in computational water replicated the phase behavior experiments on PEG-PEE assemblies (Srinivas et al., 2004a, Srinivas et al., 2004b, Srinivas and Klein, 2004, Srinivas et al., 2005). The first studies also matched some properties measured on polymer GUVs (pGUVs) such as the area expansion modulus, K_a, which proves nearly independent of polymer molecular

weight. Dissipative-particle dynamics allows longer simulation time scales (Warren, 1998, Peters, 2004, Ortiz et al.,2005), and has been used for example to understand how phase separated domains induced by differences in the hydrophilic block could register across the bilayer (Pantano et al., 2011). Finally, simulations were used to study how vesicles could be used for drug delivery by determining the release of drug payload following osmotic swelling and vesicle rupture (Ortiz et al., 2005).

2.4. Motivation for polymer approaches

While liposomes have already been used in drug delivery applications in the clinic, they have been limited by their low stability and rapid disintegration *in vivo* that prevents the controlled release of their cargo (Lasic and Papahadjopoulos, 1998, Semple et al., 1998). Liposomes are also quickly recognized and cleared by the immune system and must be modified to include an outer PEG brush to delay clearance *in vivo*. The tunability of block copolymer MW and chemistry while maintaining vesicle morphology allows polymersomes to improve on the shortcomings of liposomes (Discher et al., 2007). Section 2.4.3 summarizes the key advantages of polymersomes as well as some of the differences from liposomes.

For drug release *in vivo*, the time scale for decay should be long enough for the vesicles to reach the target. However, if it is too long, the vesicles will be cleared by the body's immune system. Liposomes exhibit limited circulation time *in vivo*, and the addition of a PEG (or PEO) to <10% of lipid head-groups creates 'stealthy' liposomes with circulation times extended from minutes or hours to 10-15 hours (Woodle, 1993; Klibanov et al.,

1990). PEG is repulsive in interactions with cells, and is the most common hydrophilic fraction of block copolymers to make polymersomes inherently stealthy (Photos et al., 2003).

2.4.1. Tuning physical properties with molecular weight for given chemistry

Liposomes are made up of constituent lipid molecules smaller than 1 kDa in size (Discher and Eisenberg, 2002). As mentioned above, polymersomes are made of copolymers that are up to 20 kDa in size, and this difference in molecular weight manifests itself in membrane thickness, d. Parameters such as permeability, viscosity, and elasticity, as measured by experiments on single pGUVs as well as on nano-vesicles, are controlled by membrane thickness d (Discher and Eisenberg, 2002, Hamley, 2005, Battaglia and Ryan, 2005, Dimova et al., 2002), and pGUV composed of membranes with much more variance in d (8 to 21 nm) than liposomes (3 to 5 nm) were used to measure these membrane properties. The thinner membrane of liposomes leads to the low stability (leakiness) and short circulation time mentioned above. Measurement of water permeation through membranes confirmed that permeation rate was much higher for liposome membranes than polymersome membranes (Discher et al., 1999). Thus, liposomes are assembled such that there is much more fluidity and permeability versus stability in the bilayer at the expense of stability. In contrast, the fluidity, permeability, and stability of polymersome membranes can be tuned by controlling the molecular weight.

Although polymersome membranes are generally thicker than liposomes, the customizability of polymers has allowed for membranes with thicknesses more similar to liposomes to be made (Battaglia and Ryan, 2005, LoPresti et. al., 2009). Amphiphilic diblock copolymers of polyethylene glycol-b-polybutylene oxide self-assembled into membranes with thickness reportedly ranging from 2.4 to 4.5 nm. Triblock copolymers (polyethylene glycol-b-polybutylene oxide-b- polyethylene glycol) assembled into thicker membranes ranging from 3.4 to 6.2 nm. The authors attributed the thinner membranes to the higher flexibility of the polyether hydrophobic block. The permeability of the membrane was found to vary with pH, and was found to be higher than that of phosphatidylcholine membranes at lower pH (Battaglia et. al., 2006). Such thin membranes might be particularly useful in the reconstitution of proteins into polymersomes.

2.4.2. Tuning properties with chemistry

Changing the chemical properties of either the hydrophilic or hydrophobic portion of the block copolymer is a means to control the characteristics of polymersomes. Three commonly employed hydrophobic chains used to make polymersomes are, in the order of increasing hydrophobicity, poly-L-lactic acid (PLA), polycaprolactone (PCL) and polybutadiene (PBD). PLA has a high degree of hydrophilicity due to the presence of an ester bond, leading to a rapid rate of hydrolysis. Thus, PEG-PLA (also abbreviated as OL) assemblies degrade soon after they self-assemble, with vesicles stable for a few days (Lee et al., 2001, Lee et al., 2002, Photos et al., 2003). PBD on the other hand is very

hydrophobic and does not undergo any appreciable hydrolysis. Consequently, assemblies comprised of PEG-PBD (OB) are stable for up to years.

PEG-PCL (OCL) assemblies have stabilities between those of OL and OB and are thus more suitable for applications in drug delivery when used in pure form. Blends of polymers that vary the percentage of degradable OL or OCL blended with inert OB were utilized to produce vesicles that have controllable release times (Ahmed et al., 2004). Such principles of blend-controlled release apply also to filomicelles (Kim et al., 2005). Blending of polymers with varying chemistry provides a powerful method to create nano-vehicles with highly customizable release times. The main mode of drug release is the hydrolytic degradation of the copolymer, specifically, via 'end-chain cleavage' and not at random points in the hydrophobic block ('random scission') (Geng and Discher, 2005). This changes the phase from vesicles to worms, destabilizing the assembly and releasing the contents (Ahmed et al., 2006a).

Environmental triggers have also been utilized to induce degradation of polymersomes, such as polymersomes that were designed to be sensitive to oxidative byproducts like H_2O_2 (Napoli et al., 2004). The hydrophobic core in PEG-(propylene sulfide)-PEG triblock copolymers was oxidized to hydrophilic groups, that destabilized the vesicle and favored micelles. pH responsive polymersomes from PEG-poly(2-vinylpyridine) (PEG-P2VP) have also been created, that fall apart after protonation of the hydrophobic core at low pH (Borchert et al., 2006). Stimuli can also be utilized to change the size of vesicles (Checot et al., 2003). Vesicles assembled from poly(butadiene)-b-poly(γ-L-glutamic acid) were shown to reversibly change size by varying the pH and ionic strength. Further,

the 1,2-vinyl double bonds were crosslinked by exposure to UV, creating systems in which the release of encapsulated drug can be controlled.

Such broad customization options are not available with lipids. However, it must be noted that, because of polydispersity inherent to synthetic polymers, each batch can vary significantly, which poses a major challenge for reproducible results. This necessitates the introduction of an additional purification step by GPC before the formation of aggregates.

2.4.3 Key Differences between polymersomes and liposomes

Since liposomes are self-assembled from natural phospholipids, they are fully biocompatible. However, they exhibit low encapsulation efficiency and stability (Lasic and Papahadjopoulos, 1998). Polymersomes are tougher, and improve upon some of the aforementioned shortcomings. Figure 2.2 depicts the general structure of polymersomes and liposomes. Some of these key differences are listed below:

- Polymer membranes are much less permeable, thus making polymersomes slow to deflate. One study estimated the shear viscosity of polymersome membrane to be 500 times higher than that of lipid membranes (Dimova et. al., 2002)

- Polymersomes relax back very slowly after deformation

- Their membranes are generally thicker and their thickness can range in a larger interval (8-21 nm). This translates to higher loading of hydrophobic drugs (Ahmed et. al., 2006)

- Molecular mobility in the polymersome membrane is much less compared to liposomes.

- For triblock copolymers, the bilayer (or two-leaflet) nature of the membrane may be lost and there could be polymers structured as loops (in one membrane half) or spanning across the membrane

- Polydispersity of polymers creates variance between batches, and poses challenge to reproducing results.

2.5. Other common block copolymers

Assemblies made with PEG-based copolymers have been found to be 'stealthy' (Photos et al., 2003). These properties in water can be attributed to the hydrogen bonding to ether oxygen atoms in PEG and high mobility in water (Discher et al., 2007). This stealthiness imparted by the PEG brush helped to delay phagocytosis, extending circulation time *in vivo*, thus making PEG an almost universal choice for the hydrophilic block. Charged hydrophilic blocks like polyacrilic acid (Schmaljohann, 2006) and polymethyloxazoline (Kim et al., 2009b) can be mixed with PEG-based block copolymers for various purposes. For example, such mixtures tune the lateral segregation of pGUV membranes (Christian et al., 2009, Christian et al., 2010).

The hydrophobic block dictates a number of properties of the polymersome membrane, and consequently there exist a number of polymers that have been utilized. Non-degradable membranes can be made to be fluid by using polybutadiene (Ahmed and Discher, 2004), polyethylethylene (Meng et al., 2009) or polydimethylsiloxane (Li et al., 2003), or membranes can be rigid by using strongly interacting glassy or semi-crystalline hydrophobic polymers such as polycaprolactone (Rajagopal et al., 2010, Ahmed and

Discher, 2004, Cai et al., 2007). Other popular hydrophobic polymers are polylactic acid (Kim et al., 2005) and polystyrene (Kazunori et al., 1993). The list of polymers can be much longer, and block ratios as well as MW are all variables that can influence physical properties measured for pGUVs, which in turn often translate to application even of nano-vesicles. Another dimension of customization can be achieved by blending lipids and polymers to create hybrid GUVs (Chemin et al., 2012, Le Meins et al, 2013).

2.6. Methods for synthesizing polymers

Diblock copolymers can be created either by using one block as a macro-initiator for the polymerization (chain extension) of the other block, or by covalently linking the two block polymers after they have been formed (conjugation). Covalently linking blocks is particularly handy when it is desired to introduce stimuli responsive groups between the two blocks (Section 1.6.2). Biodegradable polyesters are synthesized by condensation polymerization between diacids and diols or polymerization of hydroxy acids. The polymerization process requires high temperatures and long reaction times. Condensation polymerizations lead to the formation of byproducts and the polymers formed may need purification prior to use. PEG-poly(ethylene succinate) and poly(tetramethylene adipate). Ring opening polymerizations of lactones also lead to polyesters, and an example is discussed in detail in the next section.

2.6.1. Example synthesis

Chain extension requires a polymer block (initiator) with an end-group that can trigger

polymerization to be reacted with precise amounts of polymer (calculated based on the

desired molecular weight of the second block) in the presence of a catalyst and at high

temperature. An example of this type of copolymer synthesis is the polymerization of

caprolactone by methoxy-capped PEO to form PEO-PCL (OCL). Prior to this 'ring

opening' polymerization, ε- Caprolactone has to be purified by distilling it under vacuum.

This purification removes trace amounts of water in the system that also possesses

hydroxyl group required to initiate polymerization. The reactants along with the catalyst,

stannous octoate are then sealed under vacuum and reacted for 4 hours at 140 ^{o}C. A

schematic representation of this reaction is shown in Figure 2.3. Ratio of blocks can be

confirmed by ^{1}H NMR spectroscopy and the size distribution of the polymer (or

polydispersity index) is characterized using gel permeation chromatography.

Another example of chain extension is the reaction between PEO and a mixture of ε-

Caprolactone and D, L-Lactide to form OCLA. Similar to OCL, this polymer has a

polyester hydrophobic block, but has a faster hydrolysis time than OCL.

The other approach (conjugation), involves functionalizing the ends of the polymer after

synthesizing them. These end groups must be capable of reacting with each other, and

linking the blocks together when they do so. Cerritelli et al. (2007) utilized this strategy

to link together blocks of PEG and polypropylene sulfide (PPS), with a reduction

sensitive disulfide bond linking the two blocks. Thiolate terminated PPS was synthesized

by living ring-opening polymerization of propylene sulfide using benzyl mercaptan as initiator. Thioacetate PEG was deprotected to form thiolate terminated PEG, which was reacted with PPS to obtain the final copolymer. Vesicles formed were found to be sensitive to various reducing agents (like cysteine, glutathione, and dithiothreitol or DTT), aiming to simulate conditions found early in endolysosomal processing. With the disulfide bridge getting reduced and the blocks no longer linked, the assemblies destabilize and release the encapsulated payload. Chain extension provides excellent control over the polydispersity (Oltra et al., 2013), which is critical for worm formation.

2.6.2 Aggregate phase diagram

Although calculation of the packing parameter, *p*, can be useful to predicting the expected morphology of self-assembled amphiphilic block copolymers in water, mapping phase diagrams for a given polymer remains essential. These thermodynamic phase diagrams indicate which shapes are dominant in the indicated regions. The variables are hydrophilic mass fraction (f) and the MW of the hydrophobic block (M_{CH2}) in x and y axis respectively. A phase diagram of OCL is shown in Figure 2.4. It is important to note that the temperature is held constant (25 ^{o}C in Figure 2.4). Another point to be noted is that the oxygen atoms in the hydrophobic block contribute to the hydrophilicity of the polymer. Hence, the MW of the hydrophobic block is calculated by subtracting the weight of the oxygen atoms from the PCL block and the hydrophilic mass fraction f is calculated by adding the weight of the oxygen atoms to that of PEO (Rajagopalan et al., 2010). This is done because the oxygen atoms contribute to the hydrophilicity of the polymer, even though it is a part of the hydrophobic block.

One prominent point to note is that f has to be at least 0.36 for any stable colloidal

aggregates to form in water. Below this value, the PEO chains are too short to shield the

hydrophobic block from water and minimize the energy of the system. This region

corresponds to the higher end of packing parameter (p > 1). At f values just above 0.36,

the polymer exhibits low curvature (large hydrophobic block), and self-assembles into

vesicles (polymersomes). Increasing f increases the curvature and we obtain cylinder

micelles also called worms (Rajagopalan et al., 2010) and spherical micelles simply

referred to elsewhere as spheres. It is interesting to note that worms exist in a narrow

region that is embedded within the vesicle region.

It is important to note that controlling polydispersity is critical to obtaining the indicated

phases. The presence of a wide distribution of different chain lengths may destabilize

and/or favor the formation of other morphologies. Due to the narrow region in which they

exist, cylindrical micelles are particularly prone to this. Further, due to different value of

parameters for different polymers, phase diagrams are unique for a given copolymer. The

regions at given values of M_{CH_2} and f might be different for different polymers. However,

OCLA worms exist in a similar region as OCL worms.

2.7. Formation of aggregates and drug loading

A variety of methods have been utilized to self-assemble aggregated from diblock

copolymers: solvent evaporation (Rajagopal et al., 2010), thin film rehydration (Kita-

Tokarczyk et al., 2005), dialysis, and solvent injection (Kita-Tokarczyk et al., 2005) (Figure 2.5). Processes like extrusion and shear stress can be used to fine tune the final aggregate size. Of the above, solvent evaporation and thin film are the most common.

In solvent evaporation, the polymer is dissolved in a volatile organic solvent which is immiscible in water, such as chloroform. This solution is then added to water and the whole system is stirred. The organic solvent gradually evaporates and the polymer is forced into water where it self-assembles. When the organic solvent is miscible with water, dialysis method is used, where the removal of solvent by dialysis leads to the formation of aggregates.

The thin-film rehydration method starts out by dissolving the polymer in a volatile organic solvent. This solution is then added to a vial and the organic solvent is evaporated to obtain a thin film of the polymer. Water is added to the vial and at slow stirring speed (and often in the presence of gentle heating), aggregates are obtained. This method is preferred when it is desired to obtain polymersomes. Polymersomes can also be created by solvent injection technique, where a solution of block copolymers in an organic solvent is added to water slowly while stirring. During the course of aggregate formation, the solution turns turbid, with the final solution appearing milky due to the Tyndall effect.

Assemblies can be imaged using a hydrophobic dye such as PKH26 red dye. The dye partitions into the hydrophobic core of micelles or between the membrane for polymersomes (Figure 2.6). All shapes can load hydrophobic moieties, while hydrophilic ones can be loaded exclusively into the aqueous pool of the polymersomes. Dissolution of the drug in an organic solvent miscible with water followed by the solution's addition to the aggregates leads to diffusion of the drug to the hydrophobic core. Methods similar thin-film rehydration or solvent evaporation can also be utilized for drug loading. A pH gradient method is used for loading hydrophilic drugs like doxorubicin (Mayer et al., 1986).

2.8. Degradation of nano-carriers and drug release

While the nanocarriers have to be stable in circulation to avoid premature drug release, they must release their payload once accumulated in tumor. Hydrolysis can lead to degradation of polyesters by chain-end cleavage and shortens the hydrophobic block, while PEG is inert to hydrolysis. Hydrolysis increases the curvature of the assembly and a decrease in packing parameter. This changes the morphology and leads to destabilization of nanocarriers. Hydrolysis transitions polymers forming polymersomes to those for cylindrical micelles to spherical micelles (Figure 2.7). The destabilization of polymersomes leads to pores in the membrane and loss of drugs in the aqueous pool. The transition from cylindrical to spherical micelles is also accompanied by release of drug loaded in the core (Geng and Discher, 2005) (Geng and Discher, 2006). This happens because assemblies with higher curvature have smaller core for drug loading.

Hydrolysis of polyester is acid-catalyzed, and proceeds at a higher rate in the tumors where pH is lower. This ensures that nanocarriers remain stable in circulation, but degrade rapidly upon accumulation releasing drugs. Geng and Discher (2006) further determined that hydrolysis proceeds via chain-end cleavage, rather than random scission. Incorporation of pH sensitive groups between the two blocks can trigger the collapse of nanocarriers (Jeong et al., 2013).

2.9. Polymeric Nanocarriers for Gene and Drug Delivery

2.9.1. Polymeric Nanocarriers for Chemotherapeutic Delivery

Ahmed and Discher (2004) successfully controlled the release of doxorubicin from vesicles by blending degradable polyester copolymers (Polyethyleneglycol-poly-L-lactic acid, PEG-PLA or Polyethyleneglycol-polycaprolactone, PEG-PCL) with a more stable copolymer (Polyethyleneglycol-polybutadiene, PEG-PBD). Miscibility was verified by fluorescence microscopy of fluorescent copolymer. Degradation of polyester first produced pores of a size estimated to be around 10 nm from release profiles of fluorescent dextrans of different weights, which was comparable to the membrane thickness. The disintegration of uniform-sized vesicles was then checked by DLS. While no change in vesicle populations were found with time for PEG-PBD (OB) vesicles, PEG-PLA (OL) blended vesicles displayed progressive decay by splitting into two peaks. Vesicles containing OL with bigger PEO block fraction was found to disintegrate faster.

A study on the release kinetics of blends proved that increasing the OL fraction in the blend increases the rate of encapsulant release. Furthermore, the rate constant of release was directly proportional to the concentration of OL in the blend. The inertness of OL present in the bulk of the solution was established from dilution studies which demonstrated only minor deviations in the measured release time scales with varying dilution. Longer release time for PEG-PCL (OCL) blended OB (as compared to OL-OB blends) pointed to slower hydrolysis rates consistent with a more hydrophobic PCL chemistry. A lower water activity in the PCL core as compared to OL core was identified as the probable factor. Thus, varying the polyester chemistry (PLA/PCL), the percentage of blended polyester, and/or the PEG block fraction (f_{EO}) changed the time constant of disintegration providing a uniquely tunable method to regulate the release of encapsulants within the vesicle. Plots of release time against f_{EO} for blends containing 25% OL or OCL implied that the influence of hydrophobic block weight was small in comparison to f_{EO}. Ahmed and Discher (2006a and 2006b) then built on this with OL blended OB polymersomes were for the co-delivery of doxorubicin and paclitaxel into tumors. The combination of the two drugs induces a twenty-seven fold increase in apoptosis as early as one day after injection and shrinks tumor sizes by as much as sixty percent.

Polymeric micelles can increase the solubility of the poorly-soluble drugs by solubilizing the drug in its core (Kipp, 2004) and reduce off-target cytotoxicity by better delivery of the drug to the tumors (De Jong and Borm, 2008). However, they are cleared from circulation by phagocytes when they are identified as foreign. The efficiency of delivery, which is directly related to their circulation time, can be improved by using non-spherical

nanocarriers, particularly the flexible worm-like 'filomicelles'. These nanocarriers (self-assembled from amphiphilic block copolymers) have been shown to delay clearance (Geng et al., 2007), causing them to circulate longer and shifting the drug load toward the tumor. These assemblies are uniquely customizable, with the chemical composition of the hydrophobic block of the amphiphilic block copolymer controlling many critical properties of the nano-carrier such as encapsulation efficiency and flexibility (Karthikan et al., 2010). Paclitaxel (TAX) is a chemotherapeutic that is used commonly in clinic (Wall and Wani, 1995) (Wall, 1998). It stabilizes microtubules and induces aneuploidy by blocking mitosis at the metaphase-anaphase transition, which greatly increases cell death (Long and Fairchild, 1994) (Jordan et al., 1996). Being hydrophobic, it has low solubility in saline, which hinders the maximum dose that can be administered (Zhang et al., 1997). Loading onto nanocarriers can significantly improve the amount of drug solubilized (Loverde et al., 2012) This combined with better delivery (via Enhanced Permeation and Retention, (Matsumura and Maeda, 1986) (Maeda, 2012)) leads to an overall safer therapy with higher MTD. Accordingly, this system has been used to shrink tumors in vivo, and shows higher efficacy than spherical nanocarriers (Christian et al., 2009). This system can be further tuned to increase drug loading by chemical modification of the block copolymers that self-assemble to form the nanocarrier (Nair et al., 2016). Addition of aromatic blocks to PEG-PCL succeeded in increasing Paclitaxel (TAX) loading, which translated to higher cytotoxicity in vitro and in vivo. Genexol-PM, a polymeric micelle formulation composed of PEG-poly-(D,L-lactide)-paclitaxel was used in phase I study in patients with advanced refractory malignancies (Kim et al., 2004). Polymersomes composed of PEG-PLA and PEG-PBD loaded with doxorubicin

and paclitaxel shrunk tumors by 60% from the initial size (Ahmed et al., 2006a) (Ahmed et al., 2006a).

2.9.2. Polymeric Nanocarriers for siRNA and AON Delivery

Polymersomes possess the desired delivery features of vectors, but can be cheaper to synthesize than viral vectors (Korobko et al., 2005 and 2006) Vesicles formed from PBD-P4VPQI entrapped small DNA molecules such as plasmids in the aqueous lumen. These vesicles showed efficacy *in vitro* with HeLa cells within 2 hours. The cationic charge of the polymer, however, limited uptake by cells. Vesicles made of PEG-PLL were used to encapsulate DNA for gene transfer in liver and lungs (Brown et al., 2000). Polymersomes from blends of OL-OB and OCL-OB were also used for the co-delivery of oligonucleotides like siRNA and antisense oligonucleotides (AON). Both siRNAs and AONs are negatively charged and require complexation with cationic lipids. Kim et al. (2009b) showed that OL polymersome mediated knockdown was shown to be effective *in vitro* as well as *in vivo* in mouse model of muscular dystrophy. Combinations of siRNA and chemotherapeutics have gained success. Polymersomes loaded with doxorubicin and Bcl-xL siRNA (Kim et al., 2013) showed efficacy against gastric cancer cell lines than single controls.
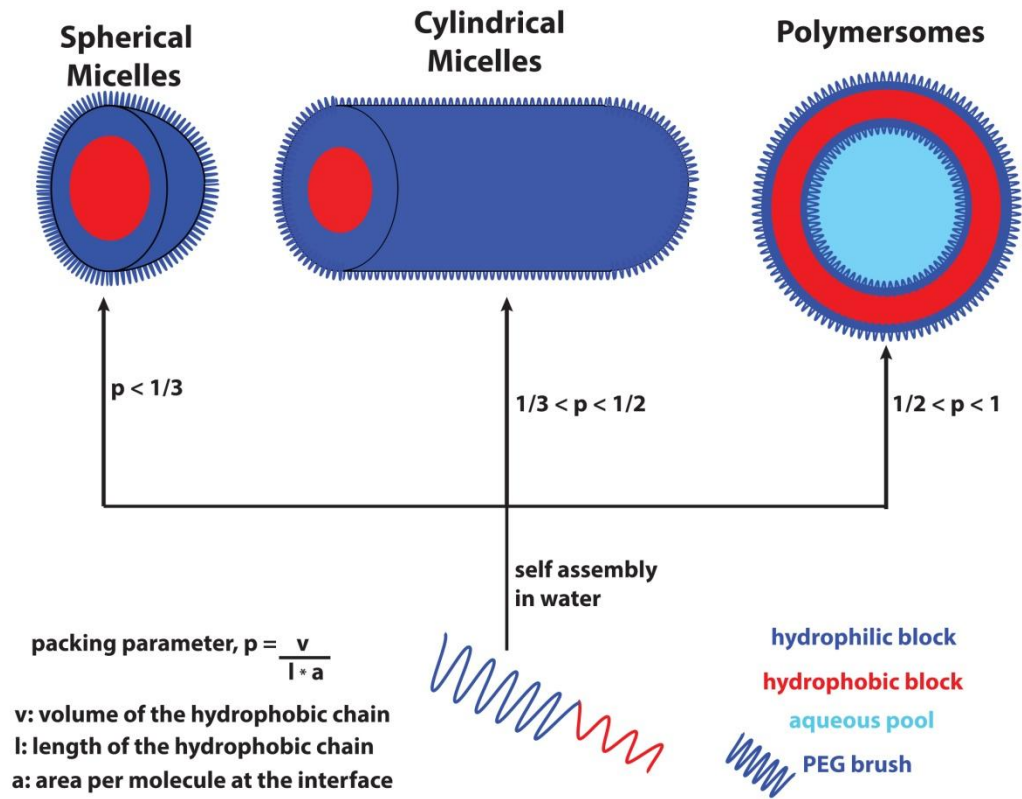
Figure 2.1. Aggregation of amphiphilic block copolymers into various morphologies. Copolymers with different values of packing parameter (p) form different assemblies as shown.
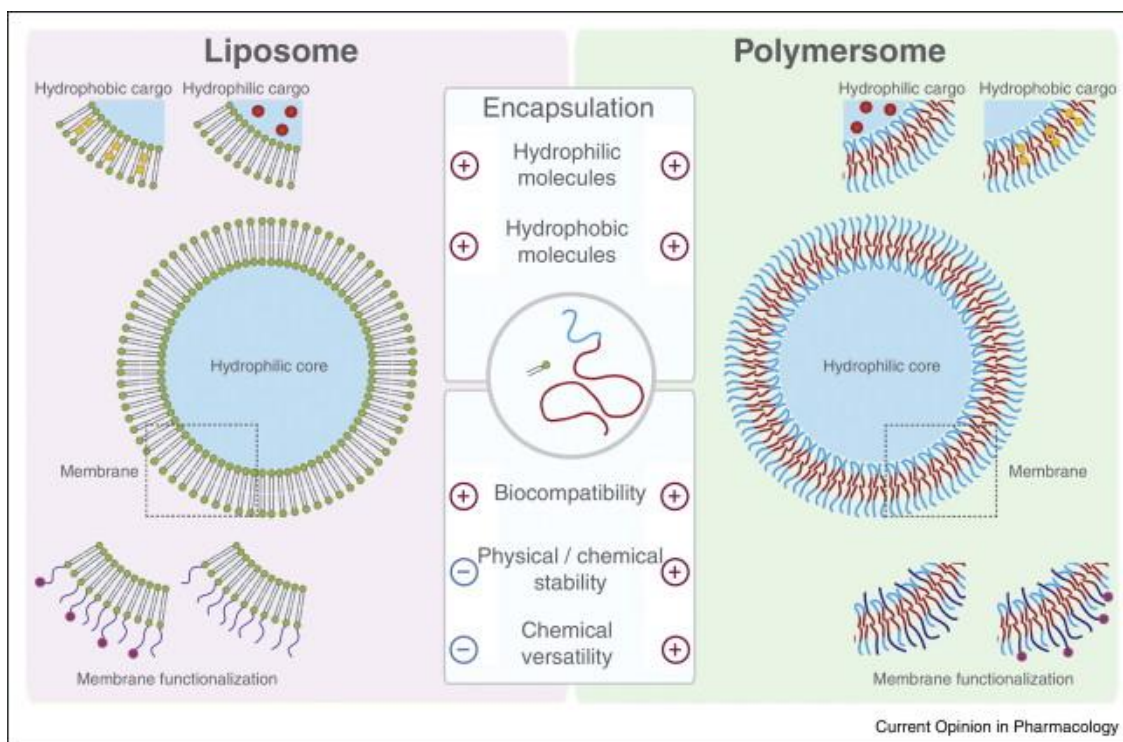
Figure 2.2. Structure of a liposome (left) and a polymersome (right) are similar. Both can be dual loaded, with hydrophobic drugs in the core of the membrane (red for polymersomes, top left inset for liposomes) and hydrophilic drugs in the water pool in the centre (blue for both). Reference: Messager et. al., 2014
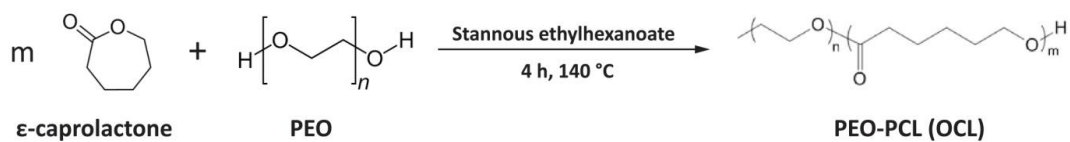
Figure 2.3. Reaction between PEO and ε-Caprolactone.
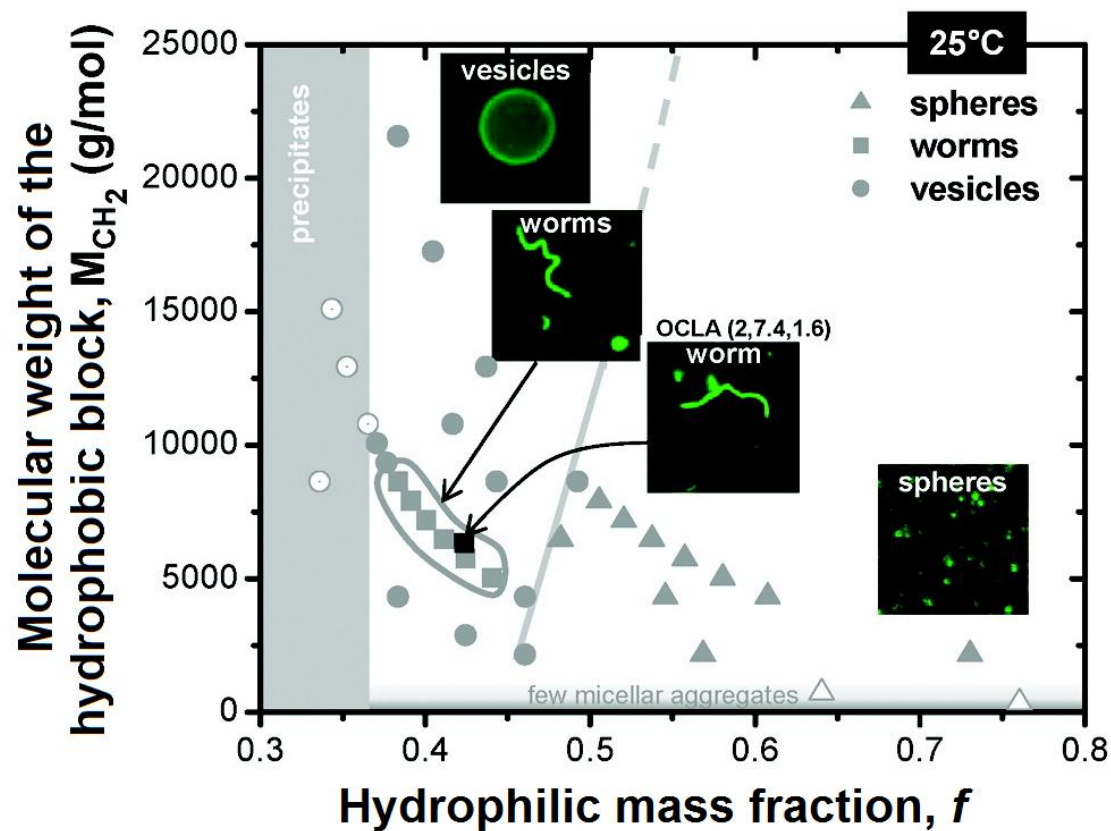
Figure 2.4. Phase diagram of OCL assemblies prepared at 25 °C. Three morphologies:

vesicles (shown as circles), worms (squares) and spheres (triangles) are represented here.

Filled gray region to the left of the diagram indicates the region where stable colloidal

assemblies are not found: open circles denote precipitates, while solid denote stable

aggregates. Insets show representative images of fluorescently labeled aggregates.

Concentration of polymer in water was 0.1 mM/mL. Reference: Rajagopalan et al., 2010
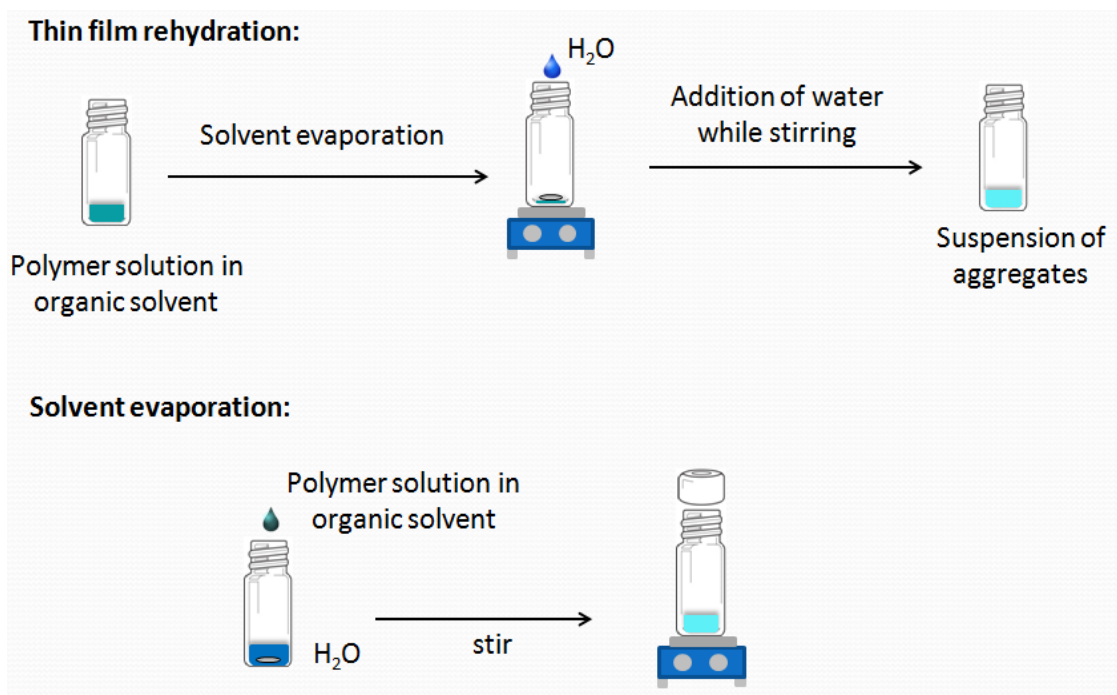
Figure 2.5. Aggregate formation by thin film rehydration and solvent evaporation.

Reference: NS Oltra
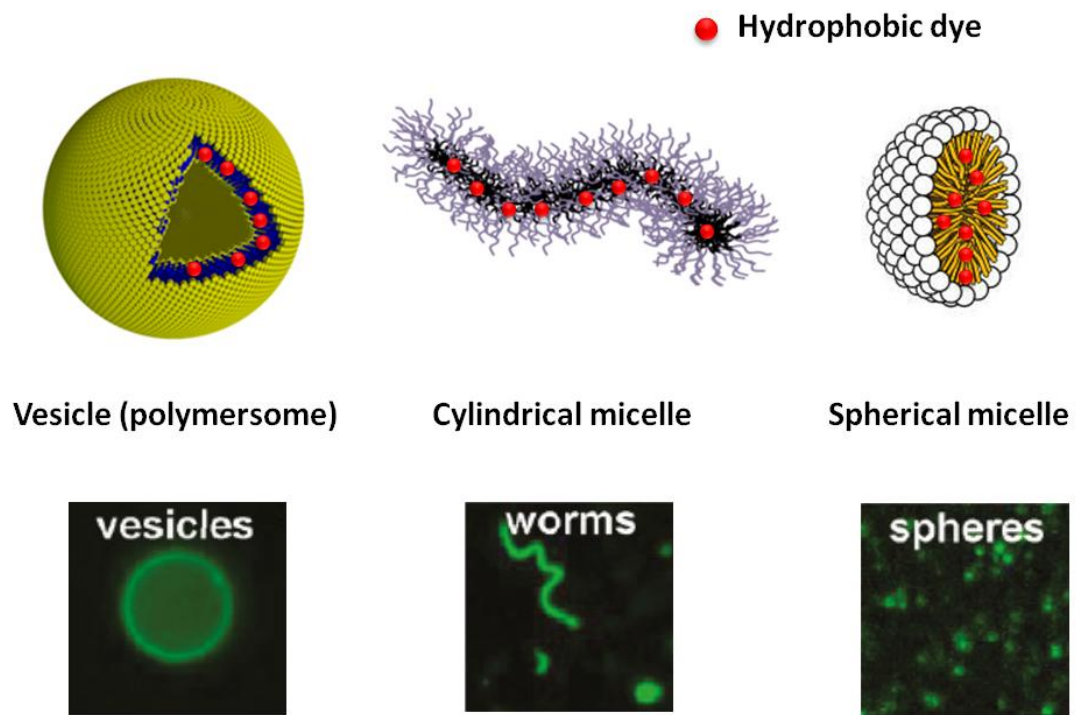
Figure 2.6. Fluorescence microscopy of different shapes formed by the self-assembly of amphiphilic diblock copolymers. These are visualized using a hydrophobic dye (red dots). Reference: NS Oltra
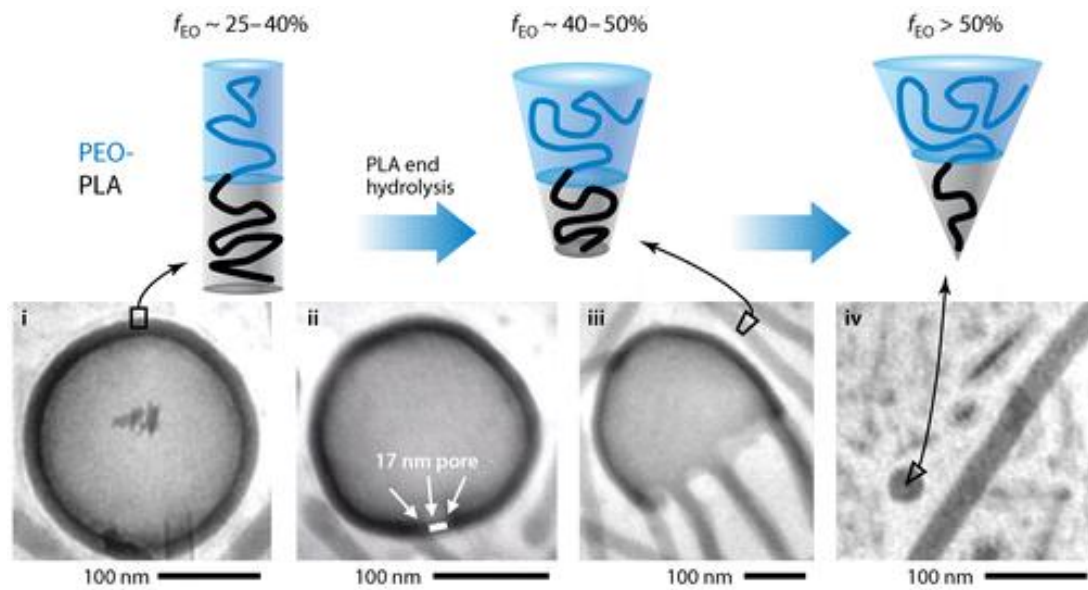
Figure 2.7. Degradation of PEG-PLA assemblies via hydrolysis. The fraction of hydrophobic block decreases and the curvature increases. The morphology of the assembly transitions from polymersomes to cylindrical micelles to spheres. Reference: Ahmed et al., 2006a

CHAPTER 3. SHAPE ADVANTAGES OF FILOMICELLES AND ITS TRANSLATION TO ANTI-CANCER TREATMENTS

(Parts of this chapter will be published as Nair, P. R., Christian D.A., and Discher, D. E. Polymersomes. The Giant Vesicle Book)

3.1 Flexibility and extended circulation time of filomicelles in vivo

The presence of stealth PEG coating on nanoparticles allows them to circulate longer. However, other factors such as shape also play a part in dictating circulating time. The non-spherical shape allows flexible filomicelles to circulate longer, based on their interaction with phagocytes. Injected worms circulated for up to a week in mice, while polymersomes circulated for three days (Figure 3.1). Another parameter that affects circulation time is the initial length of worms. During circulation, they exhibit progressive shortening in length, with worms from faster hydrolyzing polymers shortening faster. Long filomicelles (length greater than 18 μm) fragment rapidly to sizes around 8 μm (Figure 3.2). Shorter worms (length around 4 μm) shorten much more slowly.

Experiments performed on phagocytes immobilized in a flow chamber (Figure 3.3) provided more insight into the nanoparticle-immune system interaction. The immune system attempts to clear all injected nanoparticles, and spherical micelles were

internalized on contact with the macrophage. When a filomicelle was captured by a macrophage, it flexibility allowed it to align with the shear flow of the blood, break off and continue circulating. A small fraction is left behind, but the majority of the nanocarrier is avoids clearance and continues circulating.

The importance of flexibility in extending circulation time is underlined by the fact that rigid worms are cleared as rapidly as spheres, and do not exhibit the 'shape advantage' of flexible worms. Lower molecular weight polymer assembles into mostly flexible filomicelles, while rigid ones were observed when the hydrophobic block weight exceeded 9000 g/mol for PCL, when PEG weight was 2000 g/mol. higher molecular weight chains tend to pack closely and crystallize, while higher curvature in smaller chain leads to flexibility. Crystallization can be prevented by preventing regularity, i.e. by introducing defects that prevent crystallization. Addition of a small amount of lactide to caprolactone during polymerization gives PCLA, which does not form rigid worms. The formation of ordered structures is prevented by the methyl groups of lactide. These cylindrical micelles had long circulation times (increasing with higher initial length) with circulation half life up to five days for 8 μm length assemblies, which was a massive improvement over previously reported circulation times.

3.2 Selective accumulation of filomicelles in tumors

The longer circulation of filomicelles (worms) combines with preferential accumulation of worms in tumors to further increase efficacy. While spheres and worms both

accumulate in solid tumors due to the leaky vasculature, blood vessels forming normal

vasculature are not always free of defects. In these cases, smaller spheres find it much

easier than worms to penetrate into off-target normal organs (Figure 3.4). Filomicelles on

the other hand continue to circulate.

The above two phenomenon (faster clearance of spheres and more non-specific

accumulation) both combine to rapidly eliminate worms from circulation, ending up

predominantly on the liver and spleen (i.e. the MPS organs). Worms, on the other hand,

continue to circulate until they reach a tumor where they permeate out into the tumor

space due to the leaky vasculature. They can be loaded with hydrophobic drugs such as

paclitaxel as described in section 2.7 (Figure 3.5)

3.3 Increased drug loading capability of filomicelles

Loverde et al. (2012) demonstrated the effect of shape on drug loading. They used

molecular dynamics (MD) simulations to build a coarse grain (CG) model to study the

loading of paclitaxel (TAX) into spherical and cylindrical micelles. CG-MD models were

used because the constituent block copolymer assemblies were too large to simulate.

Each ethylene oxide unit was mapped onto one bead, while each caprolactone unit was

mapped onto three beads. The partitioning of TAX into the core of these nanocarriers

formed by the self-assembly of PEG-PCL was studied using a simple octanol-water

system (Figure 3.6). Calculation of force required to pull a single TAX molecule from the

core of the micelle to water outside showed that cylinders load twice as much drug as

spheres. The free energy was found to be 2.43 times lower with worms than spheres. Experimentally, the logarithm of TAX partition coefficient (proportional to free energy) was found to be 2.42 times higher for worms, agreeing excellently with theoretical calculations.

Quantification of PEG penetration into the core of the micelle showed increased penetration in the case of cylindrical micelles, which increased the loading capacity of the worms at the interface of hydrophobic and hydrophilic blocks. In spherical micelles decreased PEG penetration leads to increased water penetration into the PCL core, which is not the case in worms. Worms and bilayers have a denser PEG corona than spheres. The end result is that there is 50% more water in the core of spheres than worms. Additionally, the worm core is larger than that of the sphere due to stretching of chains. All these factors contribute to a higher loading volume and lower free energy state for TAX in worms.

After TAX loading into micelles, it remains uniformly distributed in the PCL core. Conversely, it aggregates and forms a crystalline structure in water. TAX shows a tendency to accumulate at the hydrophobic-hydrophilic interface, with the aromatic and hydrophobic groups buried in PCL. This tendency to load at the interface also explained the observation of a burst release phase observed with micelles.

3.4 Active and passive targeting with filomicelles

Worms (like other nanoparticles) exhibit passive targeting, i.e. accumulation in tumors via EPR effect. The effect is even more pronounced in worms as they circulate longer and have less non-specific accumulation. Once accumulated in the tumor, the worms degrade via hydrolysis, undergoing a change in morphology and releasing drugs (Figure 3.7).

The worm-like shape results in more surface area per volume, and these nanocarriers can be used for actively targeting tumor cells just as easily as spherical shapes. Biotin-terminated PEG containing diblock copolymers self-assemble to form biotinylated worms, on which antibodies conjugated to streptavidin can be displayed (Dalhaimer et al., 2004). These modified nanocarriers have been used to target groups displayed on the pulmonary endothelium (Shuvaev et al., 2011).

As stated previously, the hydrolytic degradation leads to shortening and destabilization of worms into spheres. The rate of degradation depends on the type of polymer and the weight of the block. PEG-PCL with a PCL weight of 4700 g/mol took 28 hours to degrade, while for a weight of 11000 g/mol, 200 hours were required (Geng and Discher, 2006). The rate of degradation in further enhanced by the observation that the terminal group on the PCL chain is oriented towards the hydrophilic part instead of being buried in the hydrophobic core (Nie et al., 2003). This makes it easier for it to get shortened by water molecules via chain-end cleavage. The lower pH in tumors also contributes towards accelerating degradation, with a drop of 2 pH units speeding the process up by 2

to 4 fold. At low temperatures, the degradation rate is minimal and there is no drug release, ruling out diffusion of drugs from core as a possibility (Ghoroghchian et al., 2006).

3.5 Drug loading of worms for anti-cancer therapy

Filomicelles can load hydrophobic small molecule drugs, and is achieved by diffusion of the drug to the core. Additionally, drug loading does not affect flexibility or rate of degradation. Paclitaxel solubility is greatly enhanced by loading on to micelles, being able to load ~5 mg/ml of TAX compared to 1 µg/ml for free TAX.

The cytotoxicity of paclitaxel loaded micelles was compared to that of free drug with *in vitro* tests. TAX loaded micelles were not only more effective than free drug, but they performed better than Cremophor EL loaded TAX (Cai et al., 2007), which is a non-ionic surfactant. Worms loaded with paclitaxel were able to shrink tumors in mice much more effectively than free drug (Figure 3.8) (Geng et al., 2007). Additionally, the tumor shrinkage was dependent on the length of the worms injected. For equal TAX dosage, tumor shrinkage increased with increasing worm length. Thus with worms, aspect ratio is another parameter that can be tuned to increase cell death, which is unavailable with polymersomes or spherical micelles.

Filomicelles also have a higher MTD of 18 mg/kg, than spheres (10 mg/kg). Both were better than free TAX with an MTD of 1 mg/kg. Higher drug loading translated into better therapeutic effect (Christian et al., 2009). TAX loaded worms injected at MTD were more effective in shrinking tumors, than spherical micelles at MTD (Figure 3.9). Consistent with the previous experiment, both were more effective than free TAX at 1 mg/kg. Additionally, tumors treated with TAX loaded worms maintained their reduced size three weeks from the start of the treatment. Apoptosis was measured in five off-target organs (liver, spleen, kidney, heart and lung) along with the tumor. While there was little preference towards tumor accumulation with free TAX, tumor specificity was observed with nanocarriers. Apoptosis in off-target organs was significantly lower with filomicelles compared to spherical ones. Assessment of biodistribution revealed that more TAX accumulation in tumors when delivered via micelles. Filomicelles led to twice as much TAX in the tumor compared to spherical micelles.

Treatment of brain tumors is complicated by the presence of a blood-brain-barrier (BBB), which limits the entry of small molecules to the brain, such as drugs. Drug delivery using filomicelles have been combined with radiation therapy to achieve success in brain tumors (Baumann et al., 2013). Radiotherapy was used to disrupt the BBB, followed by TAX loaded worms to provide a survival benefit in mice. The survival period was more than doubled after the treatment, extending lifespan by more than two months.
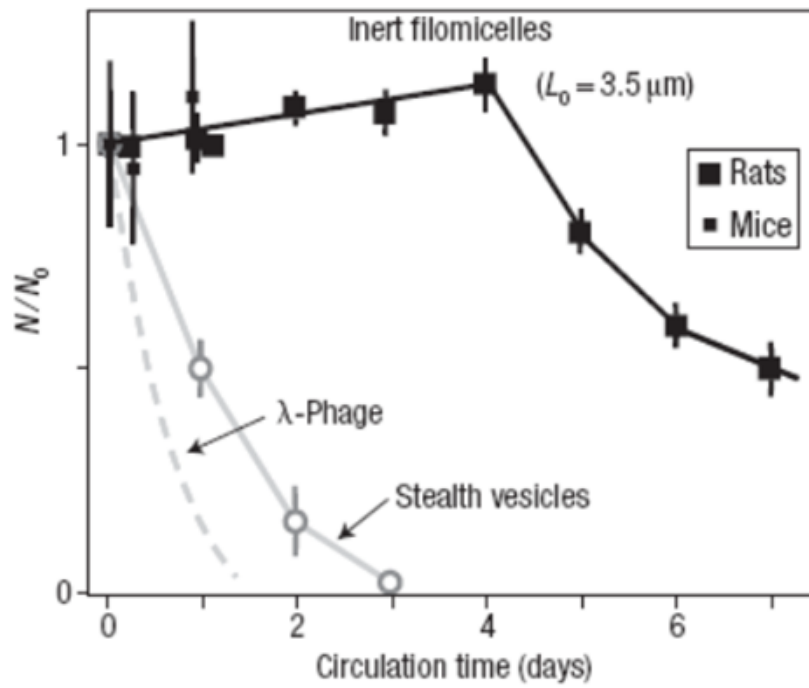
Figure 3.1 Long circulation of filomicelles compared to other carriers. Filomicelles circulate for over a week, compared to 3 days for vesicles and 2 days for phages. Reference: Geng et al., 2007
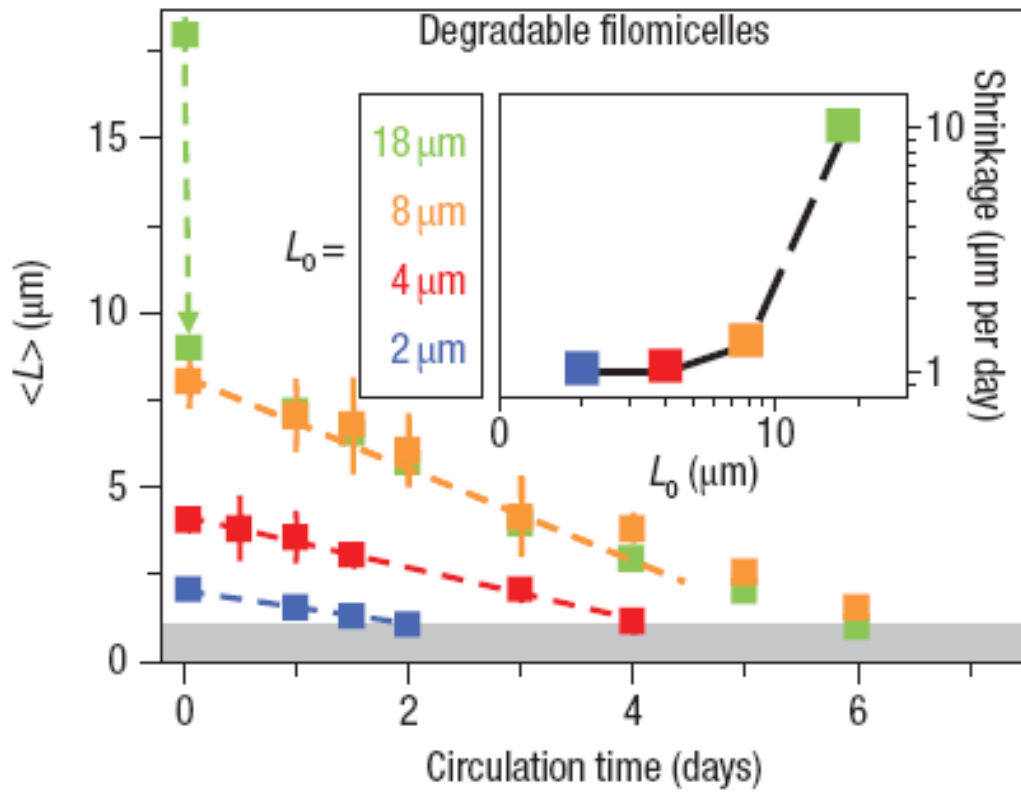
Figure 3.2 Rate of shortening of filomicelles depend on initial length. Reference: Geng et al., 2007
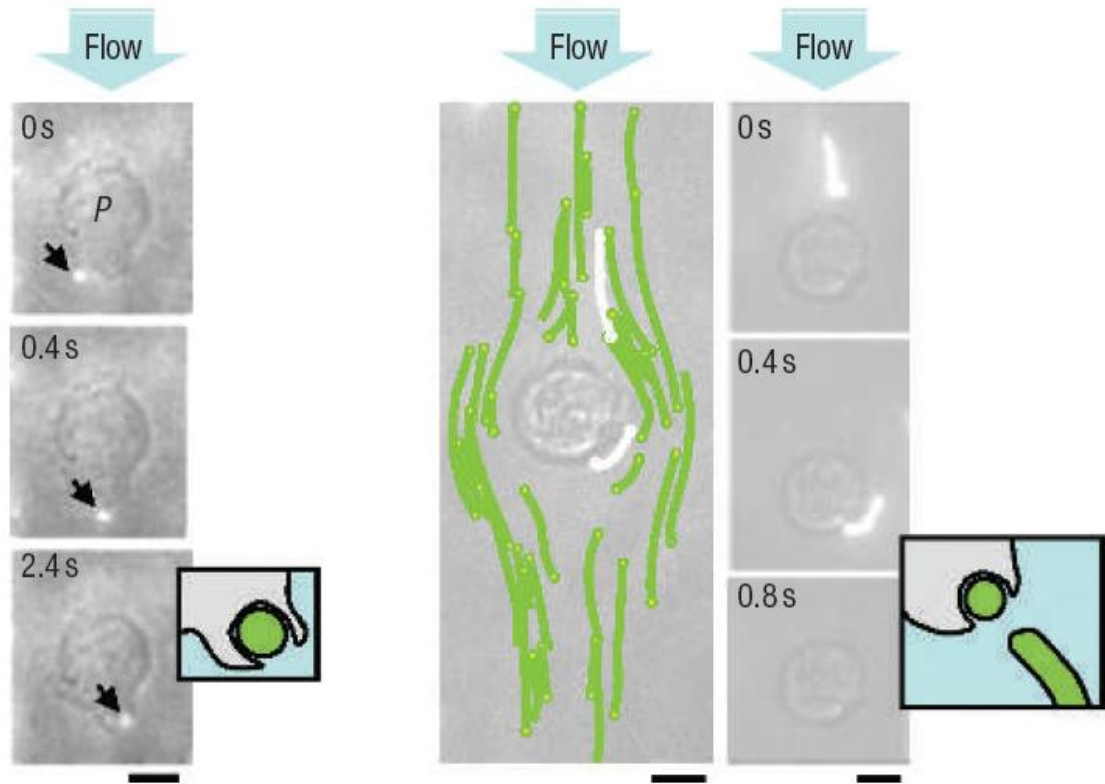
Figure 3.3 Longer circulation time of worms. Reference: Geng at al., 2007
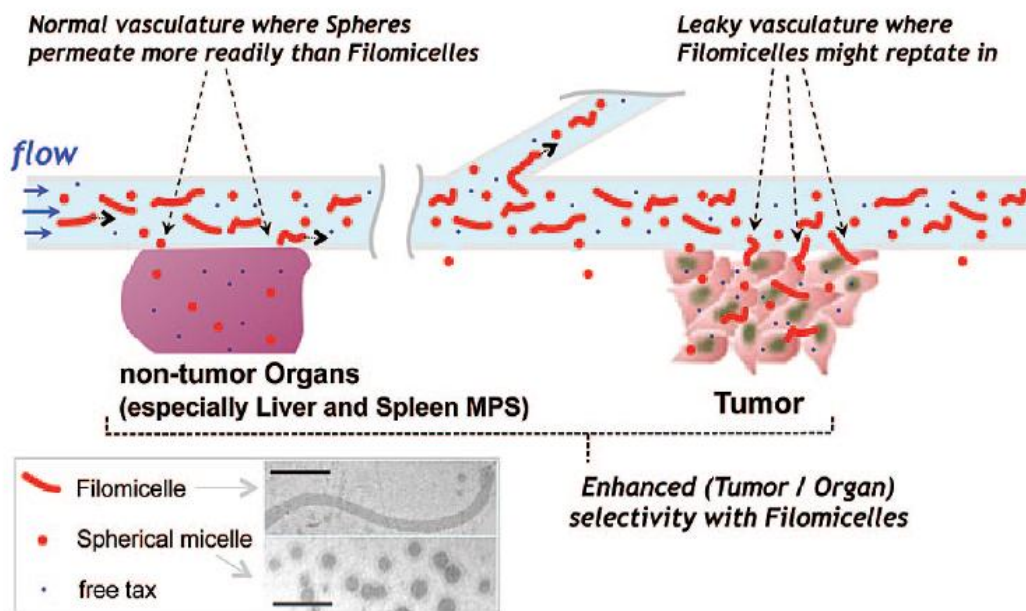
Figure 3.4 Selective accumulation of worms in tumors compared to spheres. Reference:

Christian et al., 2009a

Figure 3.5. Paclitaxel (TAX) (blue dots) loading into the core of cylindrical micelles

formed by the self-assembly of amphiphilic diblock copolymers. Reference: NS Oltra
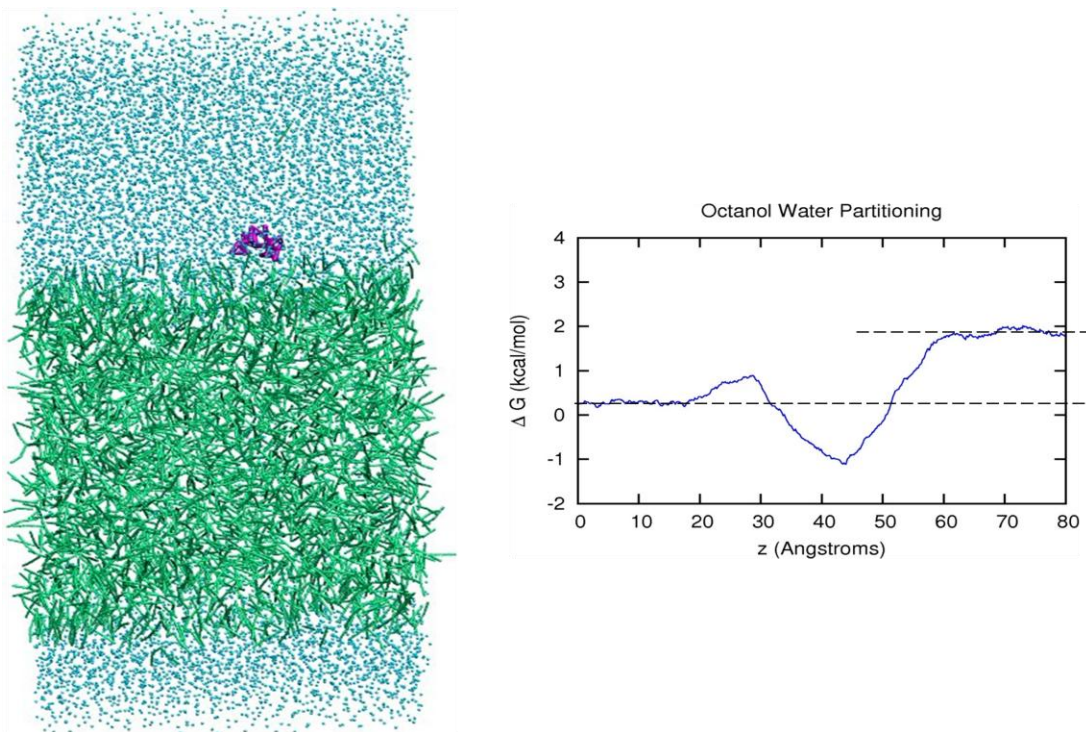
Figure 3.6 MD of TAX across CG octanol-water interface (left). Free energy change vs.

distance across octanol-water interface (right) shows minima at the interface that results

in accumulation there. Reference: Loverde at al., 2012
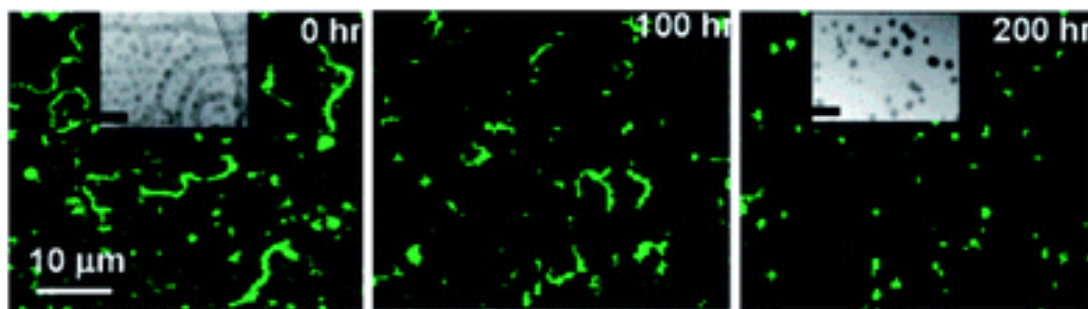
Figure 3.7 Images of PEG-PCL filomicelles showing degradation to spherical micelles over the course of 200 hours. The change in morphology is an integral part of drug release from worms. Reference: Geng and Discher, 2005
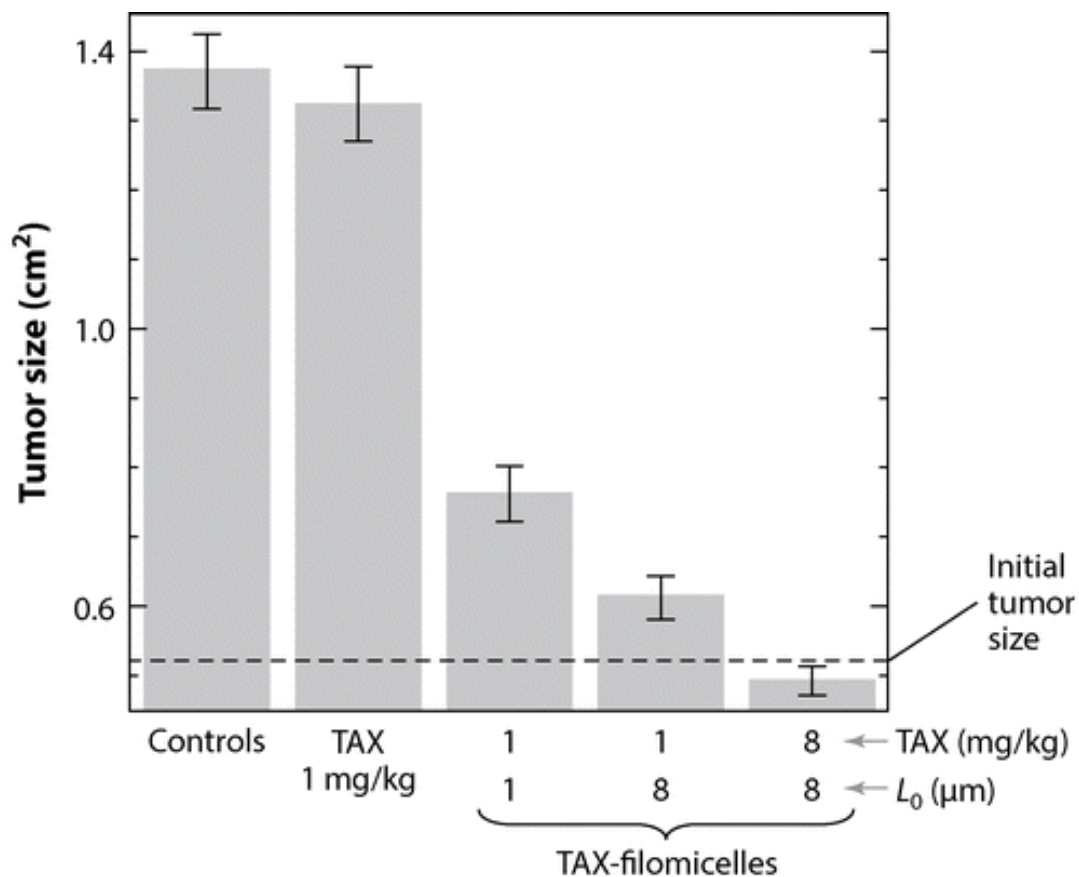
Figure 3.8. Tumor shrinkage in mice seven days after injection with free TAX or TAX worms. Loading onto worms increases the efficacy of the treatment, with the length of the worm influencing the final outcome as well. Reference: Geng at al., 2007

Figure 3.9. Tumor shrinkage in mice seven days after injection with free TAX or TAX worms. Loading onto worms increases the efficacy of the treatment, with the length of the worm influencing the final outcome as well. Reference: Christian et al., 2009

CHAPTER 4. AROMATIC MODIFICATION OF FILOMICELLES INCREASES INTEGRATION EFFICIENCY OF PACLITAXEL

Contributions: The polymer (PEG-PBCL) copolymer was provided by Alberta Research Chemicals Inc. (ARCI), Edmonton, AB, Canada as well as by Afsaneh Lavasanifar, University of Alberta. In vivo studies were performed by K.R. Spinler. Karthick S.A. performed the PEG-PCL worm shortening in Figure 4.4 B.

4.1. Introduction

4.1.1. Modification of nanocarriers

Nano-carriers can increase the solubility of poorly-soluble drugs (Kipp, 2004) such as Paclitaxel, which is a prototypical low solubility chemotherapeutic with multiple aromatic structures (Demain and Vaishnav, 2011) (Vines and Faunce, 2009) (Figure 4.1 A). TAX is an anti-mitotic aromatic chemotherapeutic. Cells that receive sub-lethal doses of TAX are more likely to develop drug resistance (Cheng et al., 2007), with selection of mutations in β-tubulin being one source of resistance (Kamath et al., 2005). Such

resistance strongly motivates many diverse efforts to increase drug efficacy, particularly by loading into nano-carriers.

As stated previously, TAX prefers the interface of PEG-PCL micelles (Loverde et al., 2012), but aromatic amino acids (e.g. tyrosine) likewise tend to localize to the interface of lipid bilayers unlike more aliphatic amino acids (Ulmschneider and Sansom, 2001). Incorporation of aromatic groups into the core of a nano-carrier could therefore increase the solubilization of aromatic drugs such as TAX for better delivery to tumor cells, and could also determine how the amphiphilic polymer or its degraded forms interact with and/or disrupt cell membranes (Vega-Villa et al., 2008)(Moghimi et al., 2005)(Vasir and Labhasetwar, 2008). Modifying the core could also affect the degradation time of nanocarriers, which is key to releasing the drugs if and/or when accumulated in the tumor. The crucial role of drug release profile on efficacy *in vivo* is highlighted by the many efforts to include moieties such as pH sensitive groups that make the nanocarrier fall apart under a right stimulus (Blanazs et al., 2009)(Chen et al., 2010). Filomicelles of different core chemistries are therefore interesting to test *in vivo* as well as *in vitro*, with a first couple of key unknowns being whether greater solubilization of an aromatic drug such as TAX impedes its release and whether changing the core chemistry alters the overall toxicity toward cancer cells (Vega-Villa et al., 2008).

4.1.2. Aromatic modification of PEG-PCL to incorporate more Paclitaxel

In this chapter, the impact of incorporation of aromatic groups in PCL via an ester group is assessed in terms of its ability to assemble into filomicelles and safely deliver TAX. Assemblies of polyethylene glycol-polybenzylcaprolactone (PEG-PBCL) (Figure. 4.1 A) were characterized by fluorescence microscopy, evaluated for drug loading/release by HPLC, and assessed for cytotoxicity using two cancer cell types. PEG-PBCL filomicelles loaded with TAX appeared more effective than either PEG-PCL filomicelles or free drug, and PEG-PBCL filomicelles also caused the greatest aneuploidy of the few surviving cells (hallmark of TAX treatment). Drug-free 'empty' PEG-PBCL filomicelles were also an order of magnitude less toxic than PEG-PCL filomicelles. Initial *in vivo* tests of efficacy of PEG-PBCL filomicelles loaded with TAX illustrate an ability to safely shrink tumors. The findings support past evidence that microns-long filomicelles are effective in cancer drug delivery but also show that efficacy might be increased by safely tuning polymer composition.

4.2. Materials and Methods

4.2.1. Materials

All chemical reagents were purchased from Sigma Aldrich Corp., St. Louis, Missouri, unless stated otherwise. Polyethyleneglycol (PEG) -Polybenzylcaprolactone (PBCL) copolymer was procured from Alberta Research Chemicals Inc. (ARCI), Edmonton, AB, Canada as well as generously provided by Afsaneh Lavasanifar, University of Alberta. Ham's F-12 growth media, FBS, penicillin-streptomycin, non-essential amino acids and

Hoechst 33342 were purchased from Invitrogen. High glucose DMEM growth media, 12-well plates, and 96-well plates were purchased from Corning.

4.2.2. Synthesis and Characterization

Polyethyleneglycol (PEG) -Polycaprolactone (PCL) di-block copolymer was prepared by the polymerization of ε-caprolactone using PEG_{2000} as macro-initiator. ε- Caprolactone was purified prior to polymerization by distilling it under vacuum at 60 ^{o}C. The molar ratios of PEG and caprolactone were adjusted to form PEG_{2000}-PCL_{7500} (as indicated in Table 4.1), which has been shown to self-assemble into filomicelles (Rajagopalan et al., 2010). The reactants along with the catalyst, stannous octoate, were sealed under vacuum and reacted for 4 hours at 140 ^{o}C. Synthesis of PEG_{5000}-$PBCL_{7500}$ (stoichiometry indicated in Table 4.2) was carried out at the same temperature, but the reaction time was 6 hours. A schematic representation of this reaction is shown in Figure 4.1 A. The PEG-PBCL reaction mixture was dissolved in 3 mL of dichloromethane and the solution was poured into 30 mL of hexane with stirring. This mixture was then decanted to remove hexane. The solid product was collected, washed with 5 mL diethyl ether, and stored under vacuum overnight. The isolated yield of the product was 72 %. Formation of the product was confirmed by ^{1}H NMR spectroscopy (Bruker BZH 360/52, 16 scans per spectrum) and the size distribution of the polymer was characterized using Gel Permeation Chromatography (GPC).

4.2.3. Filomicelle formation and characterization

Aggregates were formed in water by solvent evaporation of the copolymer dissolved in chloroform with the final concentration of polymer in water being 20 mg/mL. For every ml of aggregates, 20 mg of polymer was dissolved in 100 µl of chloroform (to give a polymer concentration in chloroform of 200 mg/ml), which was then added to 1 ml (MilliQ) water as separate phase. This mixture was then stirred for 2 days at 110 rpm with the cap lightly screwed on, to allow the chloroform to evaporate. For visualization under the microscope, 40 µl of aggregates were mixed with 0.2 µl of PKH 26 hydrophobic red dye (which had been diluted 5 times in ethanol). This dye, with emission spectra at a wavelength of 567 nm (Rajagopalan et al., 2010), was then imaged using an Olympus IX71 microscope with a 300W Xenon lamp using a 60x objective (oil, 1.25 NA) or 150x objective (oil, 1.45 NA) and Cascade CCD camera (Photometrics, Tucson, AZ). The software used was Image Pro (Media Cybernetics, Silver Spring, MD).

Phase diagram based on estimations of core block hydrophobicity (M_{CH2}) and hydrophilic mass fraction ($f_{hydrophilic}$) was calculated as per (Rajagopalan et al., 2010). Briefly, M_{CH2} is calculated as the molecular weight of the hydrophobic block minus the weight contributed by Oxygen atoms. The weight of these oxygen atoms is added to the weight of PEG block, which is divided by the total weight of the diblock copolymer to obtain $f_{hydrophilic}$ (more detailed instructions on this calculation can be found in Rajagopalan et al., 2010).

4.2.4. Drug Loading and Quantification

Paclitaxel dissolved in methanol (at a concentration of 20 mg/ml), was added to the aggregates at a final concentration of 1 mg of drug per mL of aggregate dispersion. The mixture was stirred for one hour at 150 rpm and let stand overnight to incorporate the drug into the filomicelle core. The unincorporated drug was removed by dialyzing the mixture through a membrane having Molecular Weight Cut-Off (MWCO) of 3500 Da (procured from Spectrum Laboratories, Inc., California). The dialyzed mixture was allowed to stand overnight and centrifuged at 2000 rpm for 8 minutes prior to usage. The drug loading was measured via Shimadzu prominence HPLC (High Performance Liquid Chromatography) with Pinnacle DBC18 Column (4.6x150 mm, 5 µm particles).

4.2.5. Persistence length and Mass fraction Quantification

Procedure for persistence length measurement was adapted from (Rajagopalan et al., 2010). Time-lapse images of filomicelles were taken and the end-to-end distance (R) and contour length (L) was measured using ImageJ 1.48d software. The persistence length was measured by fitting the data to a worm-like chain model as described in (Rajagopalan et al., 2010). ImageJ was used to calculate the area occupied by filomicelles and spheres in abovementioned time-lapse images. Mass fraction of filomicelles = (Area of Filomicelles)/(Area of Filomicelles + Area of Spheres).

4.2.6. Release studies

Release studies: Procedure adapted for release studies was as described in (Cai et al., 2007). Drug loaded filomicelles and free drug were dialyzed (MWCO 3500 Da) against PBS at pH 7.4 and 5.5 to simulate blood and endosome, respectively. The temperature was maintained at 37 ^{o}C. Samples were taken periodically and subjected to HPLC analysis as mentioned above (section 4.2.4).

4.2.7. Cell culture

A549 lung cancer cell line was purchased from ATCC and grown with Ham's F12 growth media supplemented with 10% FBS and 1% penicillin-streptomycin at 37 ^{o}C and 5% CO_2. EC4 mouse liver cancer cell line was cultured with DMEM High glucose growth media (4.5 g/L glucose with L-glutamine and sodium pyruvate) supplemented with 10% FBS, 1% penicillin-streptomycin and 1% non-essential amino acids at 37 ^{o}C and 5% CO_2. The cells were passaged by dissociation with 0.05 % Trypsin-EDTA (Invitrogen) and plated with fresh media as per standard ATCC cell culture protocol (2014).

4.2.8. In vitro filomicelle uptake

10000 EC4 cells were seeded in 12-well plates. Filomicelles labeled with PKH26 red dye was prepared as described above (in section 4.2.3). The next day, old media was discarded and cells were incubated with 950 μL of fresh media as well as 50 μl of 20 mg/ml labeled filomicelles. At fixed time points of 4, 24, 48 and 72 hours, cells were trypsinized, spun down and washed with PBS. They were then spun down and suspended

in 1 ml of Hoechst 33342 solution (0.01% of 10 mg/mL solution in water) for 5 minutes.

After the incubation, cells spun down and suspended in 300 µl of flow buffer (5% FBS in

PBS). Cells were run through a flow cytometer (BD LSR II) and data was analyzed by

WEASEL v3.2.1 software. A subset of cells incubated with labeled PEG-PBCL

filomicelles (one well per sample) was visualized under the microscope. The cells were

washed with Phosphate Buffered Saline (Invitrogen) and stained with Hoechst 33342

(0.05% of 10 mg/mL solution in water) (Molecular Probes, Invitrogen) for 10 minutes.

Following this incubation, they were washed with PBS 3 times and visualized under an

Olympus IX71 microscope with a 300W Xenon lamp using 60x objective (oil, 1.25 NA).

Images were taken for DNA, PKH as well as bright field and were then analyzed by

ImageJ software.

4.2.9. In vitro cell viability assay

Procedure for in vitro cytotoxicity assay was adapted from Cai et al., 2007. 5000 cells (at

a concentration of 50,000 cells/ ml of media) were seeded in 96-well plates (100 µl per

well) and incubated for a day to facilitate attachment to the bottom. The next day, old

media was aspirated and the cells were incubated with 100 µL of different formulations

and 100 µL of fresh media for 3 days (200 µL total volume). 100 µl of PBs was added as

a negative control Post 3-day incubation, the supernatant was aspirated, and cells were

incubated with 100 µL of fresh media and 11 µl of MTT solution (5 mg/mL in PBS) for

3.5 hours at 37 $^{\circ}$C and 5% CO_2. The supernatant was then aspirated and MTT formazan

crystals were then dissolved in 100 µL of DMSO per well, and absorbance was measured

using Tecan Infinite F200 plate reader at 550 nm. Cell viability was proportional to

(absorbance reading of well - absorbance of blank DMSO). Curve fitting and data

analysis was performed using OriginPro 8 software.

4.2.10. Cell death quantification

Cell death induced after treatment was measured as the number of floating cells staining

positive for Trypan Blue (Corning). After three day treatment, media was counted for

total number of floating cells (dead and alive) using a hemocytometer. Following this, the

media was mixed with equal volume of Trypan Blue solution (0.4% w/v in PBS), and

number of cells staining negative were counted. Cell death density = Total density of

floating cells - 2 × Density of cells staining negative with Trypan Blue

4.2.11. DNA content analysis

DNA content was analyzed on fixed cells as well as by flow cytometry. Cells were fixed

using 4% paraformaldehyde for 10 minutes followed by 3 PBS washes. Following this,

they were stained with Hoechst solution as described above. Cells for analysis by flow

cytometry were prepared by trypsinizing treated cells. These were then spun down,

supernatant was aspirated and cells were suspended in 1 ml Hoechst 33342 solution

(0.01% of 10 mg/mL solution in water) for 5 minutes. The cells were then spun down,

Hoechst solution aspirated and cells were suspended in 300 μl flow buffer (5% FBS in

PBS). Cells were run through a flow cytometer (BD LSR II) and data was analyzed by

WEASEL v3.2.1 software. Recovery of DNA content was performed by washing away

TAX containing media after 3 days of TAX treatment. The well was washed with PBS

and attached cells were incubated with fresh media for three more days. Following this, the remaining attached cells were prepped for flow cytometry and analyzed as described above.

4.2.12. In vivo experiments

In vivo experiments were performed on NOD-SCID mice with tumor xenografts. 200 µl of Paclitaxel-loaded filomicelles were administered via tail vein injection. The treatment consisted of four injections each, administered in regular intervals of 3 days. Tumor size was measured at regular intervals and the tumor area was normalized relative to the size at the onset of the treatment.

4.2.13. Statistical analyses

Unless indicated otherwise, mean and standard deviation are calculated for a minimum of n = 3 independent samples.

4.3. Results

4.3.1. Synthesis and Characterization of PEG-PCL and PEG-PBCL aggregates

For PEG-PCL (OCL) synthesis, the relative amount of polymerization initiator was adjusted such that the di-block copolymer had a PEG block with a molecular weight of 2000 g/mol and the PCL block a weight of 7500 g/mol. Molecular weights were confirmed by ^{1}H NMR, which was used to estimate the proportion of PEG to PCL. PEG-

PBCL (OBCL) was made per Molavi et al. (2008) with spectra verified by ^{1}H-NMR. The samples were run through a GPC to calculate PDI. A summary of the characterization of the two polymers has been provided in Table 4.3. Filomicelles made by the chloroform evaporation method (Rajagopalan et al., 2010) were visualized after incorporating the biocompatible PKH 26 red dye, and imaging indicated that OBCL could form just as many filomicelles (perhaps more) as OCL with some spherical micelles also present in all samples (Figure 4.1 B). Mass fraction calculations (Figure 4.1 B, right) revealed that 7% of the OBCL polymer formed spheres, whereas 21% did so for OCL. Filomicelles were obtained with high purity from the assembly of OBCL (Figures 4.2 and 4.3)

A phase diagram (Figure 4.4 A) based on estimations of core block hydrophobicity (M_{CH2}) and hydrophilic mass fraction ($f_{hydrophilic}$) per (Rajagopalan et al., 2010) suggests a filomicelle micro-phase dependence on PEG molecular weight rather than just hydrophilic fraction. Sphere micelle data for OBCL from Molavi et al. (2008) and Xiong et al. (2008) appears consistent with further observations here, and spherical micelles are consistently located to the lower right of filomicelle assemblies within this phase diagram. Filomicelles generated from either copolymer also required surprisingly similar amounts of nominal hydrophobicity (5000 - 6000 g/mol). Synthesis of more polymers will certainly be critical to verifying and clarifying these trends, but the production of these novel OBCL filomicelles with an aromatic core raised more important questions about stability and ability to incorporate an aromatic drug such as TAX.

4.3.2. PEG-PBCL filomicelles are initially stable and efficiently load TAX, which is released at low pH

The mass fraction of filomicelles in the aggregate solution at pH 7.4 and 37 $^{\circ}$C was quantified over time in order to track the degradation of filomicelles to spheres. The decay in OBCL filomicelle mass fraction was exponential with a time constant of ~ 700 hours (Figure 4.4 B). While this decay occurred at a near constant rate, OCL filomicelles exhibited a higher rate of degradation initially (time constant of 47 hours) which leveled off with time. Both polymers had similar mass fraction of filomicelles around day 25.

HPLC analysis of OBCL and OCL filomicelles loaded with TAX in parallel revealed consistently more integration of drug (by ~40%) into OBCL filomicelles (Figure 4.4 C).To quantify the time scale of drug release in different environments, dialysis release studies were conducted. Free drug was released efficiently (94%) and quickly in dialysis (time constant of 15 hours), compared to OBCL filomicelles at pH 7.4 and 5.5, which exhibited first order release time constants of 105 and 85 hours, respectively (Figure 4.5 A). Just 48% of the drug was released by 14 days in pH 7.4, whereas 71% was released at pH 5.5 in the same timeframe. In contrast, OCL filomicelles released 62% of the drug at pH 7.4 and 72% at pH 5.5 (Figure 4.5 B). Exponential decay curves fitted to the release profiles revealed time constants of 93 and 79 hours respectively. These results support the expectation that drug release will be minimal while circulating in the blood for many hours or days, and indicate that OBCL assemblies may be able to better distinguish between healthy and tumor micro-environments.

4.3.3. Incorporation of aromatic group maintains filomicelle flexibility

Filomicelle flexibility is important to persistent circulation since rigid filomicelles are rapidly cleared (Geng et al., 2007), and flexibility can be affected by core chemistry as well as molecular weight (Rajagopalan et al., 2010). By imaging filomicelles of different contour lengths, we estimated the persistence length, l_p, of OBCL filomicelles to be 6.1 μm (Figure 4.6 A). This differs only modestly from persistence lengths of filomicelles formed from PEG-PCL and PEG-PBD (Figure 4.6 B) despite major differences in PEG and core molecular weights as well as core chemistries.

4.3.4. OBCL filomicelle delivery to cancer cells suggests higher efficacy and safety

Human lung cancer derived A549 cells were incubated with free PKH dye or the same amount of total dye in PKH-labeled OBCL filomicelles for up to 72 hours, and the PKH intensity in the filomicelle-treated cells was plotted against time as (% of free PKH uptake). Spots of PKH were seen throughout the cytoplasm, with a decrease near the nucleus (Figure 4.7), and overall dye intensity in the cells increased with first order kinetics, fitting a time constant of 85 hours (Figure 4.8 A). Kinetic studies conducted with OCL filomicelles suggests a parabolic behavior, with PKH intensity peaking at 48 hours, and subsequently decaying. At low time scales (~ 4h), the intensities from internalized OCL and OBCL filomicelles (or worms) are similar, while OCL labeled worms accumulate more at intermediate length scales of 1 to 2 days, although the difference is intensities never exceed ~ 20%. At a longer length scale of 3 days, OBCL worms show highest intensity (20 % higher than cells incubated with OCL worms). The combination of release studies and uptake results suggest that TAX delivery to the cells

may be dominated by micellar uptake (in whole or parts of the worm) over molecular transfer (Lodish et al., 2000), which should lead to abnormal division, with cell death and/or aneuploidy (Figure 4.8 B).

To test the model, the efficacy of OBCL filomicelles loaded with TAX was evaluated for two different cancer cell lines: human non-small cell lung cancer (A549) and mouse liver cancer cell (EC4). A549 cells were treated with free TAX, TAX loaded OCL or TAX loaded OBCL for 3 days (Figure 4.9 A). Nano-carriers loaded with TAX appeared more potent in suppressing cell numbers than free TAX, and TAX loaded OBCL filomicelles (OBCL-TAX) were more potent than OCL filomicelles (OCL-TAX). Importantly, the extreme toxicity of OBCL-TAX filomicelles did not translate to systems without drug (Figure 4.9 B): filomicelles of OCL and OBCL formed at the same polymer concentration of 20 mg/mL showed empty OBCL were an order of magnitude less toxic than corresponding OCL, with TAX equivalent IC50s of 109 and 13 μM, respectively.

Efficacy of OBCL filomicelles against an EC4 liver cancer cell line produced similar results. Cell numbers were measured after incubations of 1, 2 or 3 days with either free TAX (Figure 4.10 A), OBCL filomicelles (OBCL-TAX, Figure 4.10 B) or OCL filomicelles (OCL-TAX, Figure 4.10 C). The latter were far more effective than free TAX, especially after just 1 day. At IC50 concentrations, cell death with TAX filomicelles was consistently higher than with free drug, although at more extreme concentrations (> 100 μM), cell death was higher with free TAX. Empty OBCL were once again non-toxic with an IC50 of 1625 μM, which is an order of magnitude less toxic than that found for the A549 cells. At all three time points (days 1, 2 or 3), OBCL-TAX worms were more potent than OCL-TAX worms. Empty OCL worms exhibited

significant toxicity compared to OBCL counterparts (IC50 ~ 6 μM), as seen previously in Figure 3B. After 3 days, the IC50 of OBCL-TAX was 3.5 fold lower than for free TAX (Figure 4.11 A), which highlights once again the efficacy of drug loaded nano-carriers. Some EC4 cells also detach and float as they die, with a small number of floating cells in untreated culture as well as cultures incubated with drug-free OBCL filomicelles (Figure 4.11 B). Consistent with the above counts of viable attached EC4 cells, OBCL-TAX filomicelles maximized this separate metric of cell death relative to free TAX in addition to being ~10-fold above control cultures.

4.3.5. TAX-filomicelles maximize and sustain aneuploidy

Histograms of DNA intensity in fixed EC4 cells stained with Hoechst are used to identify levels of ploidy induced by TAX as either free drug or drug delivered by OBCL Filomicelles (Figure 4.12). Untreated cells show two major peaks for diploid cells (2N) and replicating cells (≤ 4N), with very few cells showing higher intensity. However, treatment with TAX increases DNA intensity well beyond 4N intensity, consistent with incomplete cell division. Such aneuploidy is prominent in cells treated with free TAX and with OBCL-TAX (red curve) but not with empty nano-carriers (inset), which confirms the lack of toxicity. Due to the limited number of cells that can be analyzed under the microscope, DNA content of cells was also analyzed using flow cytometry (Figure 4.13 A). TAX filomicelles led again to the greatest aneuploidy when compared to free TAX, and aneuploidy was higher for OBCL-TAX compared to OCL-TAX, consistent with OBCL delivering more effectively than OCL (Figure 4.9 A).

Chemotherapy in the clinic typically involves a bolus injection or infusion followed by no delivery for a few days, and then repeated over several weeks, and so sustained effects of drugs are potentially important to efficacy. To measure the persistence of aneuploidy after TAX a treatment here, a rescue experiment was performed (Figure 4.13 B). After treatment (day 3), all cells showed high levels of aneuploidy, as noted previously (Figure 4.12 and 4.13 A). Aneuploidy always decreased post-treatment, and the rate of decrease of DNA content versus time was similar for all TAX treatments. However, only OBCL-TAX exhibits high aneuploidy (2-3 fold higher average DNA) at 3-4 days after an in vitro treatment.

4.3.6. OBCL filomicelles with TAX shrink tumors in vivo

Four injections of drug loaded filomicelles over two weeks resulted in a decrease in tumor size (Figure 4.14). Mice with control injections showed continued growth of tumors. Drug loaded filomicelles produced an immediate response as the tumor size shrunk 20% in 3 days, and 45% in 13 days compared to control. Tumors treated with OBCL-TAX filomicelles produced 30% shrinkage from initial size, which suggests potency greater than or equal to that of OCL-TAX filomicelles toward the same cancer cells in vivo (Figure 4.15 A). Also, despite the potential for any amphiphilic copolymer to lyse blood cells after intravenous injection, no statistically significant change in the number of any blood cells was measured with TAX-filomicelles (Figure 4.15 B). However, trends are consistent with TAX stabilization of microtubules in blood stem

cells and progenitors, thereby favoring (at the expense of other lineages) high

ploidy/aneuploidy megakaryocytes, which generate more platelets.

4.4. Discussion

Benzyl groups linked to the polycaprolactone backbone via a hydrolysable ester group

are similar to ester groups between caprolactone monomers, and so this cleavable linker

should and does ensure that filomicelles are stable at physiological pH (for example,

while circulating in the blood) while also hydrolyzing at low pH (like that found in

endolysosomes). The same method of filomicelle formation (chloroform evaporation

during hydration) was employed in this study as in our earlier studies (Rajagopalan et al.,

2010) in order to eliminate any impact on phase behavior due to processing, but it seems

likely that a separate phase diagram (Figure 4.4 A) is required for different molecular

weight PEG blocks as noted in (Rajagopalan et al., 2010). Nonetheless, spherical micelles

tend to be favored whenever the hydrophilic fraction is increased through a decrease in

hydrophobic mass, consistent with general ideas of micelle formation and with

degradation of filomicelle cores generating shorter lengths and spheres. While PEG-

PBCL samples formed filomicelles (average filomicelle length was 23 μm ± 8 μm, mean

± S.D.) which was twice as long as PEG-PCL filomicelles (Rajagopalan et al., 2010), role

of the incorporated aromatic group in extending the length of worms would benefit from

further study because of the different molecular weights of PEG blocks used in the two

polymers. Importantly, higher drug loading in PEG-PBCL filomicelles justified inclusion

of an aromatic group in the core (Figure 4.4 C) and also implied a high partition

coefficient in the core (Loverde et al., 2012). Drug release times of many days for the

filomicelles (Figure 4.4 B and 4.5 A) combined with the fact that filomicelles circulate in vivo for up to a week (Geng et al., 2007) imply minimal release before tumor accumulation. Rapid release at low pH favors not only endoslysomal escape (Varkouhi et al., 2011) (Miyata et al., 2011), but also release due to the lower pH prevailing in tumors (Lee et al., 2003) (Lee et al., 2008). The presence of a burst phase is seen typically with polymeric micelles at pH of 5 and 7 (Lim Soo et al., 2002), and was observed here as well.

Loading TAX into PEG-PBCL filomicelles reduced the IC50 by more than an order of magnitude compared to free drug for both cell lines tested here (Figure 4.9 A and 4.10 A). In addition to a two-and-a-half fold difference in IC50 between the OCL and OBCL filomicelles, empty OBCL filomicelles were an order of magnitude less toxic than OCL filomicelles (Figure 4.9 B). At high concentrations, even empty filomicelles became toxic to the cells, presumably due to disruption of the cell's lipid bilayer by these detergent-like amphiphiles (Vega-Villa et al., 2008)(Moghimi et al., 2005). Even slow degradation of the free end of the PCL block converts a cylinder-forming amphiphile to a higher curvature sphere-former that will be more disruptive to membranes (Cai et al., 2007). With free drug, cell viability decreased from day 1 to day 2, but then increased from day 2 to day 3 (Figure 4.10 A), which is perhaps due to degradation of TAX by hydrolysis (Tian et al., 2008) (Nikolic et al., 2011) that occurs over days (Richheimer et al., 1992) (Amini-Fazl et al., 2014). Nano-carrier cores can protect against such hydrolysis, with PCL cores protecting cisplatin from degradation (Surnar et al., 2015), and a protective effect might explain the decrease in cell viability with TAX-filomicelles from day 1 to 2 and day 2 to 3 (Figure 4.10 B).

A hallmark of TAX treated nuclei is higher DNA accumulation due to incomplete cell division, and a histogram of DNA intensities of treated cells revealed a majority of aneuploid cells (Figure 4.12). Moreover, cells treated with filomicelle-TAX appear in flow cytometry to have a narrower distribution of ploidy than free TAX (Figure 4.13 A), and heterogeneity in surviving cells has been thought to increase the chances of a drug-resistant cell (Marusyk and Polyak, 2010) (Brooks et al., 2015). In particular, low ploidy cells with DNA content similar to untreated cells likely unaffected by free drug. Furthermore, OBCL filomicelles not only induce more cell death than OCL, but the surviving cells exhibit a higher level of aneuploidy (Figure 4.13 B). Importantly, higher levels of polyploidy suggest a worse prognosis for affected cells (Gordon et al., 2012). All three treatment groups (free, PEG-PCL and PEG-PBCL TAX) exhibited a decrease in polyploidy, with such cells likely dying after drug was washed away, but even after three days of recovery, PEG-PBCL treated cells showed the highest levels of polyploidy, suggesting that TAX loading onto PEG-PBCL filomicelles might be a more durable or potent treatment.

Initial in vivo tests showed that PEG-PBCL filomicelles shrunk tumors in vivo in mice with A549 xenografts (Figure 4.14 and 4.15 A). While saline-injected controls grew consistently here and past studies already showed no effects of empty filomicelles, tumors treated with TAX loaded PEG-PBCL filomicelles (injected at 4.5 mg/kg) shrank by 25% or more in two weeks. For comparison, mice treated with TAX loaded PEG-PCL filomicelles at 4-fold higher dose (18 mg/kg) show tumor shrinkage for the first week but then a constant tumor size (Christian et al., 2009), and mice treated with free TAX at the maximum dose of 1 mg/kg exhibit only a small tumor shrinkage initially, before re-

growing, consistent with resistance and relapse. Also noteworthy was that PEG-PCL

spheres injected at 8 mg/kg produced tumor shrinkage for the first week (Christian et al.,

2009), as with PEG-PCL filomicelles, and then tumors re-grew. Continuous shrinkage

obtained with PEG-PBCL suggests a more durable or potent treatment without significant

change in hematocrit, thrombocrit, or monocyte counts in treated mice (Figure 4.15 B),

consistent with low toxicity of PEG-PBCL filomicelles.
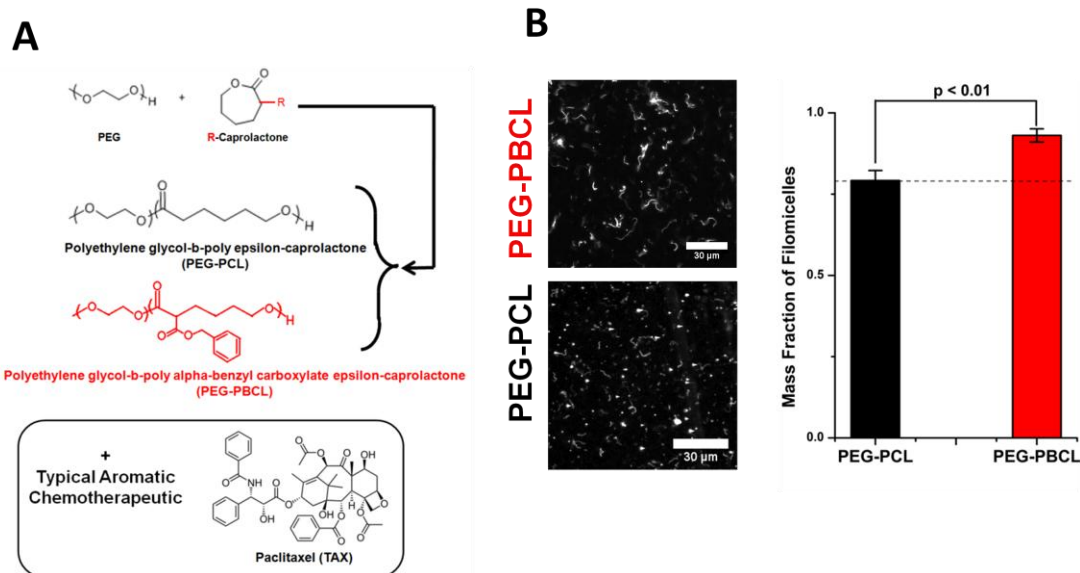
Figure 4.1. Filomicelles from different polymers **A)** PEG reacts with ε- Caprolactone (which can be functionalized with a group, R, at the alpha carbon) to form PEG-PCL (black) or PEG-PBCL (red) polymer. The aromatic group in PEG-PBCL may help load more aromatic chemotherapeutics, such as Paclitaxel. **B)** 60 x magnification images of filomicelles formed from PEG-PBCL (top left) and PEG-PCL (top right). Scale bars are 30 μm. Assemblies from the former had a higher purity of filomicelles than the latter. Quantification of mass fraction of filomicelles in aggregates (right), revealed a higher filomicelle mass fraction of filomicelles in PEG-PBCL sample (93%) than PEG-PCL (79%). The rest were spheres.
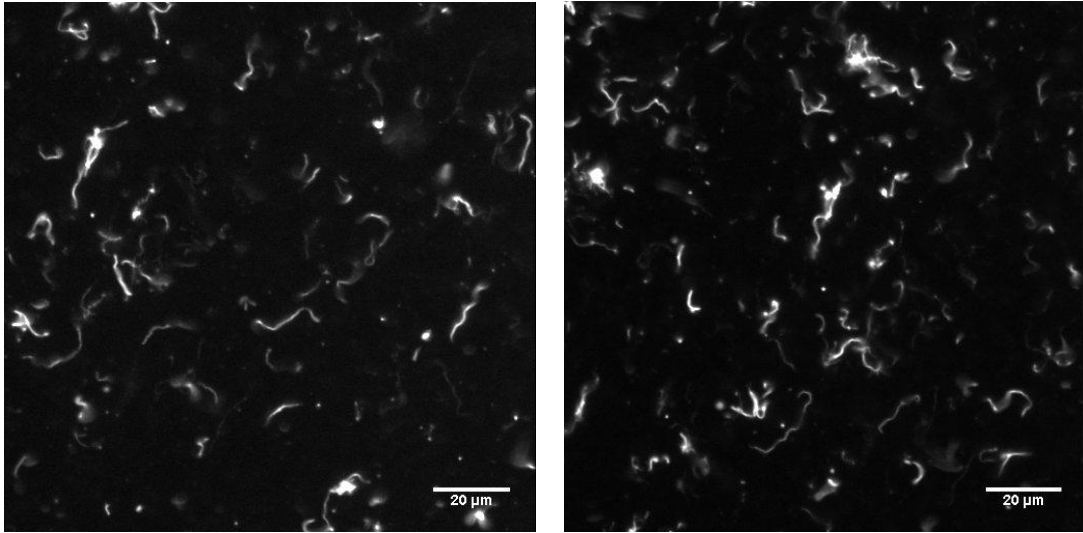
Figure 4.2. 60x magnification image of OBCL filomicelles labeled with PKH26.
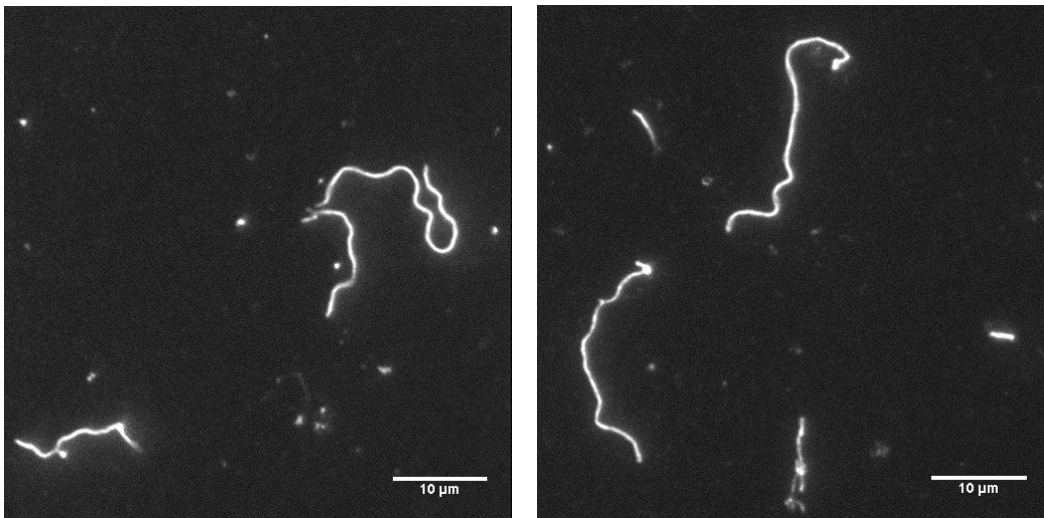
Figure 4.3. 150x magnification image of OBCL filomicelles labeled with PKH26.
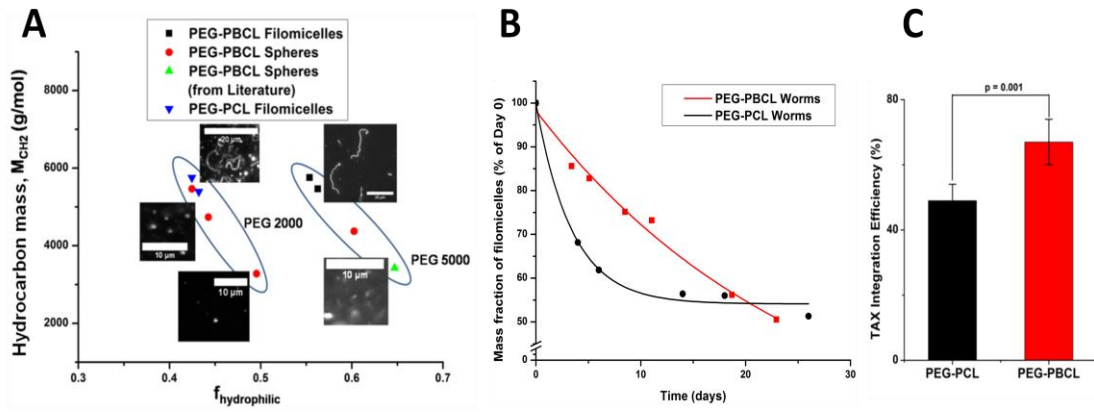
Figure 4.4. A) Phase diagram of assemblies from PEG-PBCL formed by solvent evaporation method. As with PEG-PCL, filomicelles from PEG-PBCL occupy a narrow region, with possibly different regions corresponding to the weight of the hydrophilic block. Filomicelle scale bars are 20 μm, while spherical micelle scale bars are 10 μm. **B)** Degradation of mass fraction of filomicelles with time. Rate of degradation is higher for PEG-PCL worms initially, while it remains nearly constant for PEG-PBCL. The mass fraction of worms from the two polymers becomes similar around day 25. The time scale of degradation suggests that all aggregates will be taken up by the cell as filomicelles, and not as spheres, as filomicelles circulate for roughly 8 days. **C)** Higher Paclitaxel loading capacity of PEG-PBCL vs. PEG-PCL. Integration efficiency of PEG-PBCL was 40% higher than filomicelles from PEG-PCL with an aliphatic core.
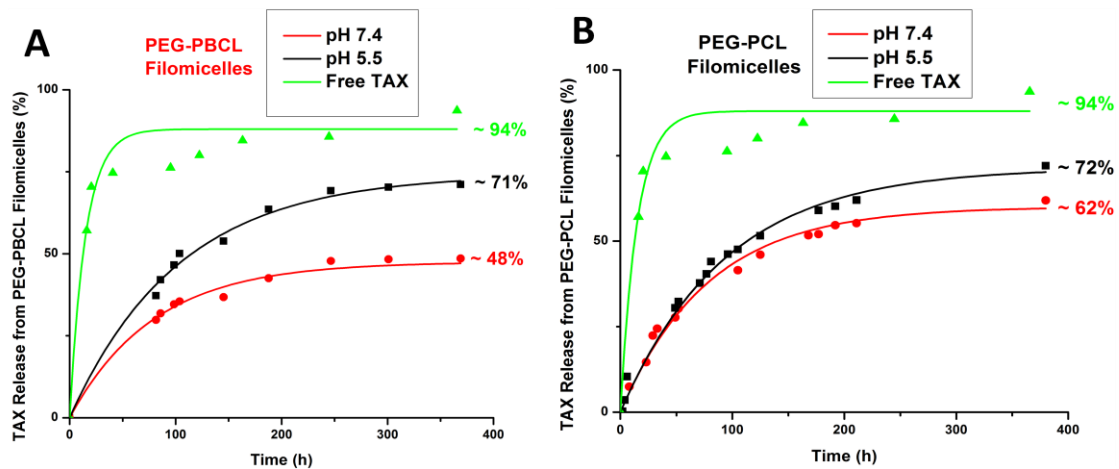
Figure 4.5. Release studies performed with PEG-PBCL and PEG-PCL filomicelles at different pH as well as free drug. The rate of release from PEG-PBCL filomicelles at pH 7.4 was much slower than that of free drug, indicating little leakage while in circulation. PEG-PCL worms in had higher drug release at the same pH. Rapid and similar release profiles at pH 5.5 for both polymers hint at rapid release after lysosomal degradation.
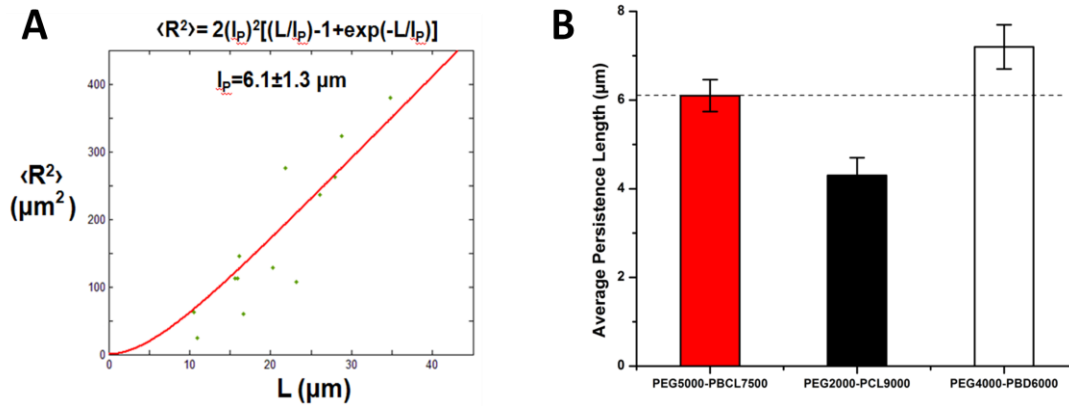
Figure 4.6. A) Model fitting during the calculation of persistence length of PEG-PBCL filomicelles. **B)** While the persistence length of PEG-PBCL is higher than that of PEG-PCL, it is lower than PEG-PBD (also proven to form flexible filomicelles).
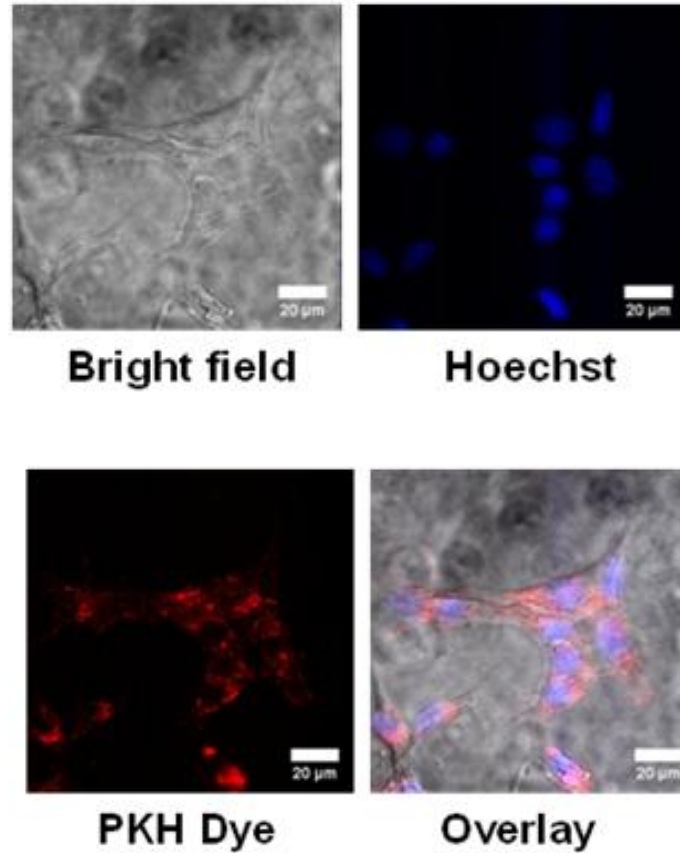
Figure 4.7. PKH, Hoechst and bright field images of cells incubated with PKH labeled filomicelles. Cytoplasmic spots of the dye after filomicelle uptake by EC4 cells can be seen after incubation for one day. Scale bars are 20 μm.
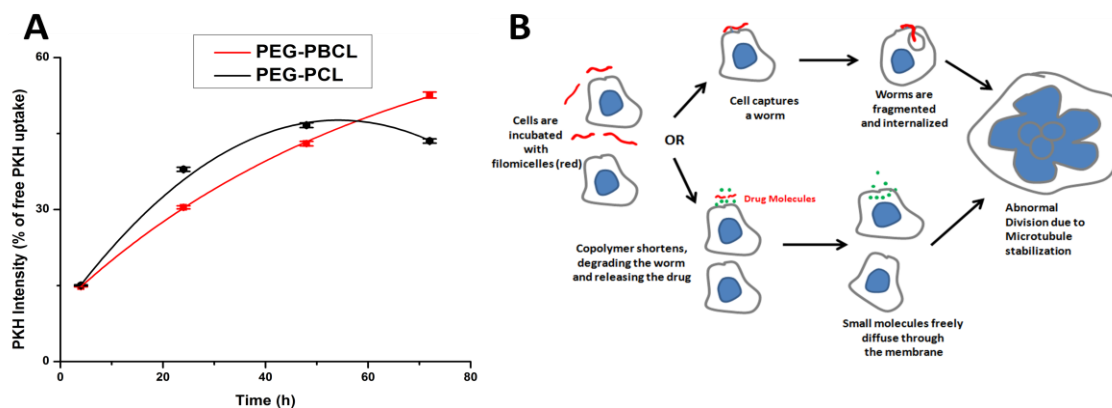
Figure 4.8. A) Quantification of PKH intensity within a cell after incubation with dye labeled filomicelles. The intensity recorded increases exponentially with time for PEG-PBCL, while it is parabolic for PEG-PCL worms. PEG-PCL worms have higher accumulation initially, but are surpassed by PEG-PBCL on day 3. **B)** Cartoon depicting the uptake of filomicelles by cells. Cells, when incubated with filomicelles, come in contact with and capture them. The cell may then proceed to chew off a part of the filomicelle. Alternatively, the constituent di-block copolymers may undergo hydrolysis leading to its shortening. The corresponding phase transition of filomicelles to spheres destabilizes the filomicelles, leading to release of the encapsulated drugs. These small molecules are then taken up by the cell.
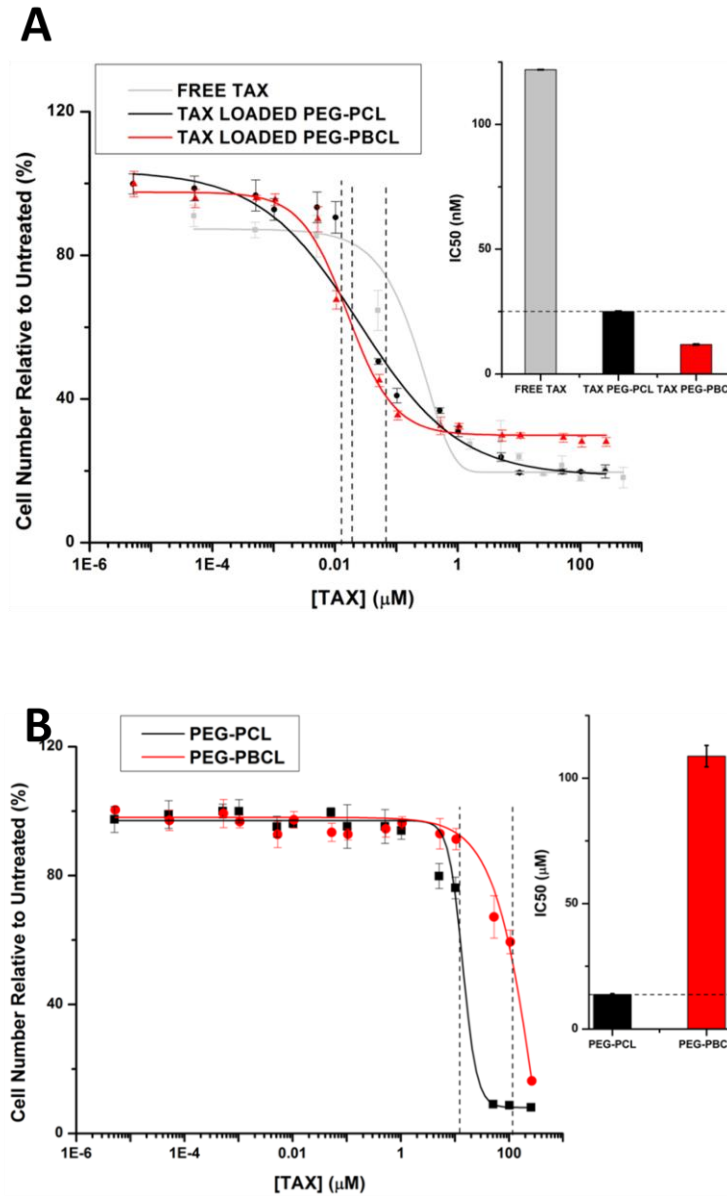
Figure 4.9. A) Effects of drug loaded micelles can be applied across various cell types. Cell viability of A549 (epithelial lung cancer) cells treated with free and polymer-loaded drugs reveal a clear advantage of loaded formulation over free drug (IC50 bar graph inset). **B)** Inertness of nano carrier (no effect of empty carriers on viability).
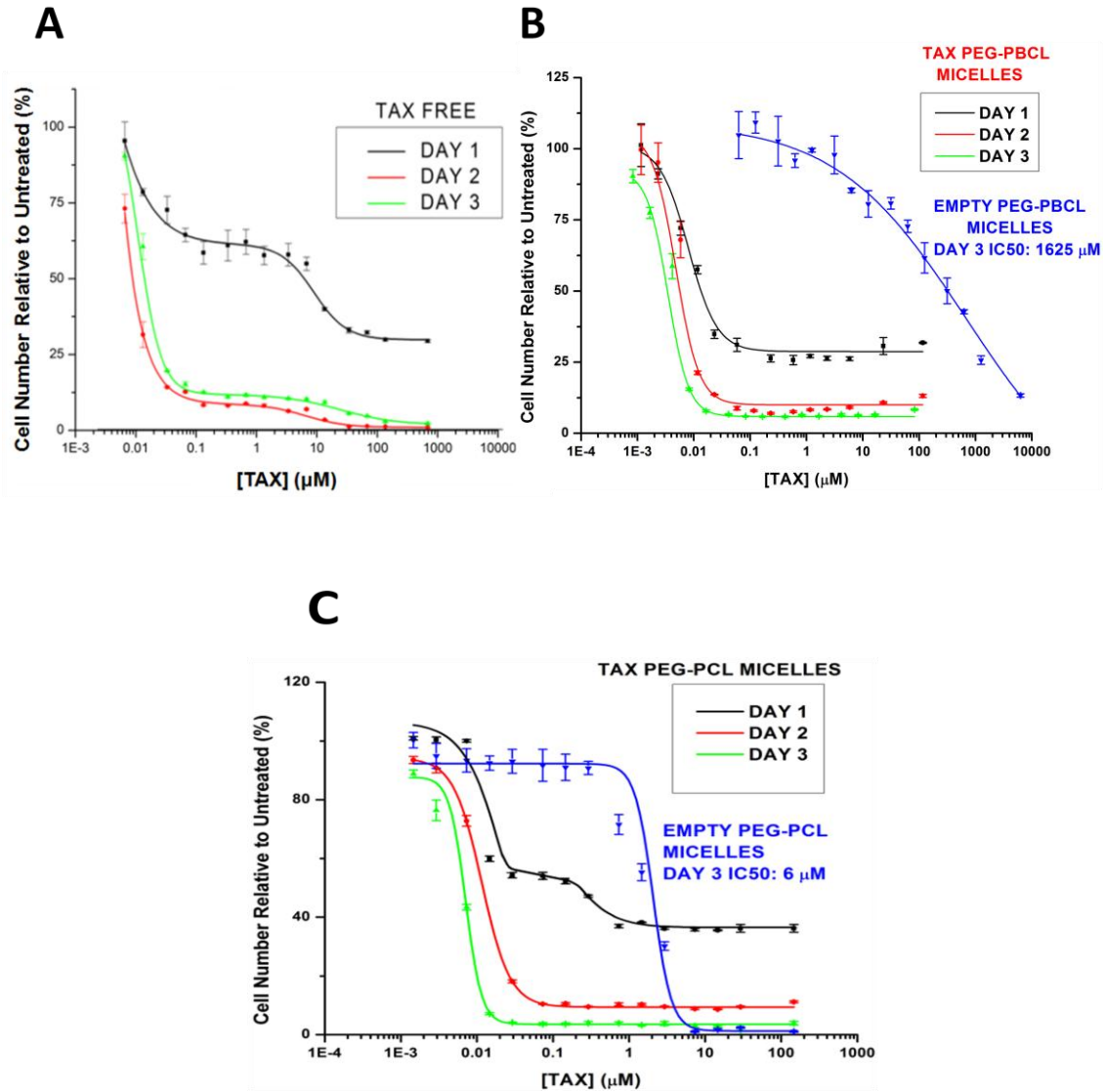
Figure 4.10. EC4 cell viability kinetics with free TAX, PEG-PBCL TAX and PEG-PCL
TAX respectively. While both free and encapsulated drugs show similar effects, cell
viability of free drug at day 3 is higher than that for day 2, presumably due to degradation
of free drug in the presence of water. Encapsulated drug is protected from hydrolysis,
which is supported by consistently decreasing viability with time. At all three time points
(Days 1, 2 or 3), the IC50 of TAX loaded PEG-PBCL worms were lower than that of
corresponding PEG-PCL worms. Empty PEG-PBCL micelles, were inert (IC50 >1500

μM). However, PEG-PCL worms exhibited significant toxicity (IC50 ~ 6 μM), as seen

previously in Figure 3B.
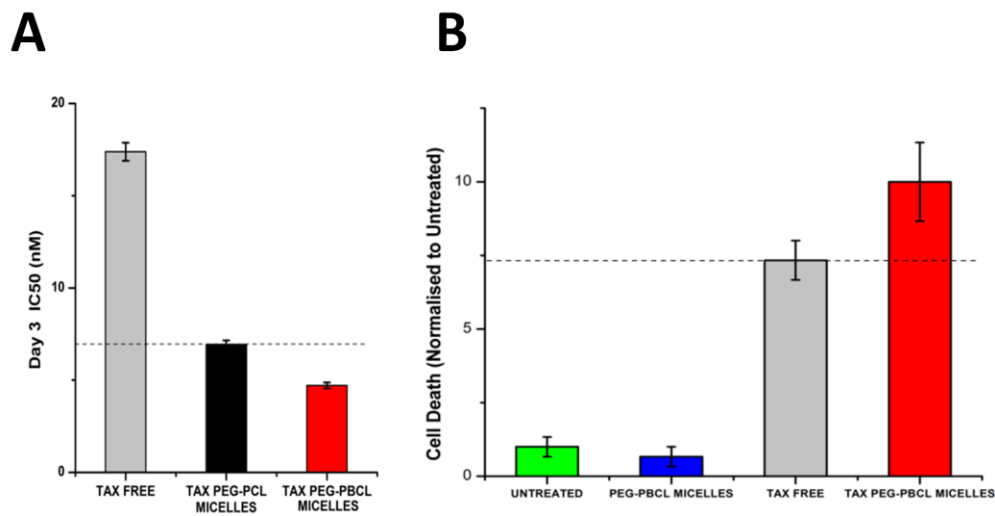
Figure 4.11. A) Bar graph representation of the IC50 values of different formulations after 3 days. Less concentration of Paclitaxel is required to induce cell death in encapsulated form than in free form, with TAX PEG-PBCL micelles being three times more potent than free drug, and 1.5 times more potent than TAX loaded PEG-PCL worms. **B)** Treatment with TAX leads to a higher number of floating cells that don't stain negative with trypan blue, indicating cell death. Cell death is minimum with untreated cells or ones incubated with empty filomicelles. Free as well as encapsulated TAX induces significant cell death, with loading on to micelles inducing forty percent more cell death.
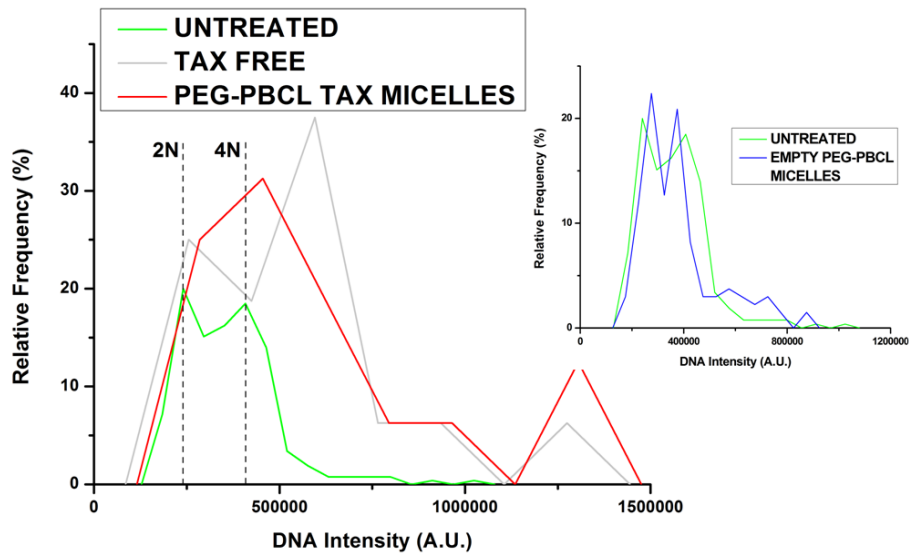
Figure 4.12. Quantification of Hoechst intensity per cell and plotting the corresponding histogram reveals aneuploidy present in TAX treated nuclei. Untreated cells reveal that a significant portion of the cells in replicating phase (labeled 4N), and rest in diploid state (2N). However, post treatment with TAX, most cells exhibit aneuploidy (i.e. number of chromosomes greater than 4N). This effect is further enhanced by encapsulating TAX in filomicelles. Empty nano-carriers do not produce an appreciable change in this distribution.
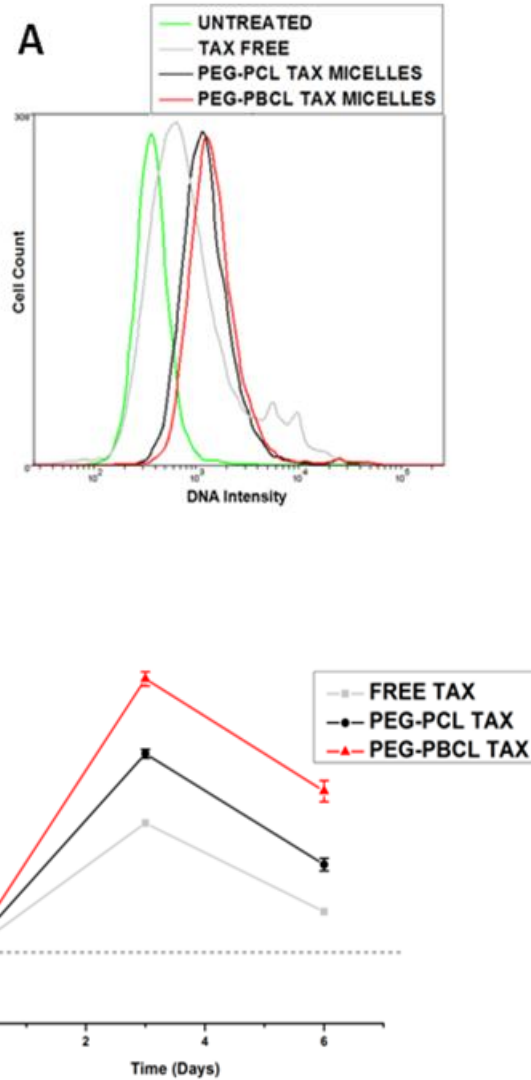
Figure 4.13. A) Quantification of aneuploidy by flow cytometry shows similar results to IF (Figure 4.12). **B)** Recovery of diploidy by EC4 cells post induction of aneuploidy after TAX treatment. Nano-carrier loaded TAX induce more aneuploidy after treatment (day 3), and still has more DNA content after 3 days of recovery.
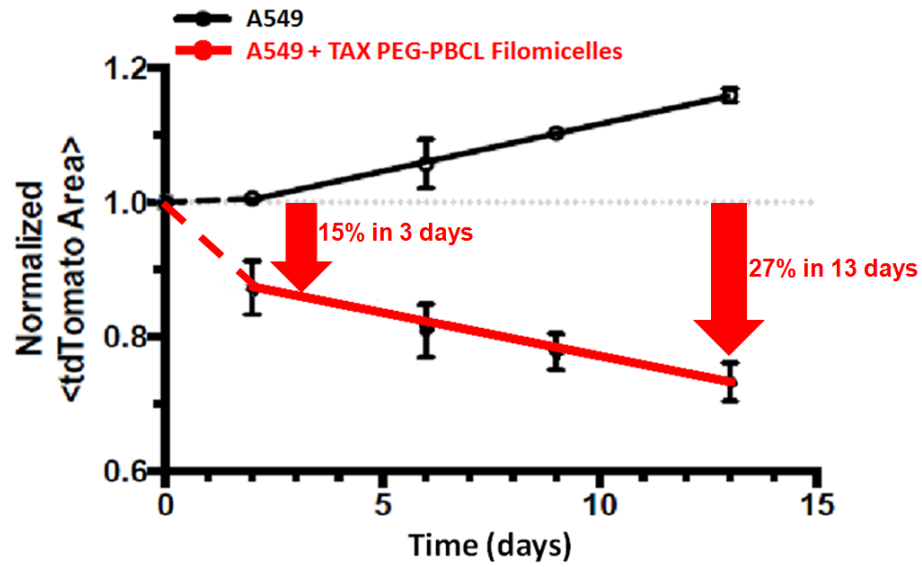
Figure 4.14. *In vivo* tumor shrinkage obtained in NOD-SCID mice with tumors established from A549 lung cancer cell line. 4 injections of PEG-PBCL filomicelles loaded with TAX were given, with each dose 3 days apart. Tumors treated with drug loaded PEG-PBCL filomicelles shrink 27% in volume from initial size after 13 days, while the untreated control grows by 15%.
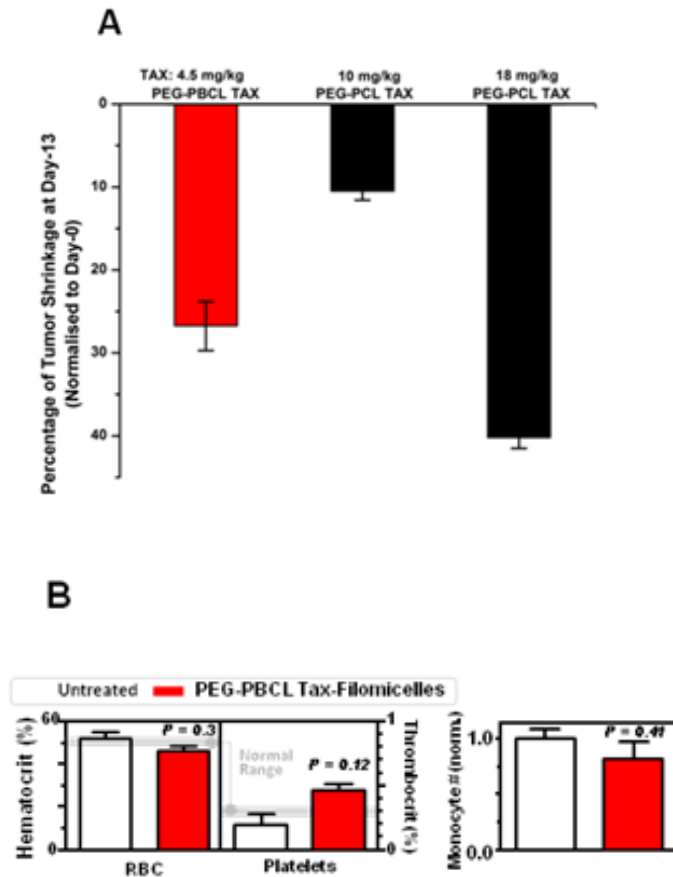
Figure 4.15 A) Comparison of tumor shrinkage obtained after 13 days of treatment.
While PEG-PBCL loaded filomicelles led to lower tumor shrinkage than PEG-PCL
counterparts, the TAX dosage was one-fourth of the latter. OCL-TAX at 10 mg/kg could
not produce sustained shrinkage, and consequently, the final tumor size was not much
smaller than initial size. OCL data from Christian et al., 2009. **B)** Mice treated with PEG-
PBCL filomicelles loaded with TAX did not exhibit adverse change in thrombocrit,
hematocrit or monocyte numbers. The changes were not significant in all three cases,
thus underlining the ability of these filomicelles to safely deliver drug to the tumors

Table 4.1: Quantities of reactants used in the synthesis of PEG_{2000}-PCL_{7500}.

Chemical	Polyethylene Glycol	ε-Caprolactone	Stannous Octanoate	PEG_{2000}-PCL_{7500}
mmol	0.27	17.53	0.04	0.27
Mass (mg)	533	2000	16	2550
Molecular Weight	2000	114.1	405.1	9500
Density (g/ml)	-	1.03	1.25	-
Volume (µl)	-	2000	13	-

Table 4.2: Quantities of reactants used in the synthesis of PEG_{5000}-$PBCL_{7500}$.

Chemical	Polyethylene Glycol	α-benzyl carboxylate ε-Caprolactone	Stannous Octanoate	PEG_{2000}-PCL_{7500}
Mmol	0.16	4.84	0.24	0.16
Mass (mg)	800	1200	96	2100
Molecular Weight	5000	248	405.1	12500
Density (g/ml)	-	1.03	1.25	-
Volume (μl)	-	2000	77	-

Table 4.3: Characterization of polymers utilized to form filomicelles.

Polymer Composition		Number Average Molecular Weight (M_n)(g/mol)	Weight Average Molecular Weight (M_w) (g/mol)	Polydispersity Index (PDI)
Block Molecular Weights	Block Repeating Units			
PEG_{2000}-PCL_{7500}	PEG_{45}-PCL_{66}	9799	15438	1.575
PEG_{5000}-$PBCL_{7500}$	PEG_{114}-$PBCL_{30}$	12533	25166	2.008

CHAPTER 5. RETINOIC ACID DELIVERY BY FILOMICELLES REDUCES PROLIFERATION AND DRIVES DIFFERENTIATION OF MURINE HEPATOCELLULAR CARCINOMA CELLS

(This chapter is a part of the manuscript being prepared for submission: Nair, P. R., Alvey C., Jin X., and Discher, D. E. Filomicelles deliver a chemo-differentiative therapy to durably control carcinoma cell fate)

5.1. Retinoic Acid

5.1.1 Synthesis of RA from retinol

Retinoic acid (RA) is a small lipophilic molecule derived from Vitamin A or retinol (Figure 5.1 A). The chief sources of intake are carotinoids and retinyl esters which are oxidized for the production of RA in the liver, spleen and bone marrow. Upon release into circulation, retinol is bound by retinol binding protein (RBP), which allows it to enter cells via a receptor mediated interaction. Once it enters the cell, retinol binds to cellular retinol binding protein (CRBP) (Lawson and Berliner, 1999). This complex is the substrate for future dehydrogenase catalyzed oxidations, resulting in retinal which is still complexed to CRBP. Retinal is then oxidized by retinal dehydrogenase to All Trans RA which is still complexed to CRBP. RA can then be further degraded to 4-oxo-retinoic acid after binding to cytochrome p450. RA can induce changes in the cell, or act in a paracrine manner after exiting the cell. Serum concentration of RA varies between 10 nM

and 100 nM (De Ruyter et al., 1979). While in the cell, RA is often bound to cellular

retinoic acid binding protein (CRABP).

5.1.2 Retinoic Acid Receptors

 RA can enter the nucleus and bind retinoic acid receptors (RARs) to modulate gene

expression. RARs belong to a superfamily of receptors including thyroid and estrogen

receptors. RARs possess ligand (RA) binding, activation, repression, DNA binding and

dimerization domains. RARs are further classified into three subtypes: α, β, and γ. There

are eight types of RARs in total (RARα1, RARα2, RARβ1, RARβ2, RARβ3, RARβ4,

RARγ1, and RARγ2). The general structure of RARs is depicted in Figure 5.1 A. The N

terminus (sections A and B) contain domains that can transactivate RAR isoforms.

Region C contains zinc finger motifs used in sequence recognition and DNA binding.

Region E contains the ligand binding domain, which can co-operate with region A/B.

This section is highly conserved. Regions D and F play a key role in the dissociation and

association of co-repressors upon binding by RA, and are located close to the C terminus.

RAR functioning involves the formation of heterodimers with Retinoid X receptor (RXR)

(Figure 5.1 C) (Theodosiou et al., 2010) (Mark et al., 2006) (Leid et al., 1992). At high

concentrations, RARs can homodimerize, but RAR-RXR heterodimers bind DNA with

higher affinity. RXRs also exist in 3 isoforms and have a similar structure to RARs. They

can be activated by binding to 9-cis retinoic acid. RXRs are a lot more promiscuous than

RARs and possess many more binding partners such as vitamin D receptor (VDR),

thyroid hormone receptor (TR), and peroxisome proliferator activator receptor (PPAR), along with orphan receptors.

RA target genes possess sections called Retinoic Acid Response Elements (RAREs) within their promoter regions which are bound by RAR-RXR heterodimers. They recognize and bind repeats of PuGGTCA (where Pu is purine residue: A or G). The binding to DNA is mediated by region C which contains the zinc finger domain. Knockout mice lacking isoforms of RAR have normal phenotype. However, mice with knockouts of RARα and RARγ exhibit mostly immature cells that do not progress past the myelocyte stage, further highlighting the role of retinoid signaling in driving differentiation.

5.1.3 Repression and activation of genes

When the RAR-RXR heterodimer is not bound to its ligand, it is bound by co-repressors such as NCoR1 and NCoR2 (also known as SMRT). Upon binding to its ligand the receptor jettisons the co-repressors (like SMRT) and undergoes a change in conformation. Mutations in region F makes RARs less sensitive to RA and unable to transactivate the target promoter. These mutants exhibit a constant association to SMRT, which associated with RARs at the carboxy terminal. SMRT can also interact with PPAR in a similar way. The interaction of RARs with SMRT varies with subtype, and RARα and RARγ interact with SMRT, while RARβ does not. When bound to its repressor, SMRT may recruit histone deacetylase 1 (HDAC1), which deacetylates histones and

leads to a closed chromatin structure inaccessible to transcription machinery. Unliganded RARs are also more susceptible to cleavage by endopeptidases compared to ligand bound receptors since ligand binding produces a change in conformation (Lin et al., 1998).

Similar to co-repressors, RARs and RXRs can also bind to co-activators such as SRC-1. RARs form a ternary complex with SRC-1 and CBP, both of whom have intrinsic histone acetyl transferase (HAT) activity, and can open up closed chromatin configurations. Additionally, CBP can acetylate subunits of Transcription Factor II E which can increase transcriptional activity. CBP can also recruit RNA polymerase II after CBP binding to phosphorylated CREB.

The regulation of accessibility of transcription machinery by modulating chromatin structures via co-repressors and activators of RARs explains how RA exerts its effects. When unbound to RA, RAR-RXR heterodimer is associated with HDACs leading to closed chromatin conformation. Upon binding to ligands, RARs undergo a change in conformation and associated with co-activators instead that acetylate histones and open up the chromatin.

5.1.4 RA target genes

RA target genes are classified based on their time of induction as early genes or cooperative response genes (Figure 5.1 D). Early genes are transcribed quickly, while

cooperate genes do not despite possibly possessing RAREs. C/EBP and p47-phox are examples of the former, while p21 and lactoferrin are examples of the latter. Both sets of genes include signaling factors that lead to activation of secondary response genes, along with factors required for differentiation (Wu et al., 2000).

C/EBP plays an important role in neutrophil maturation, adipogenesis, and liver homeostasis. It is an early induction gene, and the addition of RA lead to induction of C/EBP transcripts one hour after incubation. p21 is another protein that is involved in differentiation and regulated by RA. It is a late induced gene and arrests proliferation by inhibiting the function of CDKs. p21 gene has a Vitamin D response element (VDRE) which has been shown to bind VDR-RXR heterodimers as well as a RARE in its promoter, making it responsive to RA. Treatment with RA leads to an increase in p21 transcripts and a decrease in Cdk2 activity. Signaling pathways downregulated by RA treatment include those involved in stem cell differentiation, such as the Polycomb EZH2 network and Wnt signaling (Ginestier et al., 2009). This suggests that RA treatment may play a role in addressing chemotherapy resistance mediated by CSCs. The Akt/β-catenin pathway, which plays a critical role in proliferation and CSC self-renewal, was also downregulated after RA treatment.

5.1.5. Retinoic Acid signaling in cancer

RA can induce differentiation and arrest proliferation in cells making it potentially useful drug against cancer cells, particularly cancer stem cells (Connolly et al., 2013). RA has

been implicated in several chemo-preventive roles e.g. the RARs have been observed to be silenced in cancer cells (Virmani et al., 2000). Additionally, RA pathway transcriptionally regulates the levels of nuclear lamins (specifically Lamin A) (Swift et al., 2013) that control nuclear softness, and hence affects 3-D migration of cells (Harada et al., 2014). RA is known to induce differentiation in undifferentiated cells (including liver cells) (Huang et al., 2009) (Breitman et al., 1980), as well as to reduce proliferation of cells by arresting the cell cycle in the G1 phase (Collins, 1987) (Zhu et al., 1997).

5.1.6. Retinoic Acid in liver tumorigenesis

Another key reason behind the use of RA in our treatment is its central role in liver function, with lower levels causing and correlating with liver diseases such as Non Alcoholic Fatty Liver Disease (NAFLD) (Liu et al., 2015)(Kim et al., 2014) and fibrosis (Lee et al., 2015). RA is synthesized in the liver by oxidation of Vitamin A and is stored in fat droplets by the Hepatic Stellate Cells (HSCs) also in the liver (Blaner et al., 2009). During the development of hepatocellular carcinoma, HSCs lose RA (Shiota et al., 2005), leading to de-differentiation and increased proliferation. Thus, restoring RA levels to these cells in order to drive differentiation and arrest their proliferation is an especially attractive prospect (Sell, 2004). The central role of retinoids in regulating proliferation and driving differentiation make this a promising approach to deal with cancer stem cells. However, RA binds to serum albumin (Avis et al., 1995) for wider distribution, which might necessitate nanocarrier delivery. Based on our previous observation (Nair et al., 2016), encapsulation in the core of filomicelles might help shield RA from complexation and facilitate better delivery.

5.2. Materials and Methods

5.2.1. Materials

Retinoic acid was purchased from Sigma Aldrich Corp., St. Louis, Missouri, unless stated otherwise. FBS, penicillin-streptomycin, non-essential amino acids, MTT assay and Hoechst 33342 were purchased from Invitrogen. High glucose DMEM growth media was purchased from Corning. Lamin-A and Lamin-B antibodies were purchased from Cell Signaling.

5.2.2. Synthesis of PEG-PCL and characterization of aggregates

Polyethyleneglycol (PEG) -Polycaprolactone (PCL) di-block copolymer was prepared as described previously (Nair et. al., 2016). Briefly, the diblock copolymer was prepared by the ring-opening polymerization of ε- caprolactone using PEG_{2000} as macro-initiator at 140 ^oC in the presence of stannous octoate as catalyst. The polymer was characterized by ^1H NMR spectroscopy and Gel Permeation Chromatography (GPC). Aggregates were formed in water by solvent evaporation as described in Nair et. al., 2016. Filomicelles were incubated with PKH 26 dye and imaged at 567 nm using aggregates were mixed with PKH 26 hydrophobic red dye with emission spectra at a wavelength of 567 nm using an Olympus IX71 microscope. RA was loaded similar to before, and the loading was measured as described previously (Nair et. al., 2016).

5.2.3. Cell culture

EC4 mouse liver cancer cell line was cultured with DMEM High glucose growth media (4.5 g/L glucose with L-glutamine and sodium pyruvate) supplemented with 10% FBS, 1% penicillin-streptomycin and 1% non-essential amino acids at 37 ^{o}C and 5% CO_2. When the flasks were confluent, the cells were passaged by dissociation with 0.05 % Trypsin-EDTA (Invitrogen) and re-plated with fresh media at a density of 10%.

5.2.4. In vitro cell viability assay

Procedure for in vitro cytotoxicity assay was adapted from Cai et al., 2007. Briefly, 5000 cells were seeded in 96-well plates and treated with (different drug concentrations) the next day. Post three day incubation, the media was aspirated cells were incubated with media and MTT solution (5 mg/mL in PBS) for 3 hours. The MTT formazan crystals were dissolved in DMSO, and absorbance was measured at 550 nm. Additional cell death quantification was done by counting the number of floating cells staining positive for staining positive for Trypan Blue stain.

5.2.5. Cell fixing and immunofluorescence

Cells in 6-well plates were treated with drugs as indicated above. After the desired time-point, cells were fixed using 4% paraformaldehyde for 10 minutes followed by 3 PBS washes. Then, they were permeabilized with 0.5% Triton-X for 10 minutes, followed by 3 PBS washes. After 30 minutes of blocking with 5% BSA, the cells were incubated overnight with the primary antibody at 4 ^{o}C. The next day, the cells were incubated with

secondary antibody at room temperature for 1.5 hours and then washed 3 times with PBS. The cells were then stained with Hoechst 33342 solution (0.01% of 10mg/mL solution in water) for 10 minutes, followed by 3 more washes with PBS. The cells were fixed again and stored in PBS at 4 °C. The stained cells were visualized under an Olympus IX71 microscope with a 300W Xenon lamp using 40x objective (0.60 NA). Images were analyzed by ImageJ software.

5.2.6. Curve fitting and statistical analyses

All curve fitting and data analysis was performed with OriginPro 8 software. Unless indicated otherwise, mean and standard deviation are calculated for a minimum of n = 3 independent samples.

5.3. Results and discussion

The influence of RA on cell proliferation and differentiation revealed that free RA as well RA loaded worms arrested proliferation in cells (Figure 5.2). RA loaded micelles (red curve) dip at lower concentration than free RA (black curve). Quantification of IC50 reveals that RA worms are 200 times more potent than free RA (bar graph inset), possibly due to the encapsulated RA being protected from albumin complexation. Empty micelles are inert at physiological concentrations, with cell numbers close to that for untreated cell numbers (represented by the empty green triangle). Kinetics of cell numbers treated with free and encapsulated RA shows that free RA requires 3 days for the anti-proliferative effects to show (Figure 5.3). Cell numbers with free RA at 50 μM is the same irrespective

of treatment time (1, 2, or 3 days) and might point to increasing cell death at these high concentrations. However, encapsulated RA is more successful at stopping cell growth at physiologically relevant concentrations (~1 µM).

Arrested proliferation is reflected by a decrease in average DNA content per cell. Average intensity decreases monotonically with increasing concentrations of RA (Figure 5.4). RA loaded onto worms (red circle) were an order of magnitude more effective than that administered in free. DNA histograms after treatment with free RA show a suppression of the replicating peak (labeled 4N) (Figure 5.5). Lower number of cells with twice the DNA content leads to a decrease in average DNA intensity seen previously. While, the suppression level did not correlate with RA concentrations, RA-loaded worms suppressed the proliferating fraction more, consistent with a lower DNA content per cell seen in Figure 5.4. The effect of RA worms can be attributed to the drug alone as empty worms do not appreciably alter the DNA histogram (Figure 5.5 B, inset).

Back-calculation from cell numbers permits the estimation of percentage of cells differentiated (Figure 5.6). Differentiation follows a hill curve and reaches near maximum values after day 2, as was reflected with cell number kinetics. The monotonous increase in cell number after treatment with RA is consistent with RA not killing cells, just differentiating them. Back-calculation from the cell number data puts the proliferating fraction at ~5 % (Figure 5.6). However, it must be noted that these are binary state calculations, where the cell is assumed to either differentiate or be

unaffected. In reality, the cells would individually exhibit a wide range of division times that is extremely challenging to track with a collection of cells.

RA-induced differentiation, was also assessed through changes in levels of Lamin-A. RA initially decreases levels of Lamin-A which then rise (Figure 5.7 A). Untreated nuclei (left) are rounded with uniform Lamin-A distribution on the edges. When treated with 10 μM RA in free form, the nuclei become more elongated (right) with patchy Lamin-A distribution. Nuclear aspect ratio increases monotonously with higher concentration of RA and eventually plateaus (Figure 5.7 B), and the trend fits a hyperbolic curve well. Nuclear surface area and volume follow similar trend to Lamin-A (Figure 5.8 A and C respectively). Lamin-A levels normalized to either surface area or volume (Figure 5.8 B and D respectively) increase linearly with RA concentration. In all plots, RA in worms was an order of magnitude more effective than free drug.

To purpose behind these calculations was to estimate how much of the change in Lamin-A levels could be attributed to change in nuclear morphology. Since Lamin-A forms a meshwork at the periphery of the nucleus (Shimi et al., 2015) (Gruenbaum and Medalia, 2015), we normalized levels of the protein to the nuclear surface area (Figure 5.8 B). In order to account for the decreased DNA content (which could possibly lead to lower amount of transcripts), Lamin-A was normalized to volume as well (Figure 5.8 D). Both of these quantities scaled linearly with RA concentration, indicating that the change in

Lamin-A levels cannot be explained entirely by changing nuclear geometry, consistent with RA transcriptionally altering levels of the protein.

Finally, scatter plots of Lamin-A, Lamin-B, and DNA were plotted to figure out the trend with increasing nuclear area (Figure 5.9). All three increase linearly with increasing nuclear area, but the slope changes with treatment condition. Similar linear trends were obtained after plotting scatter plots of Lamin-A and Lamin-B vs. DNA content (Figure 5.10). Ratio of Lamin-A to B was found to be constant for a given treatment condition (Figure 5.10 C), but was found to vary with different concentrations of RA.

A

ATRA   Vitamin A

B

A/B   C   D   E   F   RAR

C

RA loaded worms

● : Retinoic Acid

RXR RAR
RARE   DNA

Transcription Factors (e.g.HoxA1, C/EBP)

Arrests proliferation, Induces differentiation, Changes nuclear morphology

Cells that do not take up RA continue to divide
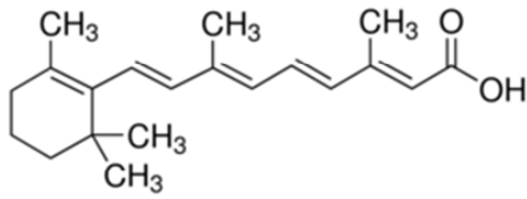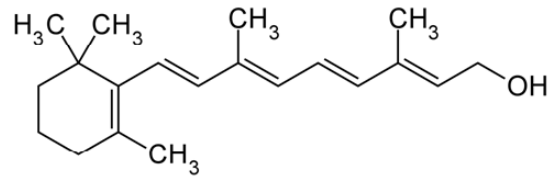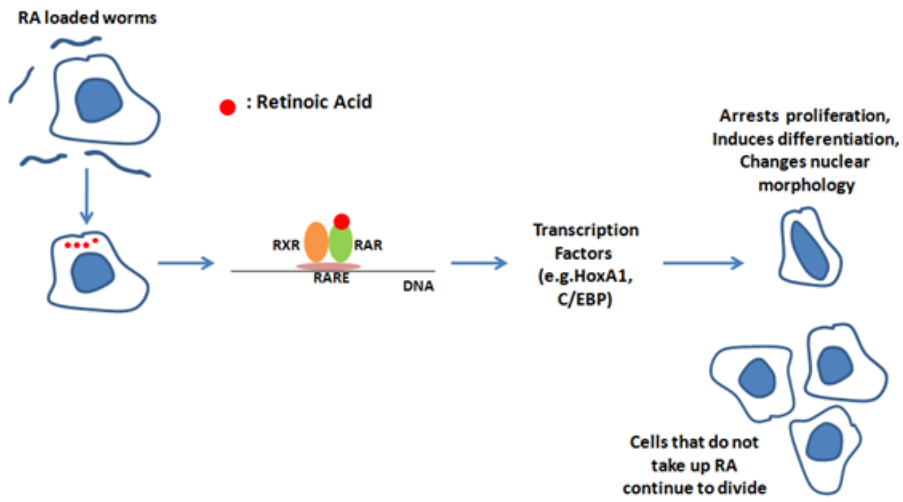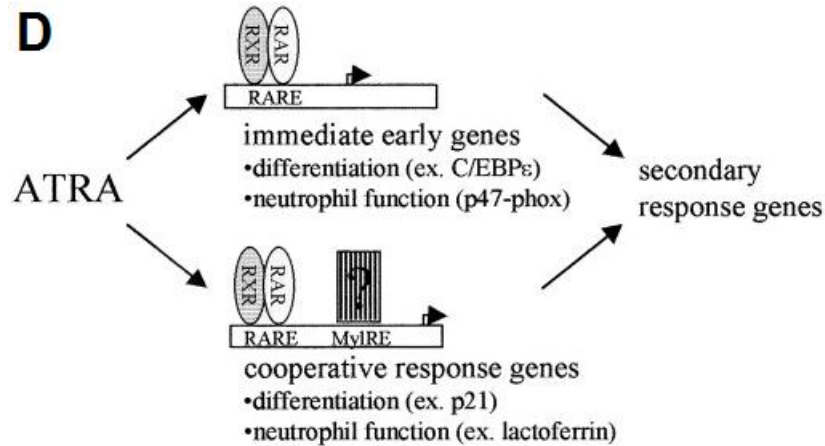
Figure 5.1. A) Structures of All trans retinoic acid (ATRA or RA), vitamin A (or retinol)

B) General structure of retinoic acid receptors. Reference: Lawson and Berliner, 1999 **C)**

Cartoon depicting effect of RA on cells. Once internalized, the worms release RA, which

binds to Retinoic Acid Receptors (RARs). The activated RARs heterodimerize with

RXRs, which in turn binds to Retinoic Acid Response Elements (RARE). This leads to

the synthesis of transcription factors (primary and secondary), ultimately leading to

proliferation arrest, differentiation and altered nuclear morphology **D)** RA binds to RAR-

RXR heterodimers that bind to RAREs. The timing of response allows the genes to be

split into two categories: early genes and cooperative response genes. Reference: Lawson

and Berliner, 1999
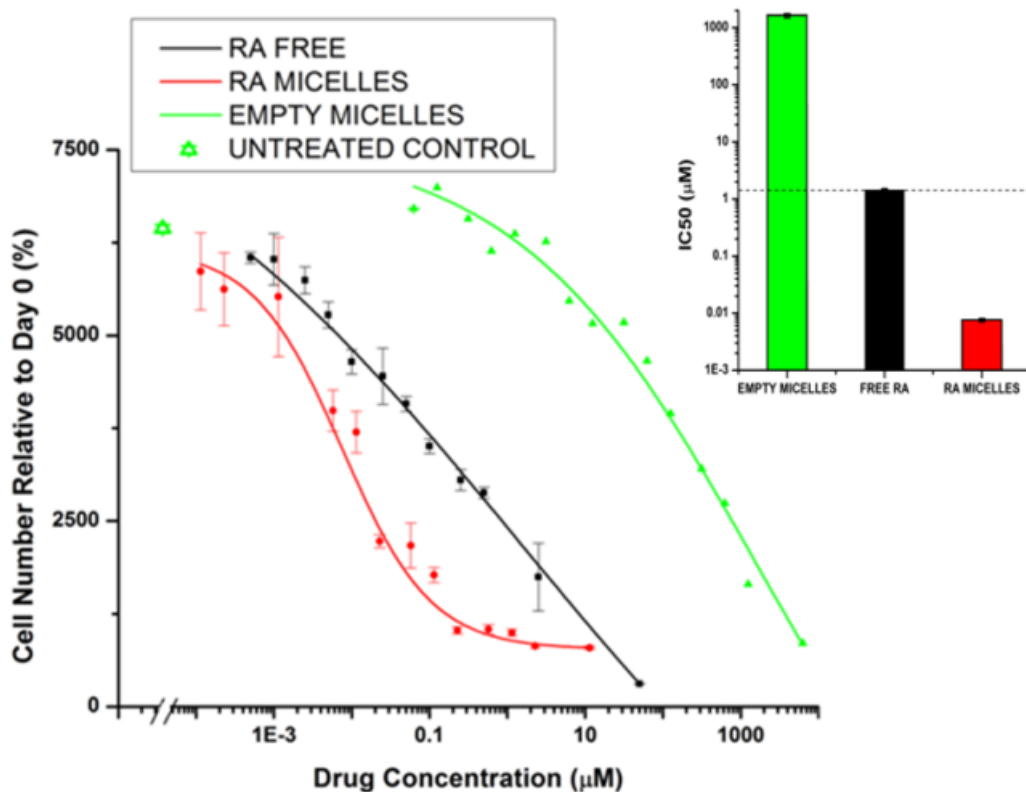
Figure 5.2. Comparison of free and encapsulated RA (bar graph IC50 inset). RA loaded micelles (red curve) are 200 times more potent than free RA (black curve). Empty micelles, in comparison, are inert. Empty green triangle represents untreated cell number after 3 days.
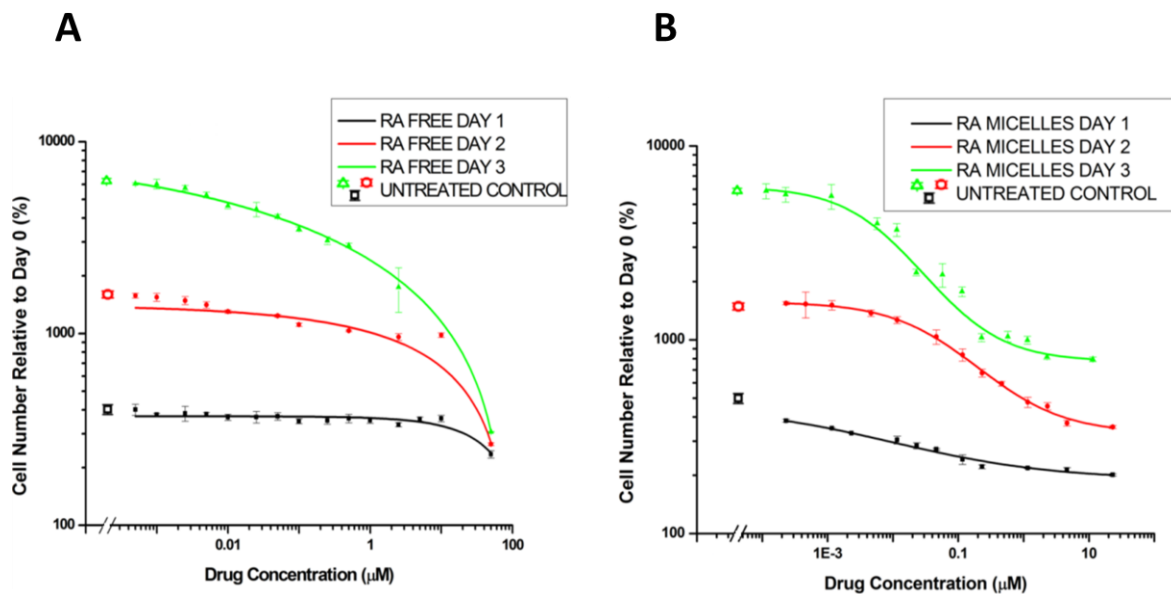
Figure 5.3. Kinetics of cell numbers treated with free and encapsulated RA. Free RA stops cell proliferation at 50 μM irrespective of treatment time. However, encapsulated RA is more successful at stopping cell growth at physiologically relevant concentrations (~1 μM).
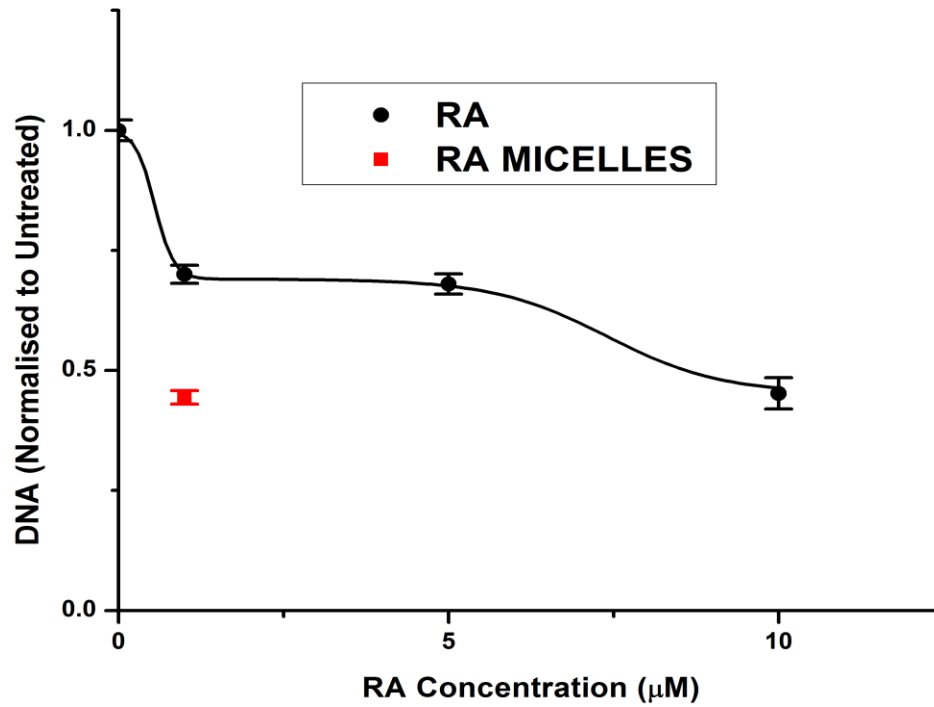
Figure 5.4. RA arrests proliferation of cells and decreases average DNA content per cell. Average intensity decreases monotonically with increasing concentrations of RA. RA loaded onto worms (red point) was more effective than that administered in free (black points).
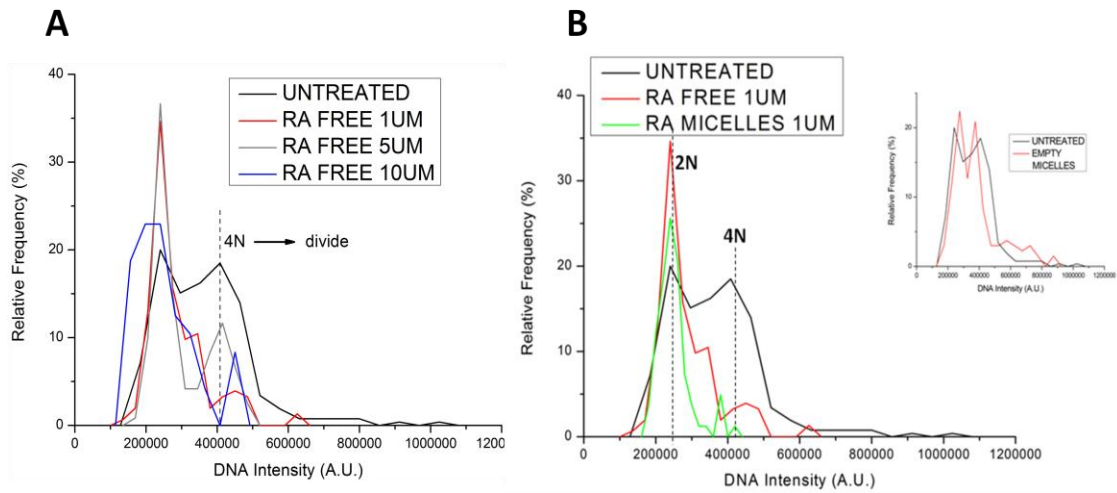
Figure 5.5. DNA histograms after treatment with free RA show a suppression of the replicating peak (labeled 4N). However, the suppression level did not correlate with RA concentrations. Worms with loaded RA suppressed the proliferating fraction even more (2N refers to normal complement of chromosomes, while 4N refers to duplicated chromosomes, acquired before cell division).
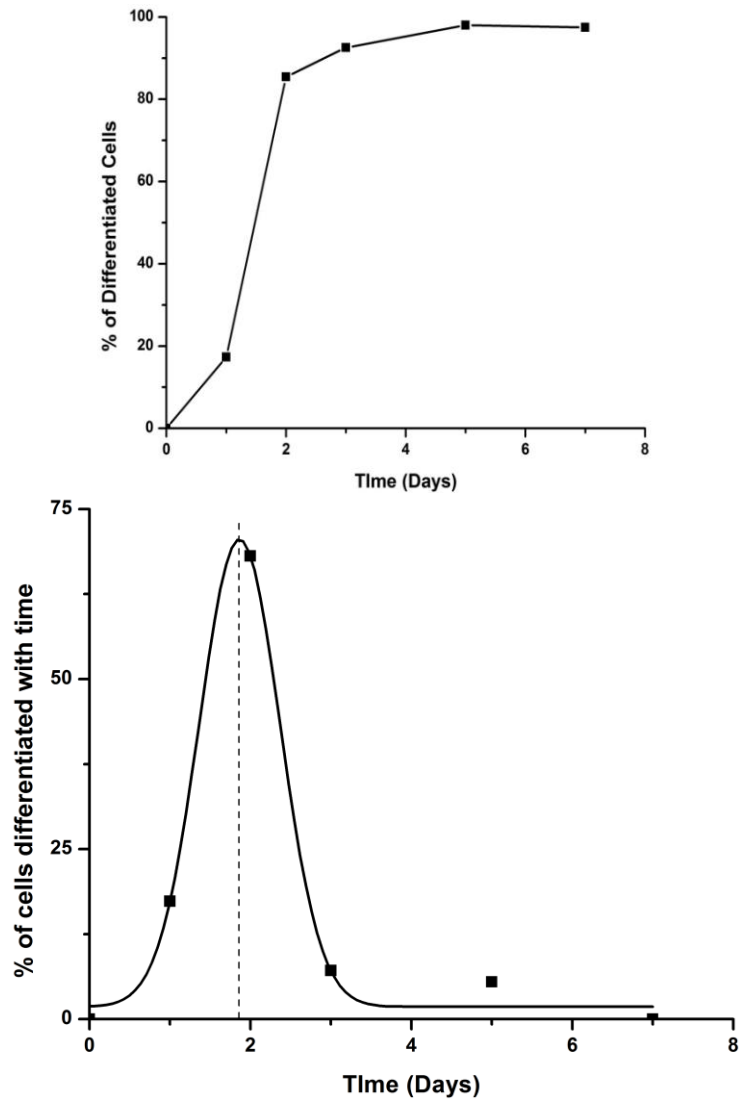
Figure 5.6. Estimation of fraction of EC4 cells differentiated by RA into a quiescent, non-proliferative state follows a hill curve. Most cells get differentiated around day 2 (2-4 cell cycles) after incubation with the drug (bottom), consistent with necessitation of secondary transcription factors to enforce the decisions. Note that this is a simple estimation by back-calculation from cell number data.
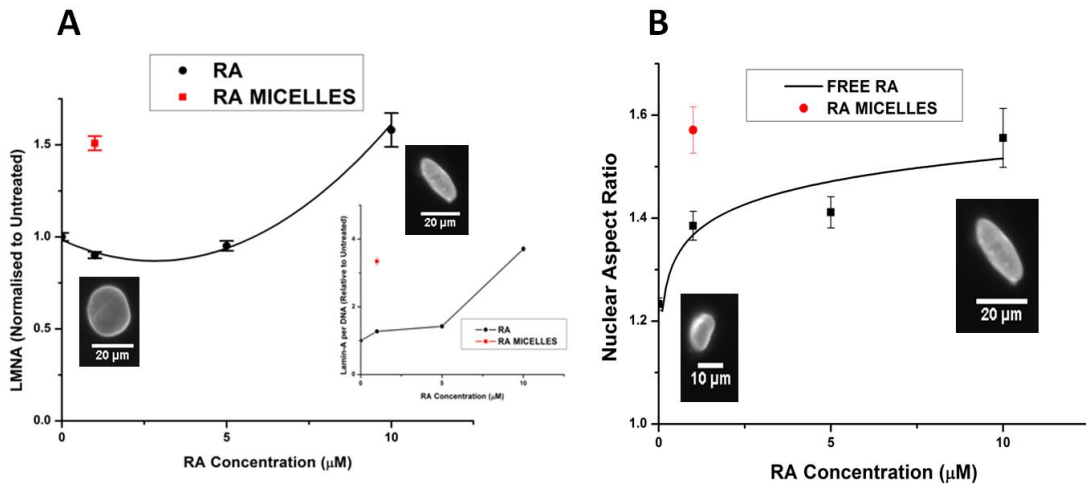
Figure 5.7. RA induces differentiation of cells **A)** RA affects levels of Lamin-A (a marker of differentiation), with RA in nanocarriers being an order of magnitude more effective than free drug. While levels of Lamin-A initially decrease before increasing, Lamin-A normalized to DNA content increases with RA concentration. Comparison of images of treated and untreated nuclei clearly reveal changes in morphology. Untreated nuclei (left) are rounded with uniform Lamin-A distribution on the edges. When treated with 10 μM RA in free form, the nuclei become more elongated (right) with patchy Lamin-A distribution. Treatment with RA increases levels of Lamin-A (normalized to DNA), hinting at differentiation. **B)** Nuclear aspect ratio increases hyperbolically with RA concentrations. As with Lamin-A levels, encapsulated RA is an order of magnitude more effective than free RA.
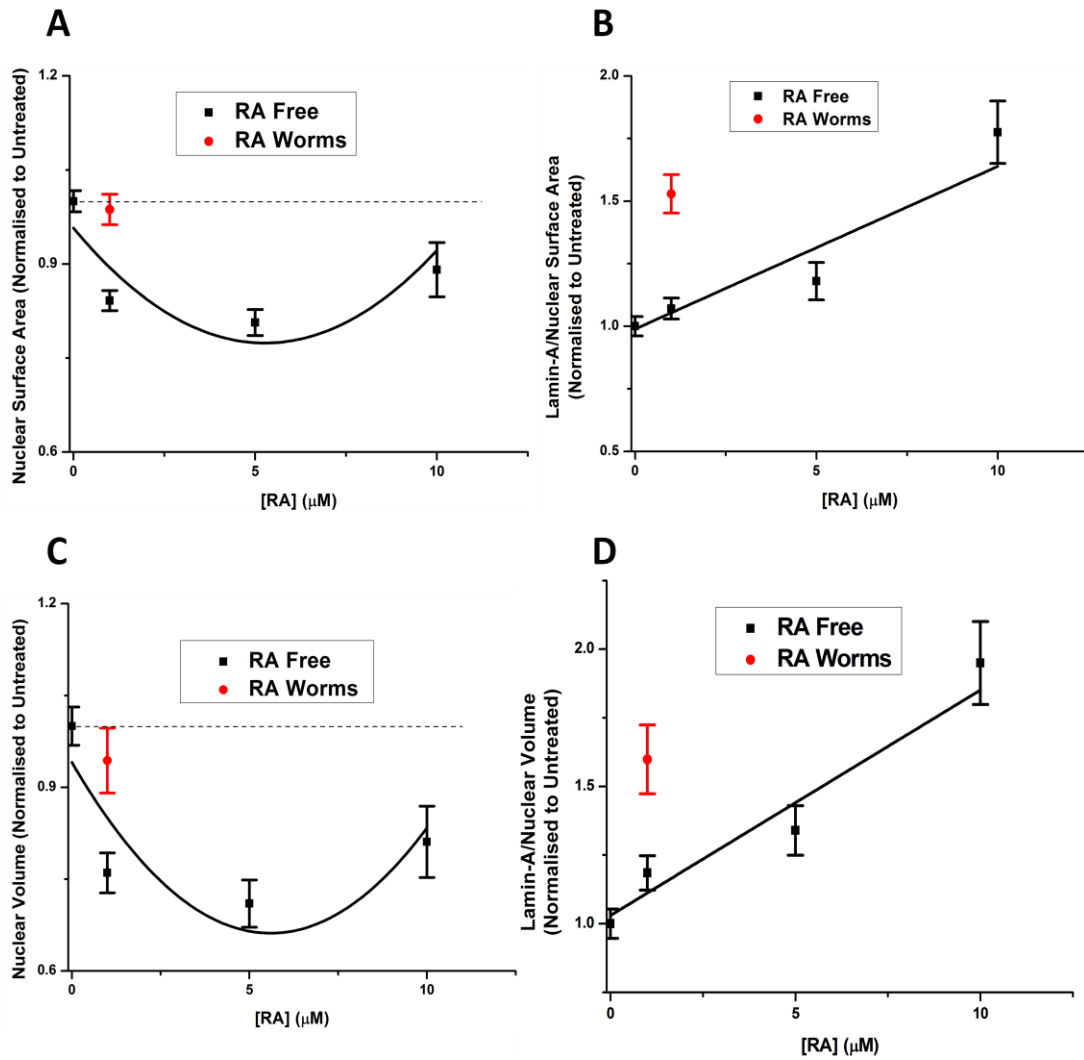
Figure 5.8. A) and **C)** RA has a parabolic effect on nuclear surface area and volume. As with previous plots, encapsulated RA is an order of magnitude more effective than free RA. **B)** and **D)** Levels of Lamin-A normalized to either nuclear surface area or volume increase linearly with RA concentration, indicating that changes in protein level are not solely due to change in nuclear shape (morphology).
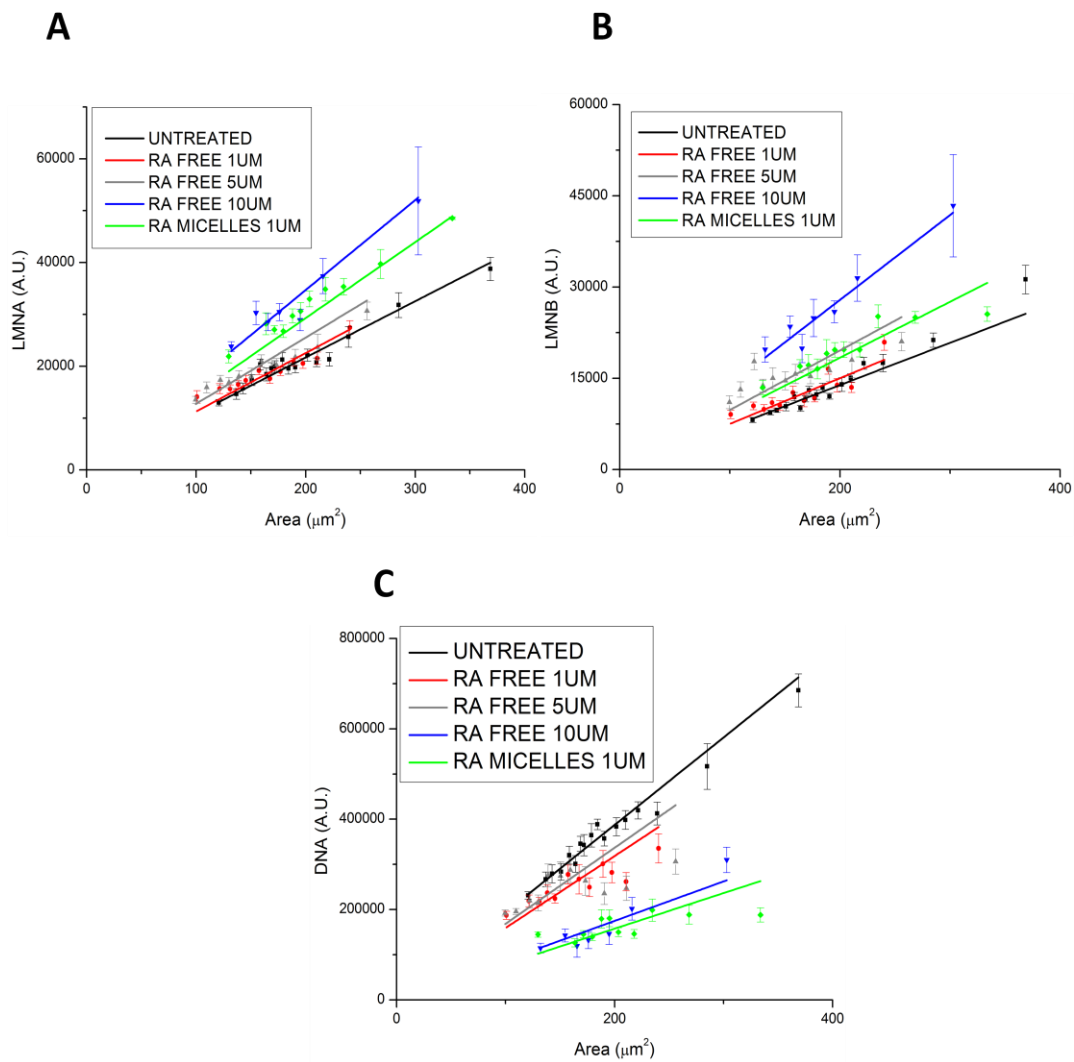
Figure 5.9. Scatter plots of Lamin-A, Lamin-B, and DNA vs. area. All three increase

linearly with increasing nuclear area, but the slope changes with treatment condition
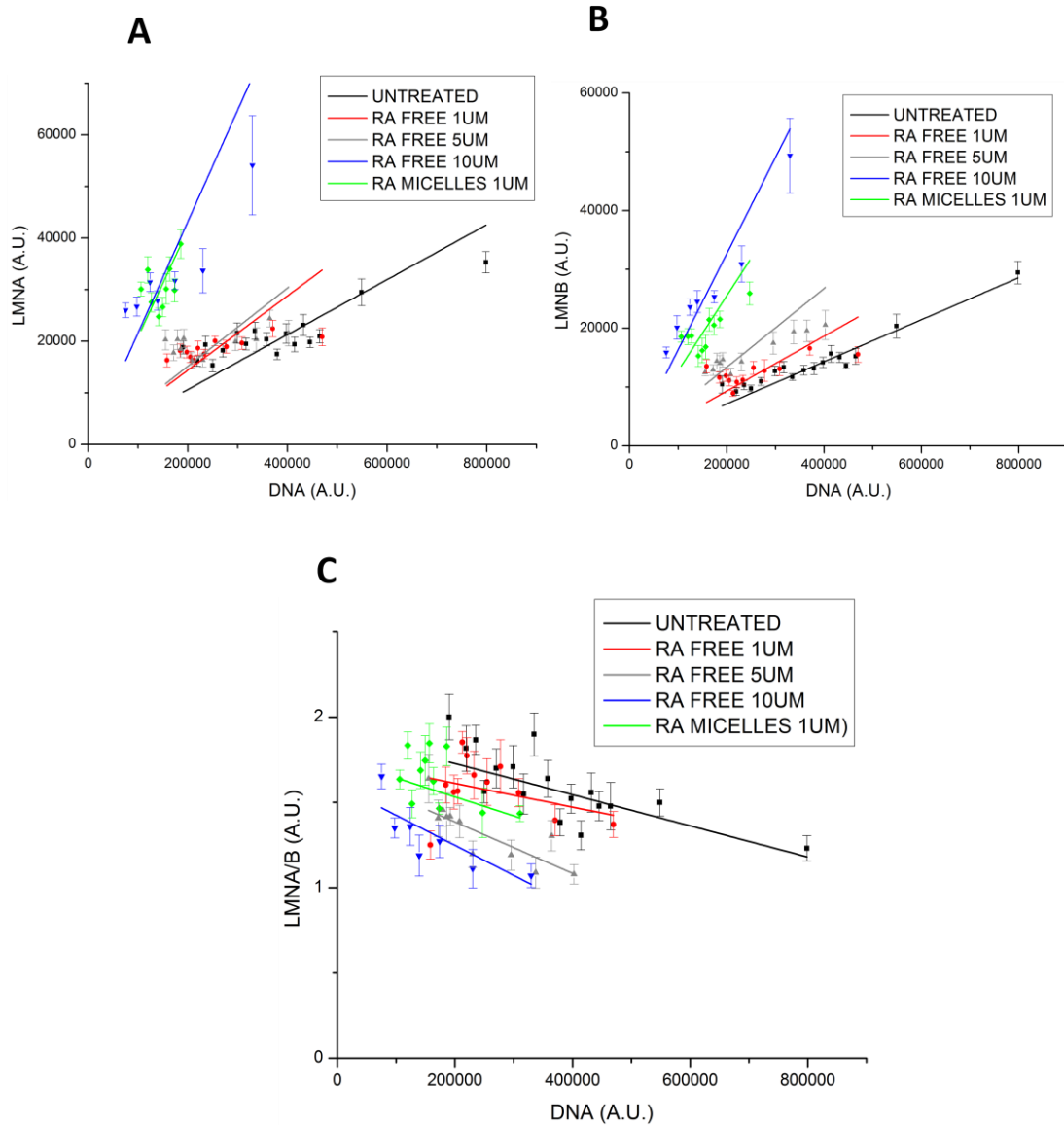
Figure 5.10. Scatter plots of Lamin-A, Lamin-B, and Lamin-A/B vs. DNA. Both increase

linearly with DNA content, but the slope changes with treatment condition

CHAPTER 6. CHEMO-DIFFERENTIATIVE THERAPY SHRINKS TUMORS WHILE REDUCING RESISTANCE

(This chapter is a part of the manuscript being prepared for submission: Nair, P. R., Alvey C., Jin X., and Discher, D. E. Filomicelles deliver a chemo-differentiative therapy to durably control carcinoma cell fate)

Contributions: X. Jin established orthotopic liver models *in vivo.* C. Alvey performed *in vivo* imaging with IVIS Spectrum for data shown in Fig. 6.19 A.

6.1. RA as a part of chemo-differentiative therapy

6.1.1. PML-RAR fusion in acute promyelocytic leukemia (APL)

APL is characterized by a block in differentiation at the promyelocytic stage, and is a subtype of AML. Translocation t(15; 17) is found commonly in APL cells (Nasr et al., 2008) (Soignet et al., 1998). The involved genes are RARα (at chromosome 17) which fuses with PML (Promyelocytic leukemia protein) located on chromosome 15. PML is a tumor suppressor protein involved in the formation of nuclear structures like PML-nuclear bodies. Similar to RARs, PML is involved in differentiation, specifically, hematopoietic differentiation. PML is also required for RA induction of target genes.

Due to its vital role, RA is already being used in clinics for treating acute promyelocytic leukemia (APL) (Tallman et al., 1997) (Weis et al., 1994). Combination of RA and arsenic trioxide have induced complete remission in majority (>90%) of APL cases (Jing et al., 2001) (Soignet et al., 1998). Treating the leukemic cells with superphysiological (1 µM, 10 times the maximum serum concentration) caused them to differentiate into neutrophils, leading to complete remissions in 23 of 24 patients. Treatment with RA also restores PML localization in the nucleus, which is disrupted by the fusion protein. The RARα part of the fusion lacks the transactivation domain (regions A and B in Figure 5.2) at the N terminus. The remaining domains are intact, which permits it to bind to RA and RAREs and exert its effect. Conversely, the PML part is truncated at the C terminus, losing a part which is a phosphorylation target. The fusion protein, however, retains the region that binds to the co-repressors of RARα such as SMRT and NCoR.

To summarize, retinoid signaling can induce differentiation, and blocking it can lead to a block in differentiation likely due to the repression of RA target genes. RA exerts its effect through RARs, which is diminished in fusion proteins, leading to incomplete differentiation and leukemia.

6.1.2. Development of chemo-differentiative therapy (Paclitaxel and Retinoic Acid)

Combination of RA with a conventional chemotherapeutic such as Cisplatin (Zhang et al., 2013) Paclitaxel (Hong et al., 2011) has been shown to be a promising option. However a detailed study of the underlying mechanisms as well as the optimal dosage

remains unclear, with the function of RA in regulating multiple pathways (Connolly et al., 2013) adding to the complexity of the challenge. As with previous chapter, delivery using filomicelles will be attempted in order to increase efficacy of treatment.

Keeping this strategy in mind we decided to combine Paclitaxel with Retinoic Acid (RA), which is a derivative of vitamin A. Herein, we report a chemo-differentiation therapy that is an improvement over conventional chemotherapy, when drug resistance and relapse are considered (Figure 6.1). Filomicelles dually loaded with TAX and RA display higher potency in vitro and in vivo. Dual drug treatments led to the most cell death as well as highest cell size and DNA content in surviving cells (hallmark of TAX treatment). Additionally, Lamin-A (marker of differentiation) levels were highest with combination treatment, indicating probable synergy between the two drugs. Crucially, the fraction of resistant cells arising after treatment was massively reduced. This combination had significantly more impact on the reduction of key proliferation proteins, particularly Ki-67. Despite the central role of RA in liver function, we were able to extend the efficacy of the combination to cell lines derived from lung, bone and muscle. Finally, the treatment was translated in vivo, shrinking subcutaneous xenografts as well as orthotopic liver tumor models with effects being durable. The results demonstrate two major avenues of chemotherapy improvement: drug combinations and the use of nanocarrier systems to increase potency and efficacy of drug delivery.

6.2. Materials and Methods

6.2.1. Materials

All chemical reagents were purchased from Sigma Aldrich Corp., St. Louis, Missouri, unless stated otherwise. Ham's F-12 growth media, FBS, penicillin-streptomycin, non-essential amino acids, MTT assay and Hoechst 33342 were purchased from Invitrogen. High glucose DMEM growth media and Dispase were purchased from Corning. Lamin-A, Cyclin D1 and Ki67 antibodies were purchased from Cell Signaling.

6.2.2. Synthesis of PEG-PCL and characterization of aggregates

Polyethyleneglycol (PEG) -Polycaprolactone (PCL) di-block copolymer was prepared as described previously (Nair et. al., 2016). Briefly, the diblock copolymer was prepared by the ring-opening polymerization of ε- caprolactone using PEG_{2000} as macro-initiator at 140 $^{\circ}$C in the presence of stannous octoate as catalyst. The polymer was characterized by ^{1}H NMR spectroscopy and Gel Permeation Chromatography (GPC). Aggregates were formed in water by solvent evaporation as described in Nair et. al., 2016. Filomicelles were incubated with PKH 26 dye and imaged at 567 nm using aggregates were mixed with PKH 26 hydrophobic red dye with emission spectra at a wavelength of 567 nm using an Olympus IX71 microscope. Paclitaxel and RA were loaded and the loading was measured as described previously (Nair et. al., 2016).

6.2.3. Cell culture

A549 lung cancer, Huh7 liver cancer, U2OS bone sarcoma, and RH30 human rhabdomyosarcoma cell lines were purchased from ATCC and grown as per as per standard ATCC cell culture protocol (ATCC Animal Cell Culture Guide 2014). EC4 mouse liver cancer cell line was cultured with DMEM High glucose growth media (4.5 g/L glucose with L-glutamine and sodium pyruvate) supplemented with 10% FBS, 1% penicillin-streptomycin and 1% non-essential amino acids at 37 $^{\circ}$C and 5% CO_2. When the flasks were confluent, the cells were passaged by dissociation with 0.05 % Trypsin-EDTA (Invitrogen) and re-plated with fresh media at a density of 10%.

6.2.4. In vitro cell viability assay

Procedure for in vitro cytotoxicity assay was adapted from Cai et al., 2007. Briefly, 5000 cells were seeded in 96-well plates and treated with (different drug concentrations) the next day. Post three day incubation, the media was aspirated cells were incubated with media and MTT solution (5 mg/mL in PBS) for 3 hours. The MTT formazan crystals were dissolved in DMSO, and absorbance was measured at 550 nm. Additional cell death quantification was done by counting the number of floating cells staining positive for staining positive for Trypan Blue stain.

6.2.5. Rescue experiments to determine RA-TAX durability

50000 cells were plated in 6-well plates and allowed 24 hours for attachment. After 1 day, the media was exchanged with fresh one, and cells were incubated with free RA-

TAX combination (1 µM and 10 nM) or PBS (negative control). Free RA (1 µM) and

free TAX (10 nM) were the positive controls. After the 3-day incubation, the drug

containing media was aspirated, wells were washed with PBS and surviving cells were

incubated with fresh media. After this, the old media was replaced with fresh media twice

a week until the cells were analyzed by flow cytometry. At fixed time intervals, 3 wells

of each control as well as treatment group were detached from the plate by trypsinization,

stained for DNA (with Hoechst 33342 solution (0.01% of 10mg/mL solution in water) for

5 minutes) and run through a flow cytometer to record cell number.

6.2.6. In vitro 'relapse' studies

As with cell viability studies, 5000 cells were seeded in each well of 96-well plates, with

each well representative of a tumor. As was done with the abovementioned durability

studies, cells were treated with different formulations (free RA-TAX, free TAX, TAX

loaded worms or RA-TAX loaded worms) for 3 days, after which media was washed out

and cells were incubated with fresh media. The cell numbers were monitored in each

well, as were the number of wells with a resistant colony. For every time point, the

number of wells with a resistant colony were recorded and a plot of percentage of wells

relapsed vs. time was plotted.

6.2.7. Cell fixing and immunofluorescence

Fixing and immunofluorescence was carried out similar to that in previous chapter. Cells

in 6-well plates were treated with drugs as indicated above. After the desired time-point,

cells were fixed and permeabilized, followed by blocking with 5% BSA. The cells were

incubated overnight with the primary antibody, and then secondary antibody. The cells

were then stained with Hoechst 33342 solution and fixed again. The stained cells were

visualized under an Olympus IX71 microscope with a 300W Xenon lamp using 40x

objective (0.60 NA). Images were analyzed by ImageJ software.

6.2.8. Intracellular protein staining and flow cytometry analysis

The cells were detached with 0.05% Trypsin, spun down and washed with PBS. They

were fixed with 1.6% paraformaldehyde for 10 minutes and permeabilized with 0.1%

saponin for 10 min. The cells were then spun down, resuspended with the conjugated

antibodies and incubated for 1.5 hours and stained for DNA with Hoechst 33342 solution

(0.01% of 10mg/mL solution in water) for 5 minutes. After this incubation, cells spun

down and suspended in flow buffer (5% FBS in PBS). Cells were run through a flow

cytometer (BD LSR II) and data was analyzed by WEASEL v3.2.1 software.

6.2.9. Establishment of Xenograft Model for Liver Metastasis of Tumor

All animal experiments were approved by Institutional Animal Care and Use Committee

of the University of Pennsylvania and in accordance with NIH publication No. 86-23.

Eight to ten-week-old NOD-SCID-IL-2Rgc null mice (NSG) were purchased from the

Stem Cell and Xenograft Core of University of Pennsylvania (Philadelphia, PA) and

housed in a specific-pathogen-free facility. Mice were anesthetized using 4% isoflurane

in 3 L/min O_2, after which isoflurane percentage was maintained 2%. To examine the

therapy for liver metastasis of tumor, 10^6 of A549 human lung cancer cells labeled with tdTomato were injected into the murine liver. Briefly, the anesthetized mouse was placed supine, maintaining inhalational isoflurane anesthesia (2% (v/v) in 2 L/min O_2) with a nose cone. For analgesia, buprenorphine SR (1 mg/kg, ZooPharm, Fort Collins, CO) was subcutaneously injected on the animal's flank. The skin was shaved and the skin on the ventral abdomen and partial thorax was sterilized with chlorhexidine swab (Professional Disposables International, Inc. Orangeburg, NY. Cat. # B10800). Using sterile sharp scissors (Roboz Surgical Instrument Co., Inc. Gaithersburg, MD. cat. # RS-5916), a 15mm of mid-line abdominal incision was made and the linea alba was opened to enter the peritoneal cavity. 25 µl of tumor cells suspension (10^6 /25 µl of 25% Matrigel in PBS) was loaded into an insulin syringe with 30 G 1/2 inch needle (MHC Medical Products, LLC, Fairfield, Ohio. cat. # 08496-3035-11). The left lateral lobe of liver was then exposed using forceps (Roboz Surgical Instrument Co., Inc. Gaithersburg, MD. cat. # RS-8254). The liver was stabilized with a cotton-tip applicator (Fischer Scientific, cat. # 23-400-125), and the syringe was positioned inserting the needle into the liver and advancing the tip along the subserosal plane for a few millimeters. The tumor cell suspension in the syringe was gently discharged and the needle was removed from the liver. The puncture site was gently pressed with a cotton-tipped applicator to prevent leakage of the tumor cell suspension and to achieve complete hemostasis. Finally, the incision was closed with an absorbable 4-0 sutures (Ethicon Inc. Somerville, NJ. cat. # VR494).

6.2.10. In vivo experiments

In vivo experiments were performed on NOD-SCID mice with subcutaneous tumor xenografts or a xenograft model for liver metastasis of tumor (as described above). RA-Paclitaxel loaded filomicelles were administered using tail vein injection (250 µl per injection). The treatment consisted of four, six, or eight injections each, administered in regular intervals over 2 to 3 weeks. Tumor size was measured at regular intervals using calipers and Perkin Elmer IVIS Spectrum located at Penn Small Animal Imaging Facility (SAIF). The tumor area was normalized relative to the size at the onset of the treatment. Caliper measurements (for subcutaneous tumors) as well as mouse body weight were recorded twice a week.

6.2.11. Tumor disaggregation and anti-human staining

After the mice were euthanized, the tumors were excised and diced into pieces no larger than 1 mm^3. These chunks were then incubated with digestion buffer (containing 9 mg collagenase, 3 ml dispase and 200 µl of 1 mg/ml DNAase solution) for 20 minutes at 37 $^{\circ}$C. The digested mix was passed through a 70 µm filter and the filtrate was spun down to obtain a cell pellet. Any RBCs present were lysed with RBS lysis buffer (Corning) and Fc-blocked with CD32/CD16 antibody (Cell Signaling) for 10 minutes to prevent non-specific staining. The cells were then incubated with primary and secondary antibodies for 30 minutes each. The cells were then washed with 5% FBS, stained with Hoechst (10 min) and run through a flow cytometer (BD LSR II).

6.2.12. Curve fitting and statistical analyses

All curve fitting and data analysis was performed with OriginPro 8 software. Unless indicated otherwise, mean and standard deviation are calculated for a minimum of n = 3 independent samples.

6.3. Results

6.3.1. Combination of RA with chemotherapeutics

Three chemotherapeutics (Paclitaxel, Oxaliplatin, and 5-Fluorouracil) were combined with RA and the cell viabilities were studied on EC4 cell line to identify the best candidate to form a combination with RA (Figure 6.2 A, B and C). IC50 values were calculated from the cell viability curves (Figure 6.2 D). Paclitaxel exhibited the most improvement upon the addition of RA (more than a 2.5 fold decrease from free TAX), while the IC50 of Oxaliplatin was reduced 1.5 fold. Addition of RA had minimal effect on the potency of 5-fluorouracil. To evaluate a sample combination chemotherapy, we investigated the combination of Paclitaxel (TAX) and 5-Fluorouracil (5FU) on A549 cells (Figure 6.3 A). Combination of the two drugs were not as potent as TAX (black curve), as indicated by a rightward shift. They were however more effective than 5FU (dashed red curve). Further, the potency of the combination was dictated by TAX content, i.e., mixtures with higher amount of TAX were more successful than those having higher 5FU. All this pointed to the lack of synergy between the two drugs. Quantification of IC50 values (plotted in bar graph representation in Figure 6.3 B)

underlined the same message. All plots in Figures 6.2 and 6.3 were generated with free

drug data, and the primary purpose was to evaluate synergies between drugs.

6.3.2. Combination of RA with Paclitaxel

Experiment similar to that conducted in Figure 6.3 A was performed to evaluate the

performance of TAX-RA combination (Figure 6.4 A), and to find the optimal drug ratio.

Three molar ratios were tested: 3:100, 1:100, and 1:300 (TAX:RA) on A549 cells, and all

combinations were found to be more potent than either single drug. 1:100 was found to

have the lowest IC50 (3 nM, quantified in Figure 6.4 B), ~30 fold lower than free TAX

(95 nM). The other two combinations had comparable IC50s (15 and 18 nM), despite an

order of magnitude difference in TAX content, which might hint at synergy between RA

and TAX. RA was comparably cytotoxically inert, with an IC50 of 72 µM. Hence, a

molar ratio of 1:100 between TAX and RA was chosen and adhered to in future in vitro

experiments. To further confirm the efficacy of the combination and to assess its

performance when loaded onto worms, EC4 cells were treated with RA, TAX or RA-

TAX encapsulated in worms. Drug loaded worms led to a lower IC50 (and hence, more

potency) than free drugs (Figure 6.5 A). RA-TAX worms were synthesized by loading

RA and TAX separately into worms, and then mixing them to obtain desired

concentrations. This method was chosen to make it easier to control final drug

concentration, and the combination was three times more potent than free form, as were

TAX worms when compared to free TAX. RA benefitted the most from loading into

worms, as observed earlier. A bar graph depicting the IC50s is shown in Figure 6.5 B,

with RA-TAX exhibiting the lowest IC50 among all tested formulations. Empty worms

were inert at desired physiological concentrations, and cells incubated with empty worms did not show any abnormal nuclear morphology when stained for nuclear lamin-A (Figure 6.5 A, top). Cells treated with RA were more elongated (Figure 5.7 A), and cells treated with TAX or RA-TAX displayed massive blebbed nuclei (a hallmark of TAX treatments that will be revisited later). To further confirm the potency of this combination, cell survival and death were directly measured by flow cytometry and Trypan blue staining respectively (Figure 6.6 A and B). Cell numbers were similar for untreated and empty worms, while they were much lower for drug treatments, especially for TAX and RA-TAX treatments. As expected, cell density was lowest and cell death was highest for RA-TAX worms treatment. To gain further insight into the kinetics of the treatment, we studied cell viabilities after days 1, 2 and 3 following treatment with free RA-TAX (Figure 6.7 A). While the curve is largely flat for day 1 with free RA-TAX, a dip in cell numbers is observed after day 2. The response curve for day 3 exhibits a bi-phasic behavior. Similar kinetics study with RA-TAX loaded worms (Figure 6.7 B) led to similar curves that increased in steepness with passing time. Finally, the difference in performance between separately loading RA and TAX (as was done previously) and loading both drugs together (co-loading) was assessed (Figure 6.8 A and B). While there is no difference between the curves at very low or high concentrations, co-loading worms (perhaps unsurprisingly) is more effective at the desired intermediate concentrations. Quantification of IC50 revealed a four-fold decrease in co-loaded worms from separate loading. Quantification of integration efficiency revealed no loss for RA, while loading efficiencies were higher for TAX with co-loaded worms than separately loaded (Figures 6.8 C and D). Although separate loading allows the precise control of final drug

concentration, the absence of any loss in integration efficiency made co-loaded worms the system of choice for all following experiments.

6.3.3. Durability of RA-TAX treatment and reduction in vitro 'relapse' studies

Even though the combination leads to a more potent treatment, as mentioned earlier, the aim of this study was to seek a more durable cure. This 'durability' was assessed by a simple rescue experiment (Figure 6.9), where cells were treated with drugs and incubated with fresh media post-treatment. The cells treated with RA consistently increase in number (red curve), and the difference in slopes indicate that a fraction of the cells exposed to RA have been differentiated and have lower proliferation. The slope decreases sharply from day 1 to day 2, consistent with the differentiation data in Figure 5.6. In accord, there is little change in the proliferation rate past day 2. TAX treated cells decline in number initially (black curve), but cell death plateaus after a week. Inset figure shows a typical frame at this time point with TAX affected cells among normal-looking 'resistant' cells. After more time, proliferating cell numbers overtake dying ones, leading to cell numbers rising. RA-TAX treated cells (green), on the other hand, consistently decrease in number, indicating a more durable treatment and all cells die-off around day 30. A larger scale quantification of in vitro 'relapse' (Figure 6.10), showed that most cells treated with free TAX relapse (92%), consistent with the observation of resistance in Figure 6.9. This rate is much lower for RA-TAX treated cells (15%), 22 days after treatment, indicating that in around 85% of wells treated with free RA-TAX, all cells die-off, indicating a much more durable treatment than single drug like TAX. Loading TAX onto micelles (Figure 6.10, right) might decrease IC50, but only manage to slightly delay

the relapse by a couple of days. 89% of TAX treated wells still experience relapse, highlighting the limitation of a single drug. The efficacy of RA-TAX was greatly improved via loading onto micelles, with no relapses in cells observed after 30 days.

6.3.4. Potential Synergy of RA with Paclitaxel

To comprehend the influence of one drug on the other, we visited the hallmark of TAX treatment i.e. increased cell size and DNA accumulation (measured by forward scatter and Hoechst intensity respectively). As expected, both TAX (1.5 times the untreated size) and RA-TAX (2.7 times the untreated size) showed increased cell size (Figures 6.11 A and 6.12 A). However, cell sizes for TAX treated cells had returned back to normal by day 9 (1.06), while it was 3.1 for RA-TAX treated cells after 29 days. Similar to cell size, DNA content (Figure 6.11 B) was also increased for TAX (2.8 times relative to untreated) and RA-TAX (3.8). Similar to cell size, DNA content was back to normal after day 9 (1.09), while it was still high for RA-TAX treated cells after day 13 (5.8). By day 29, it had declined to 1.2, which combined with the increased cell size suggested that DNA synthesis was hindered after treatment. DNA content decreases for RA due to lower number of proliferating cells (0.7), but similar to TAX, returned to normal (1.08) within 9 days. Normalization of DNA to area (Figure 6.12 B) showed that cells treated with TAX (single drug or as a part of the combination) had lowest values, suggesting that DNA synthesis might be affected after treatment. Histogram of DNA content (Figure 6.12 C) further shed light on the DNA content in surviving cells and reaffirmed that drug loaded worms induced the most polyploidy.

As the initial role of RA was to increase levels of differentiation in surviving cells, we measured levels of Lamin-A (Figure 6.13). Levels of the protein (normalized to DNA content) increased with drug treatments from RA only to RA-TAX, as well as from free drug to drug-loaded worms. Highest values were obtained with RA-TAX worms (3.6, normalized to untreated), which was an improvement over free RA-TAX (2.8). Both values were higher than those for free RA (1.27) and RA loaded worms (3.3). Flow cytometry scatter plots of Lamin-A vs. DNA reveal a shift in population of cells staining high for both proteins and provide a more detailed insight onto the different populations of cells existing after treatment (Figure 6.14 A).

6.3.5. Effect of RA-TAX on key proliferation proteins

While the combination treatment greatly reduces the proliferation of surviving cells (Figures 6.9 and 6.10), the basis for this remains unclear and cannot be fully attributed to differentiation and mitosis block. Measurement of levels of Ki-67 and Cyclin D1 (Figure 6.15 A) provided more insight into this. Measurement of absolute protein levels revealed a decrease in levels of both proteins (Ki-67:1.1 and Cyclin D1:1.6, normalized to untreated) compared to TAX treated cells (Ki-67:1.7 and Cyclin D1:1.9). The levels were presumably higher than untreated due to the greatly increased cell size (Figure 6.11 A), with affected nuclei up to 4 times larger in size than that for untreated cells. Cells treated with RA had the lowest Cyclin D1 levels (0.9). The effect of dual drug treatment on Ki-67 levels is further highlighted in Figure 6.15 B. Images (40x magnification) of cells treated with TAX alone (top) and with RA-TAX combination (bottom) reveal larger nucleus (as expected). However, cells treated with TAX alone still stain positive for Ki-

67 (top right), while those treated with RA-TAX are null to low for the same (bottom right). These effects are further improved by using worms for delivery (Figure 6.16 A), with Ki-67 levels 62% of that for free drug treatment. Cyclin D1 levels show a modest decrease too (6%) compared to free drug. A histogram of Ki67 and Cyclin D1 levels after treatment (Figure 6.16 B) reveals a much larger fraction of cells staining null for these proteins. This progressively increases from no treatment to free drug to micellar drug delivery. Flow scatter-plots of Ki-67 v. DNA and Cyclin D1 vs. DNA show a shift in populations towards cells with higher DNA and lower proliferation proteins (Figures 6. 14 B and C).

6.3.6. Resistance to RA-TAX treatment and expansion of the treatment across different cell lines

During the course of the study, cell colonies acquiring resistance to RA-TAX worms were isolated and expanded to better study the characteristics of resistant cells. The doubling times were measured, and all resistant cells were found to have higher doubling time (and hence slower rate of replication) than EC4 cells (Figure 6.17 A). The resistance was evident in the dose response curves (Figure 6.17 B), with more resistant cells displaying a rightward shift and higher IC50 than normal EC4 cells. This data along with cell doubling times were used to calculate the degree of resistance. The resulting scatter plot of proliferation rate against the degree of resistance displayed an anti-correlative trend (Figure 6.17 C). The colony with the slowest replication rate (denoted as RTMR2), had the highest fraction of resistant cells. As expected, untreated EC4 cells had the fastest

replication and lowest resistant fraction. All other colonies lied between these two extremes.

The efficacy of RA-TAX on c-myc driven EC4 cells might be representative of its effect on an aggressive tumor. However, the central role of RA in liver tumorigenesis would imply the applicability of this treatment to other hepatocellular carcinoma cell lines. With Huh7 cell line, the combination was found to be more effective than either of the free drug alone (Figure 6.18 A, RA-TAX IC50: 3 nM, TAX IC50: 13nM). Another point to note is that this was despite the lack of responsiveness to RA (IC50: 5μM) compared to EC4 cells (IC50: ~10 nM). This efficacy despite varying response to RA raises the question of applicability of this combination outside of liver cancer, and tests on A549, U2OS and RH30 cell lines do confirm this (Figures 6.18 B, C, and D). RA-TAX worms exhibit a much lower IC50 (1 nM), than TAX loaded worms (25 nM) in A549 cells, and this theme was repeated with U2OS (RA-TAX IC50: 3 nM, TAX IC50: 8 nM) and RH30 cells (RA-TAX IC50: 1 nM, TAX IC50: 4 nM). Dose responses of all cell lines to free drugs also reveal higher efficacy of free RA-TAX over single drugs (Figure 6.19).

6.3.7. RA-TAX potency can be translate in vivo to shrink subcutaneous xenografts

The efficacy of dual drug delivery in vitro was replicated with in vivo models. As a preliminary experiment, free RA-TAX injections (TAX: 1.4 mg/kg, RA: 0.002 mg/kg) were administered via tail vein injections to NOD-SCID mice with subcutaneous A549 xenografts (Figure 6.20 A). Four injections over the course of 11 days led to a modest

141

(15%) shrinkage in tumor size, while the growth of the tumor was arrested for ~25 days. RA-TAX worms led to a more durable shrinkage in a similar model (Figure 6.20 B). Six injections of RA-TAX loaded worms (administered at TAX: 1.5 mg/kg, RA: 0.1 mg/kg) led to a 25% shrinkage of tumors, and most importantly, the tumors did not resume an upward trend nearly 45 days from the start of the treatment. Additionally, there was no decrease in mice body weight with either of the above treatment (Figures 6.27 A and B).

Efficacy of RA-TAX worms could be extended to in vivo xenografts with other tumor lines. Injections in NOD-SCID mice with HepG2 subcutaneous tumors suppressed the growth of tumors (Figure 6.21 A). In mice treated with RA-TAX worms, the tumors grew by 30%, while untreated tumors more than tripled in size during the same time frame (3.2 times from the start of treatment). Unlike A549 xenografts, free RA-TAX produced minimal retardation in tumor growth, with final size 2.5 times from the onset of treatment. The dosage of RA and TAX was similar to that from previous experiments. The rapid growth of untreated tumors (compared to A549 xenografts), prompted the isolation of tumor from mice, disaggregation and staining of tumor cells with anti-human antibody to stain the HepG2 cells (and distinguish them from mouse cells). The non-homogenous composition of the tumor was evident upon plotting a histogram of anti-human stain and comparing it with that for pure HepG2 cells (Figure 6.21 B). Only 0.2% of the tumor cells stained positive for HepG2 (Figure 6.21 C) for untreated, while 0.14% cells stained from RA-TAX worms treated tumor. While the effect of free RA-TAX treatment was not reflected in tumor size, only 0.1% cells from those tumors were HepG2 cells. To better comprehend the question of optimal dosage in vivo, mice with

subcutaneous A549 xenografts were administered with altered drug dosage. The TAX dosage was increased (2.2 mg/kg) from previous experiments, while the dosage of RA was halved (0.05 mg/kg) (Figure 6.22 A). As seen previously, RA-TAX worms suppressed the growth of tumors, with effects lasting ~25 days after the last injection. However, the lowered RA dosage was evident in that the tumors failed to shrink. A second round of treatment with triple the RA dosage (0.15 mg/kg) was much more successful in shrinking tumors. Mice previously treated with RA-TAX worms as well as untreated were injected with RA-TAX worms, while those injected with free drug in the first round remained untreated. Injected mice exhibited tumor shrinkage, while (now) untreated mice experienced an increase in tumor burden. The higher dosage led to a drop in body weight (indicating toxicity), however these mice bore orthotopic liver tumors (next section), which hinder the normal functioning of liver and might lead to weight loss, especially ~80 days post tumor establishment (Figure 6.27 C). It should also be noted that mice who were treated with RA-TAX worms previously tolerated the second round of injections better than mice that were previously untreated, calculated by rate of loss in body weight.

Finally, mice were injected with a higher dose of RA (0.35 mg/kg) and TAX (2 mg/kg) during an extended round of injections (8) in attempt to figure out the maximum drug dosage that could be withstood (Figure 6.22 B). RA-TAX worms shrunk subcutaneous A549 tumors by ~50%, with tumors remaining shrunk 20 days after the completion of treatment. Single drug controls arrest the growth of tumors 15-20 days after treatment, but fail to produce shrinkage in size. During the same time frame, untreated tumors more

than double in size. Despite bearing liver tumors as well, the mice treated with RA-TAX show little loss in body weight (Figure 6.27 D) and were alive the longest. All other groups exhibited weight loss.

6.3.8. RA-TAX efficacy can be extended to shrink orthotopic liver tumors in vivo

In order to test the delivery potential of worms to orthotopic tumors, mice were injected with HepG2 cells in the liver to form an orthotopic tumor mimicking a 'metastasis' model. Liver tumors excised from mice treated with RA-TAX worms were much smaller, and showed ~60% shrinkage compared to untreated (Figure 6.23 A and quantified in 6.23 B). Disaggregation of an adjacent 'normal' liver lobe was then performed to comprehend the effect of RA-TAX worms on metastasis of cells from established liver tumor to adjacent lobes. A much larger population of cells in normal liver lobes stained positive for anti-human stain (2.18%) compared to RA-TAX worms (0.87%) treated, and this is evident in the histogram of anti-human stain intensities, which reveals a small peak with untreated liver lobe (inside red box) (Figures 6.24 A and 6.24 B). To further elucidate the efficacy of RA-TAX worms on liver tumors, mice bearing orthotopic A549 tumors (also bearing A549 subcutaneous tumors that were shrunk in Figure 6.22 B) were injected with either the dual drug therapy (RA-TAX worms, green curve) or single drug controls (RA worms, red curve, or TAX worms, blue curve). As with previous experiments, untreated mice were the negative control (black curve). As observed previously, dual drug treatment was the most efficient, initially shrinking liver tumors but failing to immediately arrest the re-growth. The tumors did not exhibit any re-growth once the treatment was finished, and remained so for ~20 days. The final tumor size was similar to that during the start of the

144

treatment. Tumors grew with single drug controls and untreated mice. Quantification of

total (subcutaneous plus liver) tumor burden in mice recapitulates and reaffirms the

previous observations (Figure 6.25 B). Dual drug treatments produced the only shrinkage,

with TAX loaded worms being the next best treatment but producing only a minor

improvement over untreated tumors (large data point indicates average for data points

with horizontal trend line). This led to a survival benefit as depicted by the Kaplan-Meier

curve in Figure 6.25 C. RA worms were ineffective in arresting tumor growth, consistent

with previous results. Quantification of the above data (Figure 6.26) indicated that RA-

TAX worms shrunk total tumor load by 18% compared to start of treatment and was 45%

the size of final untreated tumor, while TAX treated tumors grew by 52%. Final tumor

sizes for untreated and TAX treated tumors were similar, with latter 84% the size of the

former, and only the combination succeeded in shrinking tumors compared to the start of

the treatment.

6.4. Discussion

The emergence of drug resistance in clinic and the subsequent relapse of tumors often

lead to death. A simple solution in clinic has been to use combination chemotherapy,

either with two different drugs (often acing though perpendicular pathways in the cell) or

combining a drug with radiotherapy. As explained above, RA is an essential molecule

derived from vitamin A, and is an attractive option as a part of a combination. As seen in

figures 6.2 A to C, addition of RA decreases (even if it is minimal for 5-FU) the IC50,

and this may be attributed to RA working through an independent pathway from the

chemotherapeutics. Oxaliplatin and 5-FU damage DNA and induce apoptosis, while TAX

stabilizes microtubules and induces aneuploidy by blocking mitosis at the metaphase-anaphase transition, leading to bigger and blebbed nuclei (Figure 6.5 A inset). This eventually causes the affected cells to apoptose. RA, in contrast does not induce cell death at physiological concentrations (~ 1μM), simply arrests the proliferation and drives the differentiation of cells. This can be inferred from Figure 6.6, where RA is a negative control and has low density as well as low cell dea-th. This manifests itself in similar trends when cell viability is plotted against drug concentration. Figures 6.2 and 6.3 were performed with free drug, and its sole purpose was to select the best candidate. It highlights an advantage of chemo-differentiative therapy over combination chemotherapy that was examined in Figure 6.3. Despite TAX and 5FU being used in clinic for advanced gastric cancer (Kim et al., 1999)(Murad et al., 1999) and breast cancer (Buzdar et al., 2007),they failed to synergize, consistent with previous reports (Kano et al., 1996)(Johnson et al., 1997). While the combination of Paclitaxel and RA has received limited exploration in colon (Hong et al., 2011), brain (Karmakar et al., 2008) and breast cancers (Pratt et al., 2006), it has not (to the best of our knowledge) been studied with liver cancer, despite RA being synthesized and stored in the liver.

But as mentioned above, RA complexes with albumin and binds to it tightly at concentrations above 0.5% albumin (Avis, 1995). Additionally, TAX is susceptible to hydrolysis, reducing its activity (Nikolic et. al., 2011) (Amini-Fazl et. al., 2014), and loading TAX into nanocarriers may protect it (Nair et. al., 2016). This is confirmed by the decrease in IC50 upon loading drugs, especially for RA. Similar improvements in IC50 for TAX and RA-TAX hinted that majority of the loss in cell numbers was dictated

146

by the action of TAX. The inertness of empty worms attributed the potency of drug-loaded worms solely to the drugs (and not the carriers themselves) and further outlined the inertness of polymeric nanoparticles. The lipids forming the cell membrane and the amphiphilic diblock copolymers that self-assemble to form the worms are structurally similar. This may allow the worms to destabilize the cell membrane, leading to the toxicity and cell death observed with high concentrations of empty worms. This claim is backed up by higher cell density and lowest cell death in figure 6.6. Higher cell density on plates with RA, free or worm loaded, supports the claim of different mechanism and induction of minimal cell death. It should be noted that even though RA and TAX lead to similar trends, they work by completely different ways different mechanisms. TAX blocks cell division at metaphase-anaphase stage, leading to cell death, while RA arrests proliferation and is Lamin-A regulator (Swift et al., 2013).

Cell viability kinetics (Figure 6.7) is consistent with the hypothesis that TAX might first kill susceptible cells, and suggests that the anti-proliferative effect of RA may not interfere with the anti-mitotic action of TAX. The timeframe for action (~2 days) agrees with that for RA to take effect (RA exerts its effects through secondary response proteins (Wu et al., 2000) (Lawson and Berliner 1999)). Higher integration efficiency of TAX in the presence of RA (Figure 6.8 C) may suggest that the presence of RA might help load TAX into the core of the worms, possibly by increasing the hydrophobicity of the core. However, there was no benefit in the reverse case, and loading of RA was similar with or without TAX. However, concentration of RA was 100 fold higher than that of TAX, which might obscure any cooperativeness. The higher efficiency of co-loaded worms

(Figure 6.8 A and B) suggests that the simultaneous presence of both RA and TAX is required. Further supporting this hypothesis is the inadequacy of separately-loaded RA-TAX worms. While they do produce a better performance in dose response tests *in vitro*, their performance is no better than that of TAX alone during the rescue/relapse studies (data not shown). When separately-loaded RA-TAX worms are injected *in vivo*, their performance was found to be worse than free RA-TAX. While free RA-TAX produced 15% shrinkage in Figure 6.20 A, separately-loaded RA-TAX worms produced ~7% shrinkage (data not shown). As has been proven subsequently, co-loading permits the successful translation of the potency of RA-TAX to worm loaded systems *in vitro* and *in vivo*, suggesting that both RA and TAX need to be present together while being taken up by the cell.

The plateauing and subsequent re-growth of almost all wells containing TAX treated cells explains the acquisition of resistance and subsequent re-growth observed in tumors and is observed frequently *in vivo* as well as in clinic (Hattinger et al., 2016)(Alkema et al., 2016). The above experiment was with free drugs, and the benefits of loading on to micelles could be evident as either lower relapse rates or delay in relapse among treated cells or a combination of the two. While loading the drug onto nanocarriers decreases the IC50, the relapse rate was not significantly different from free drug treatment, indicating a contradiction between *in vitro* potency and long term prognosis. TAX-loaded worms may delay the onset of relapse by a couple of days *in vitro* compared to free TAX, but the final outcome does not change. It is also interesting to note that irrespective of being worm-loaded or free form, relapse rates peak around day 10 (20 cell cycles) and remains

148

mostly constant after 15 days (30 cell cycles) *in vitro*. This transient nature of single drug treatment is further highlighted by tracking the cell size and DNA content with time, which return to normal within a week after the drugs are washed off. The inability of RA-TAX treated cells to continue synthesizing DNA may just be one of the mechanism that prevent the rise of resistant clones. Combined with highest levels of Lamin-A achieved after RA-TAX treatment (suggestive of differentiation of surviving cells), this indicates that either drug enhances the effect of other drug, and as seen with RA on TAX, makes the effects durable. This might suggest some sort of synergy between the two drugs and further supports the observations from Figures 6.2 C and D as well as 6.4.

Another key point that is once again highlighted is the massive improvement offered by loading RA into worms that lead to a 2.6 times increase in protein levels. This further supports our hypothesis that loading RA into worms protects it from complexation with albumin, and increases its efficacy. The decrease in levels of Cyclin D1, but not Ki-67 reiterates the claim that RA arrests cell proliferation (by arresting the cell cycle regulated by Cyclin D1), and might have minimal effect on protein synthesis by itself. The durability of RA-TAX combination, however, might be better explained by its inhibitory role on protein synthesis (via Ki67) rather than regulation of cell cycle (Cyclin D1). This is most striking in the images with cells stained for Ki-67 (seen in Fig. 6.15 B). However, the effect on Cyclin-D1 might be underestimated here, as EC4 cells constitutively express c-myc (main reason behind their rapid proliferation), that is known to constitutively activate cell cycle via Cyclin-D pathway (CDK4/6 and Cyclin D genes) (Obaya et al., 2002) (Liao et al., 2007) (Qu et al., 2014). Greater effect of drug-loaded worms is

consistent with previous experiments, as well as with the hypothesis that lower levels of Ki-67 dictate the loss of proliferation in surviving cells.

In the scenario of acquisition of resistance, the anti-correlative trend in Figure 6.17 C supports the observation that this drug resistance can be a burden to cell proliferation (Wilson et al., 1997) (Lee, 1993). It must be mentioned here, that the resistant colonies were expanded and given sufficient time to recover from the stress of exposure to drugs. The cells were isolated, grown with fresh media and passaged for about 200-250 cell cycles before any measurements were conducted, suggesting that the acquired resistance was not transient. This observation, coupled with the rapid proliferation rate of EC4 cells, suggests a situation where resistant cells that may arise, would have a distinct proliferative disadvantage and would eventually be outcompeted by normal cells that escape the effect of drug. Hence, even if resistant cells may arise after RA-TAX treatment, they will be outcompeted, resulting in a less resistant tumor. At this point, they may be treated again and the whole process will be repeated. Similar rationale has been used to develop competitive therapies such as 'evolutionary double bind therapy' (Cunningham et al., 2011) (Orlando et al., 2012) (Gatenby et al., 2009), and could one day be an integral part of chemotherapy.

Extension of durability of RA-TAX treatments to in vivo models was done with subcutaneous xenografts in NOD-SCID mice. Both free RA-TAX as well as RA-TAX worms produced tumor shrinkage, and all treatments were durable, with tumor sizes

remaining almost constant ~20-25 days after treatment. TAX and RA dosages used were low in the first three experiments, with TAX doses an order of magnitude lower than the MTD (Christian et al., 2009), and then gradually ramped up in future ones. This precaution was borne out of the *in vitro* dose responses that indicated that RA-TAX combination was more potent than TAX, and one might stand to reason, should have lower MTD than it. This was reflected in the later experiments (Figure 6.27 C and D), where mice did not gain weight like they did previously (Figure 6.27 A and B). However, RA-TAX treated mice lost little weight unless they were old (~8 months).

Finally, having built up the entire rationale on the vitality of RA to liver function, we tested RA-TAX worms on mice bearing orthotopic tumors. RA-TAX treated mice had their liver tumors shrunk, while TAX failed to do so, validating our reasoning. However, mice with orthotopic liver tumors exhibited a higher mortality rate than NSG mice with only subcutaneous tumors, which might presumably be due to compromised liver function, leading to shutdown of vital processes (El-Serag et al., 2008)(Shirabe et al., 1999). But, as seen in Figure 6.18, the efficacy of the combination can be extended to cells derived from tissues outside the liver. This might suggest that the success of the combination might hinge on a function of RA that is common to all cells. RARs and RAREs regulate a number of processes in all tissues and one of these might be the target of this combination, one that ultimately impacts at least protein synthesis (as seen by lower Ki67 levels). Larger scale studies, transcriptomics and proteomics might help elucidate the same. The focus of this study however, has been to highlight two key improvements over conventional chemotherapy: i) the benefits of a chemo-differentiative

therapy over single drug treatments or combination of chemotherapeutics, and ii) the

improvement offered by nano-carriers, that greatly increases efficiency by better delivery,

increased loading and may shield the payload from any unnecessary interactions

(degradation or complexation). While the concept of chemo-differentiation has been

demonstrated in the case of APL (Jing et al., 2001) (Soignet et al., 1998), the advantages

of nanocarriers are yet to be fully appreciated in a clinical.
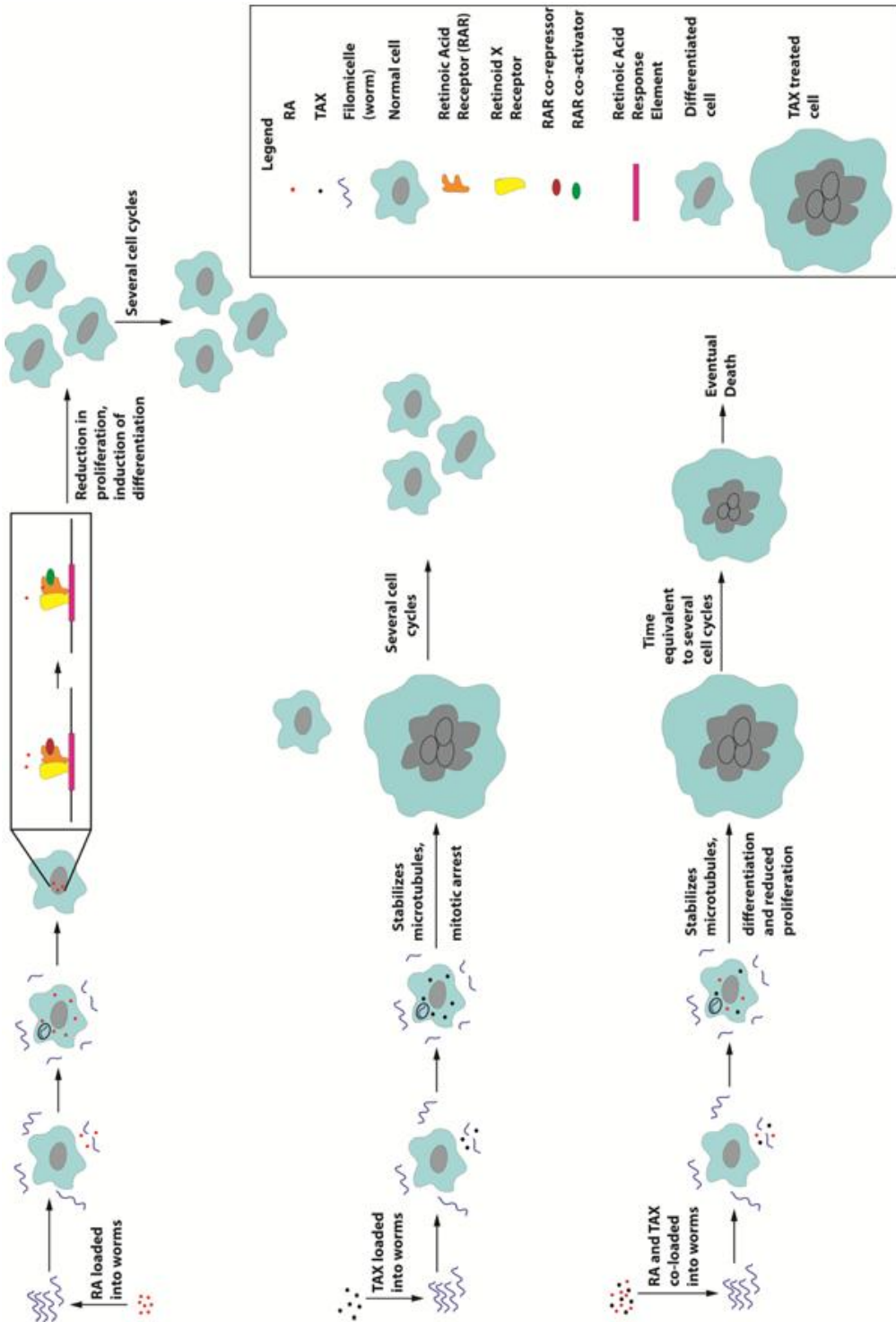
Figure 6.1. Durability of combined RA-TAX treatment. Each drug has its own mode of action, but the effects are transient with single drug. Dual drug treatment is more irreversible and can reduce drug resistance.
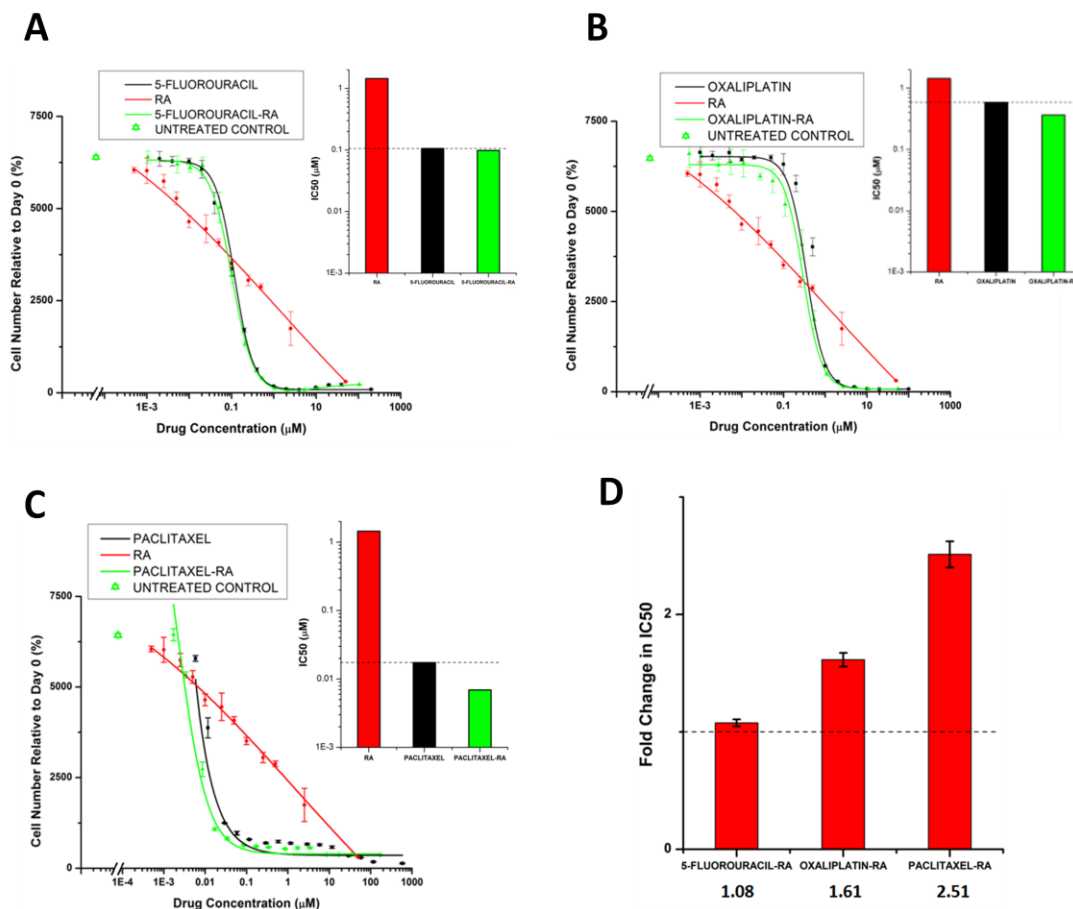
Figure 6.2. Synergy between different drugs tested with free drug solutions.

Combinations of RA with **A)** 5-Fluorouracil, **B)** Oxaliplatin, and **C)** Paclitaxel. While all

combination treatments had a lower IC50 on EC4 cells than the involved

chemotherapeutic, the change in IC50 was different for each combination. Empty symbol

represents untreated control. **D)** Bar graph representation of the fold change in IC50 with

RA-drug combination. Combination of 5-fluorouracil shows negligible change in IC50,

and oxaliplatin-RA showed a 1.6 fold change in IC50, signifying some synergy.

However, combination of RA and Paclitaxel had a 2.5 fold reduced IC50 than parent

chemotherapeutic (Paclitaxel), signifying maximum synergy among the three

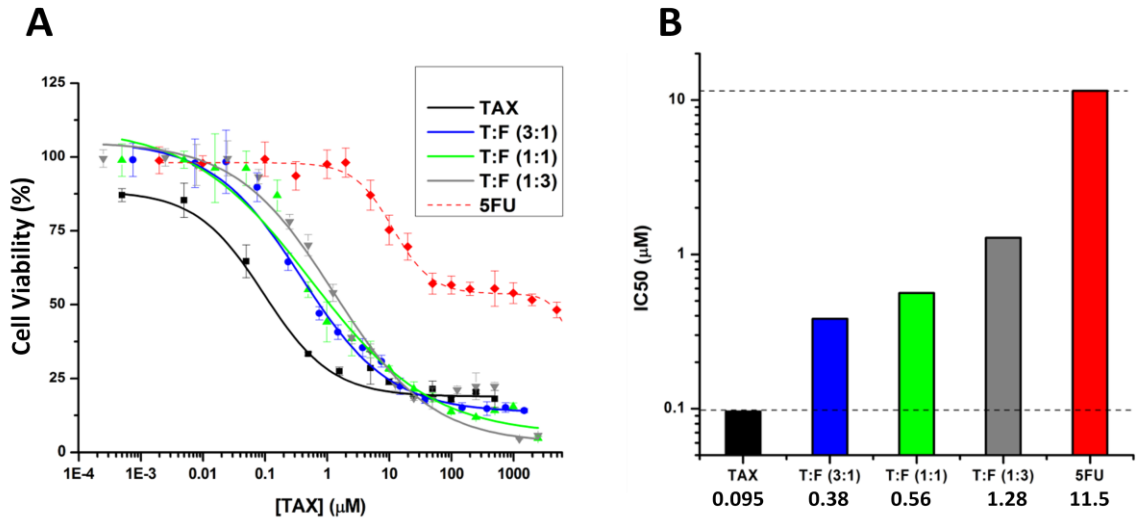combinations and the best candidates for further experiments.

Figure 6.3. A) The combination of Paclitaxel with 5-Fluorouracil depicts combination chemotherapy. Curves of drug combinations (tested on A549 cells) lie between that of the single drugs indicating lack of synergy. **B)** Bar graph depiction of the IC50 quantification of Paclitaxel-5-Fluorouracil combinations.
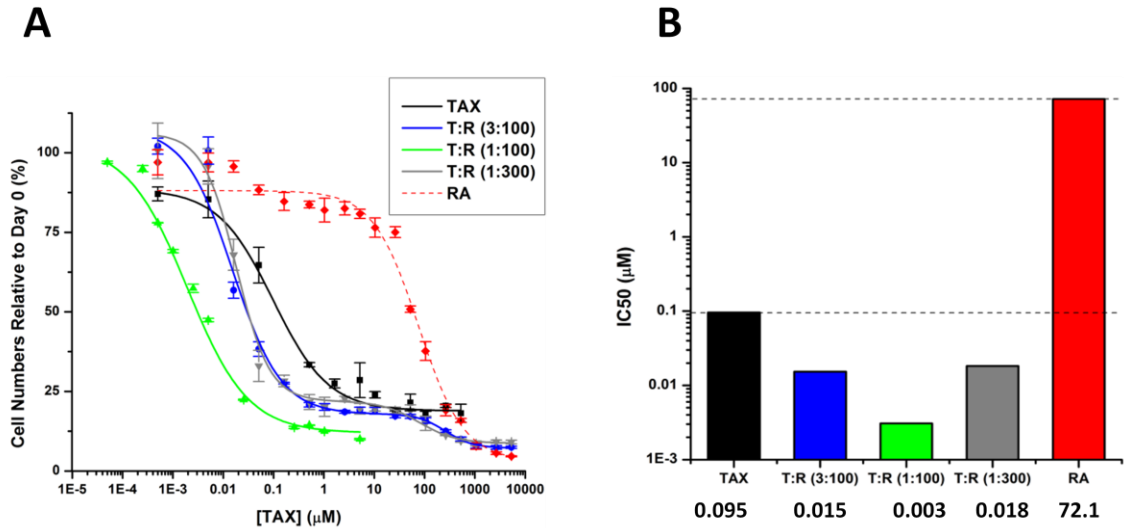
Figure 6.4. A) Combination of a Paclitaxel (black curve) with RA (red) for a chemo-differentiative treatment is better than that of two chemotherapeutics. Curves of combinations lie beyond (left) of either single drugs when tested on A549 cells, hinting at synergy between TAX and RA. Combination at 1:100 molar ratio (green curve) between TAX and RA respectively was the most potent combination. **B)** Bar graph depiction of the IC50 quantifications of the free drug combinations tested in Figure 6.4 A
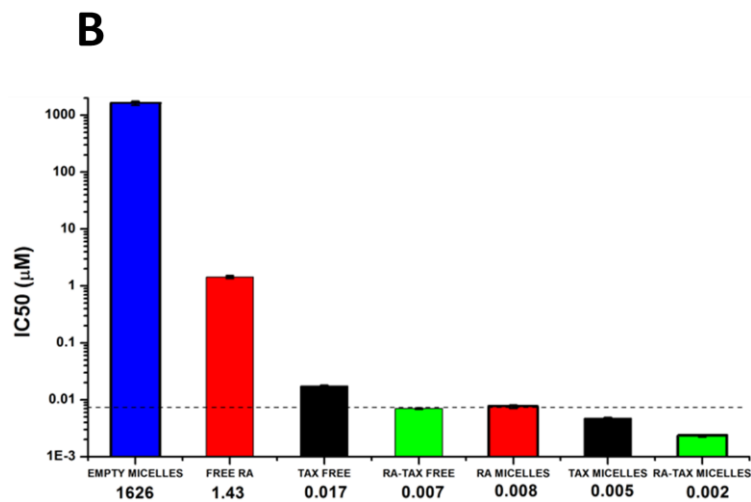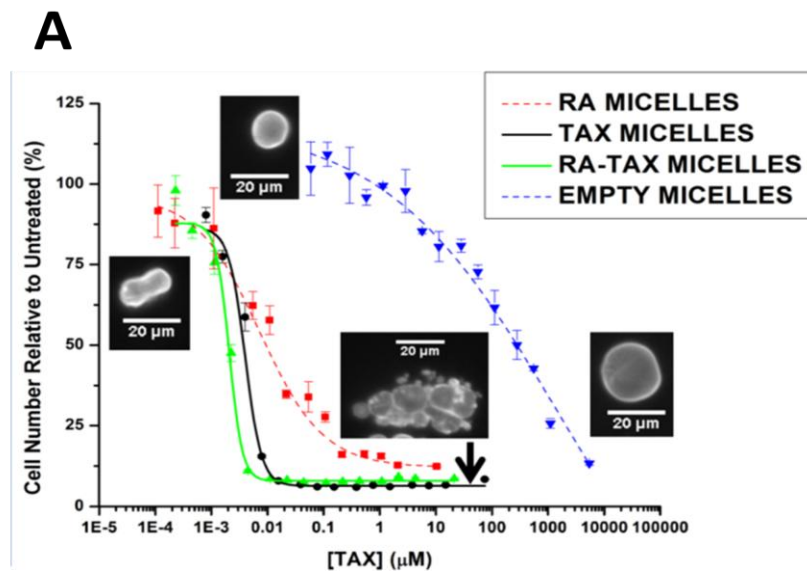
Figure 6.5. A) Testing of RA, TAX, and RA-TAX loaded worm micelles on EC4 mouse

liver cancer cells. TAX (black) has a much lower IC50 than RA (red) as it induces

apoptosis instead of arresting proliferation. However the combination of RA-TAX is

more effective than either drug alone, with its IC50 less than half of that for TAX. Empty

micelles (blue curve) were inert at the desired concentrations. Nuclei treated with

Paclitaxel (TAX) exhibit massive blebbed nuclei due to incomplete division (bottom).

Untreated nuclei (top) in contrast are smooth and rounded. **B)** Bar graph representation of

IC50 of different formulations. Micellar RA-TAX had the lowest IC50 among all tested formulations; almost 3 times lower than that of free drug.
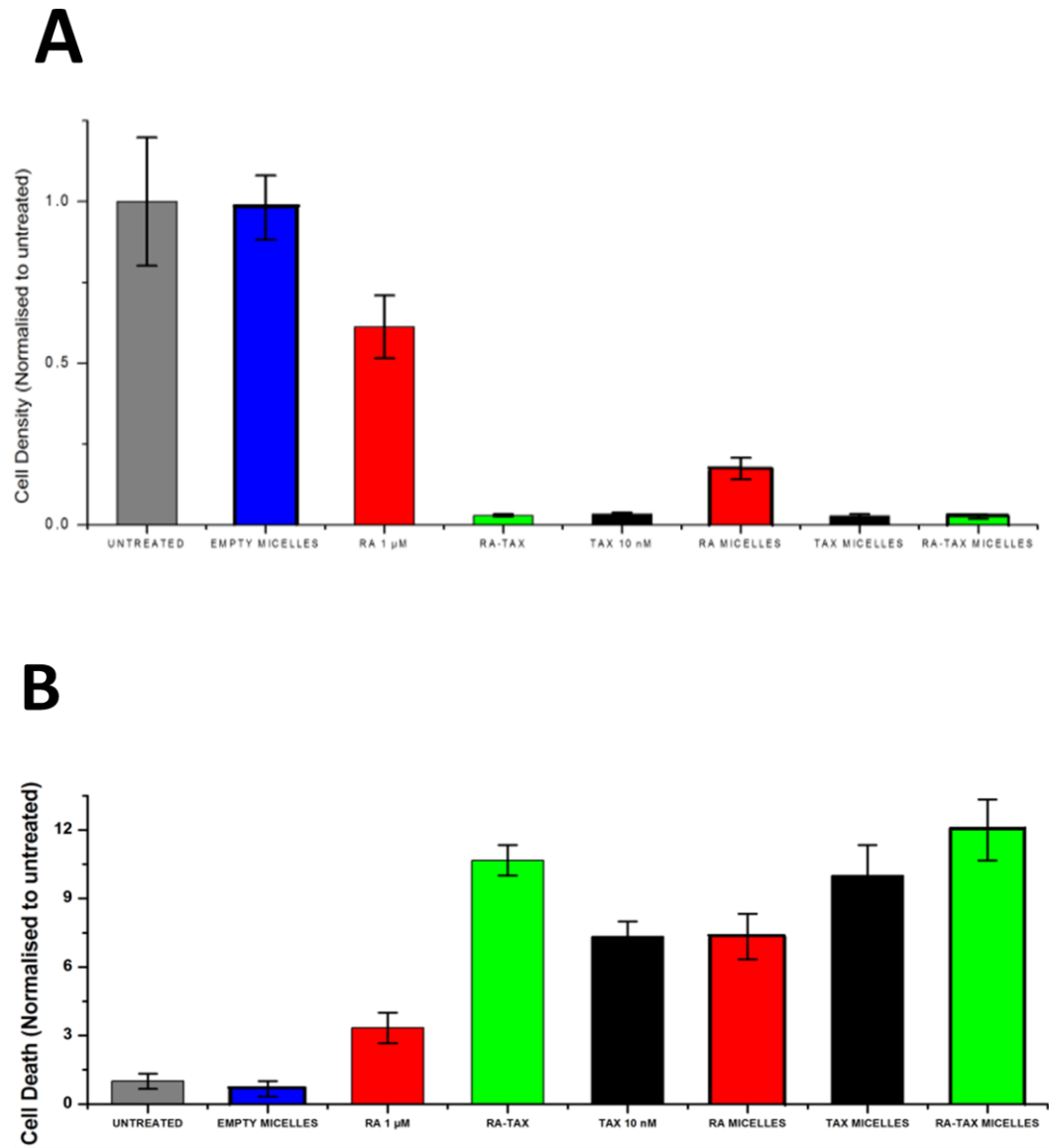
Figure 6.6. Cell density and Cell death measurements done on well plates further highlight the potency of the system. RA-TAX treated cells had the lowest cell density on plate (A) and the highest cell death (B). As with previous experiments, worms were more effective than free drug.
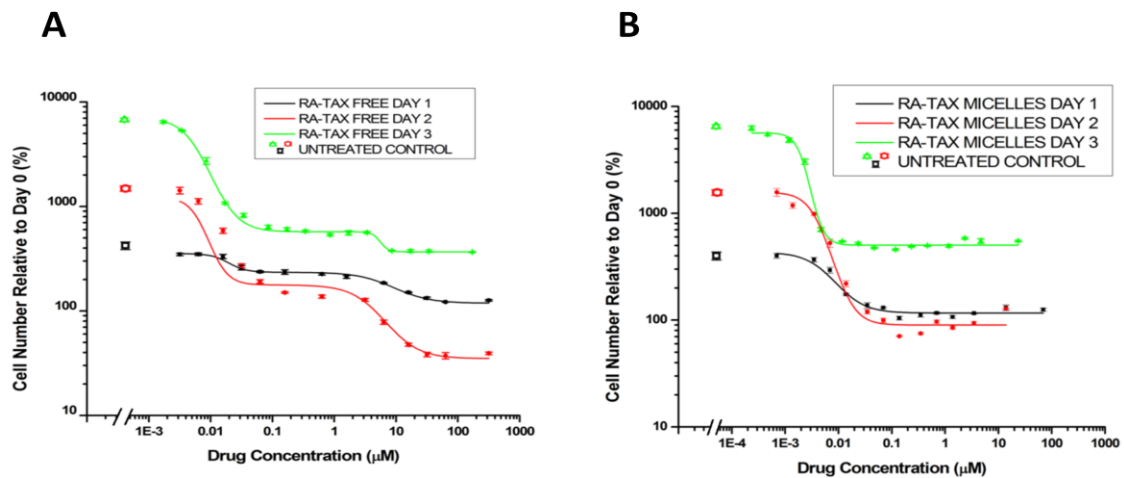
Figure 6.7. Kinetic studies reveal an effect as early as a day, with peak death observed after two days. Complexation of RA with albumin, hydrolysis of TAX, and subsequent recovery may limit the efficacy of the drug in free form. These limitations may be overcome to certain extent by loading them onto worms.
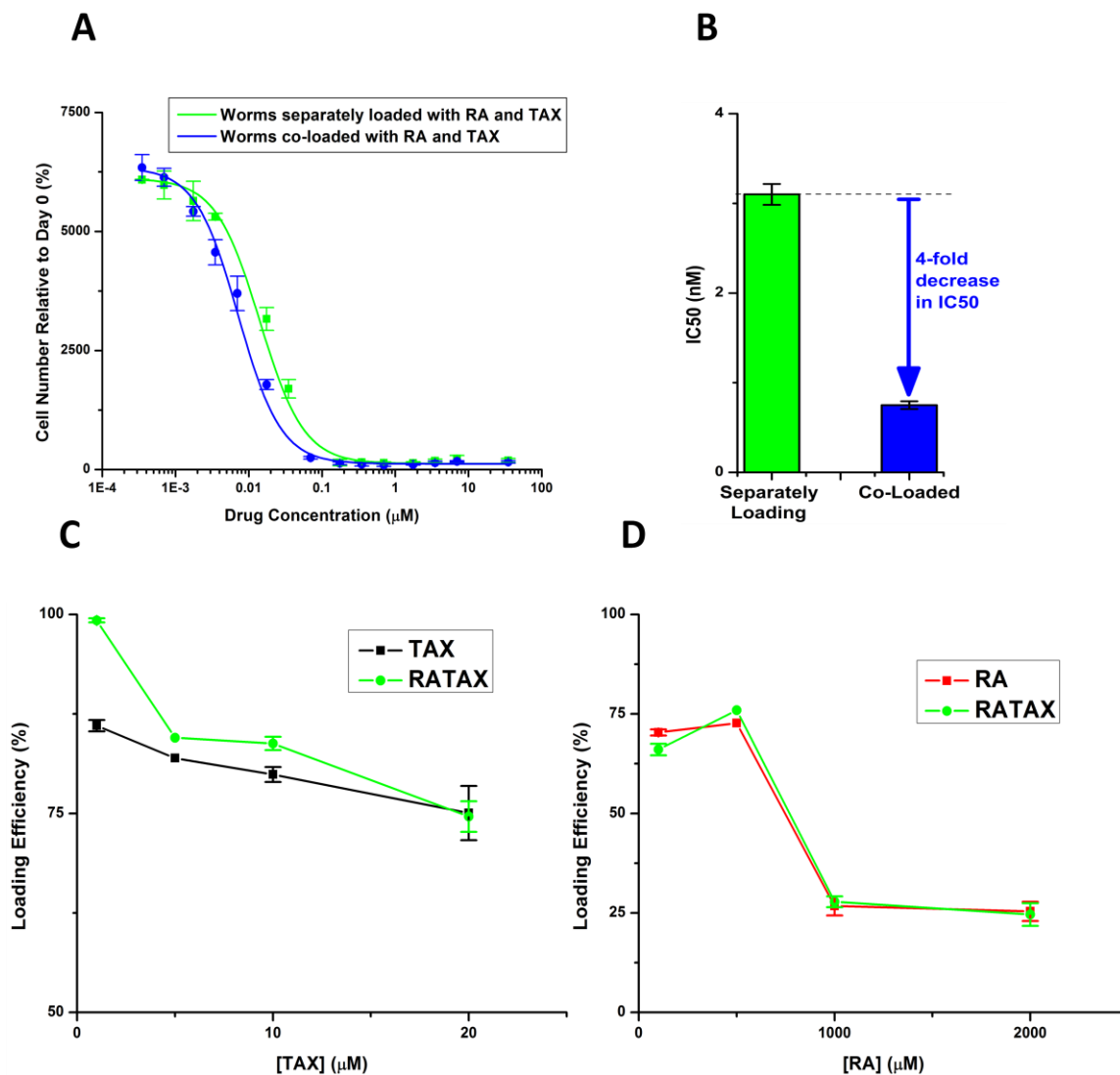
Figure 6.8. A and B) Delivery systems with two payloads can be co-loaded onto the same micelle or on separate micelles which are then mixed. At high concentrations, both are equally effective. However, at therapeutic concentrations (around IC50), co-loaded micelles are 4 times more potent than separately loaded worms (quantified in bar graph). At lower concentrations, separate loading is beneficial. Co-loading of drugs does not decrease encapsulation efficiency of either drug (compared to separate loading **C)** and **D)** Quantification of drug loading efficiency with change in added drug concentration reveals a decrease with increasing concentrations (as expected). Vitally, there is no loss

161

in integration efficiency between single and dual drug loading for either drug. Presence of RA may help increase the loading efficiency of TAX, although a reciprocal effect seems to be absent with RA loading.
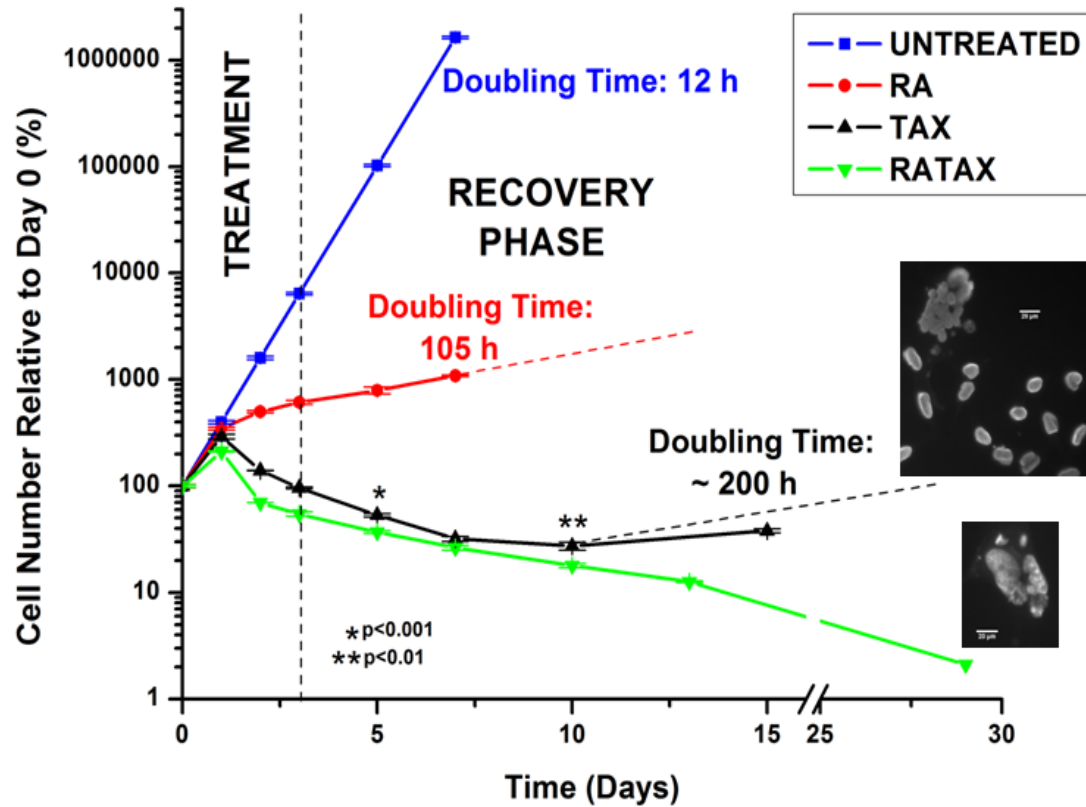
Figure 6.9. Cells treated with RA consistently increase in number. This is consistent with RA not killing cells, just differentiating them, and the difference in slopes indicate that a fraction of the cells exposed to RA have been differentiated and have lower proliferation. TAX treated cells decline in number initially (similar to initial tumor shrinkage), but cell death plateaus after a week when proliferating cell numbers overtake dying ones. RA and TAX treated cells, on the other hand, consistently decrease in number, indicating a more durable treatment. Around 30 days after treatment, all cells die off.
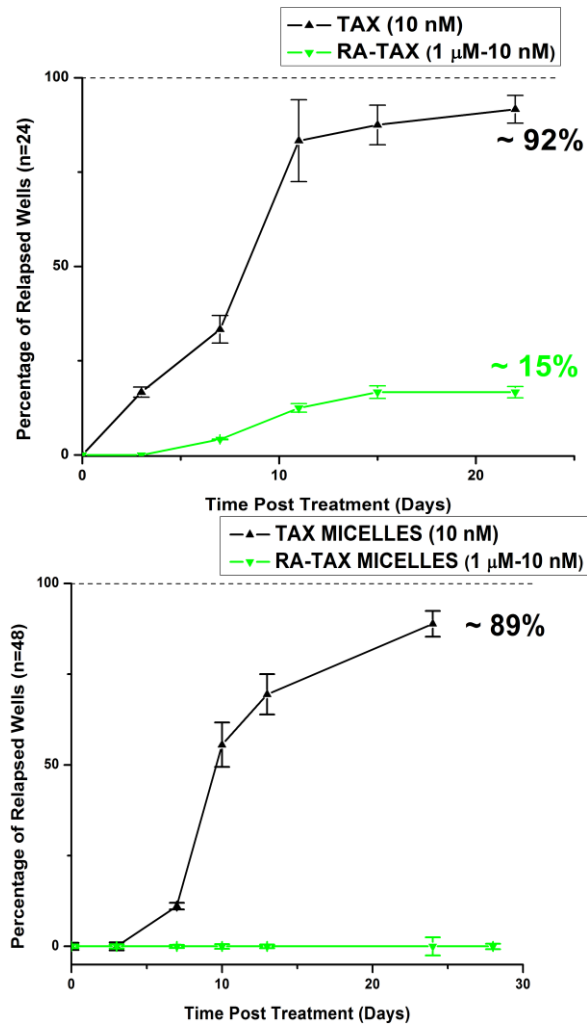
Figure 6.10. Consistent with previous plot, most cells treated with TAX relapse (92%), the rate is much lower for RA-TAX treated cells (15%) 22 days post treatment, indicating that around 85% of cells (and their progeny) exposed to RA-TAX die off, indicating a much more durable treatment than single drug like TAX. Loading TAX onto micelles increase efficacy, but only manage to delay the relapse (89% of TAX treated wells experienced relapse), highlighting the limitation of a single drug. It also interesting to note that loading TAX onto micelles delays relapse compared to free TAX. The efficacy of RA-TAX was greatly improved via loading onto micelles, with no relapses in cells observed after 30 days.
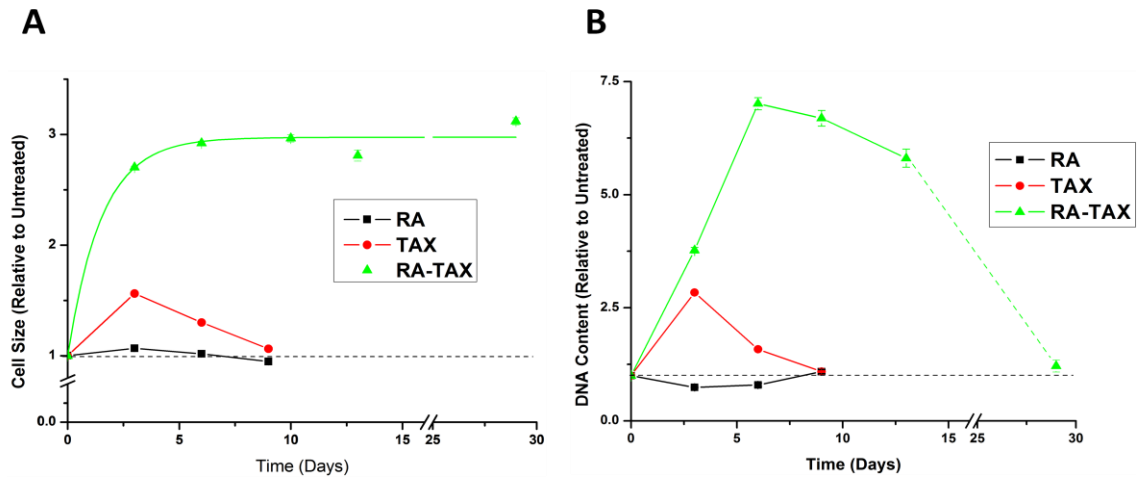
Figure 6.11. Quantification of DNA content and cell size after drug treatment. DNA content increases for TAX and RA-TAX due to incomplete cell division; it decreases for RA due to lower number of proliferating cells (and hence lower DNA replication before division). DNA content for cells treated with single drugs return to normal after about 6 days (about 3 days after treatment), indicating the transient nature of single drugs, whereas DNA content for RA-TAX decreases much slowly. While DNA content decreases as cells with high accumulation die off with time, DNA synthesis might be inhibited after exposure to RA-TAX combination, which might prevent them from rising again. Increased DNA accumulation leads to bigger nucleus and hence larger cell size. DNA content with time for cells with rescue performed after treatment with RA, TAX and RA-TAX. Cell size for single drugs return to normal within 3 days, indicating the transient nature of single drugs that has been underlined throughout this study. But they remain consistently high for combination treatment.

166
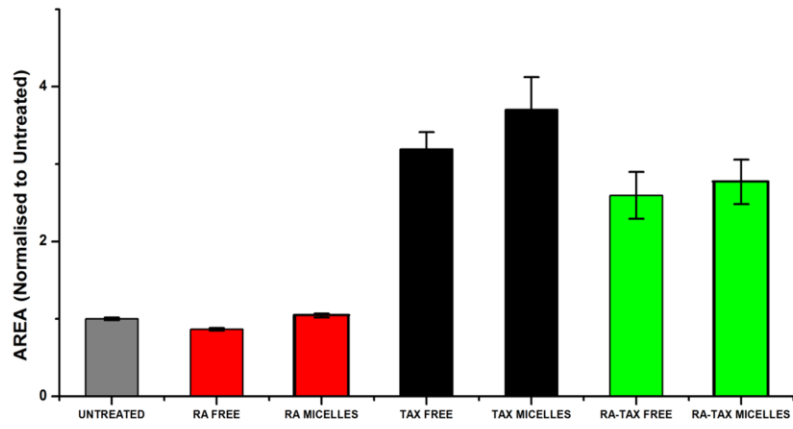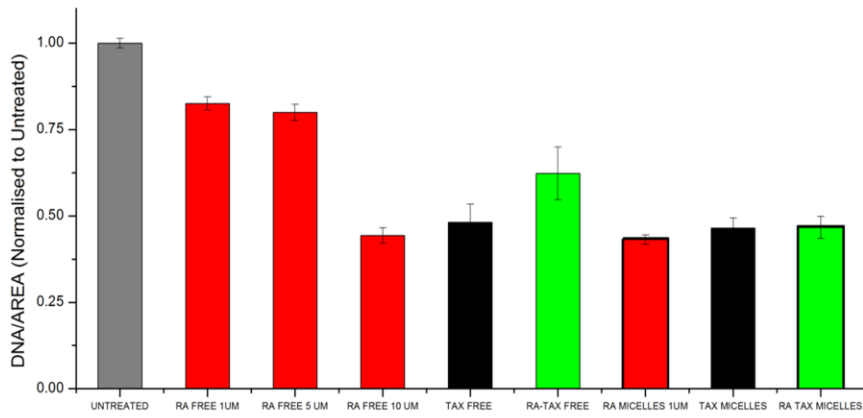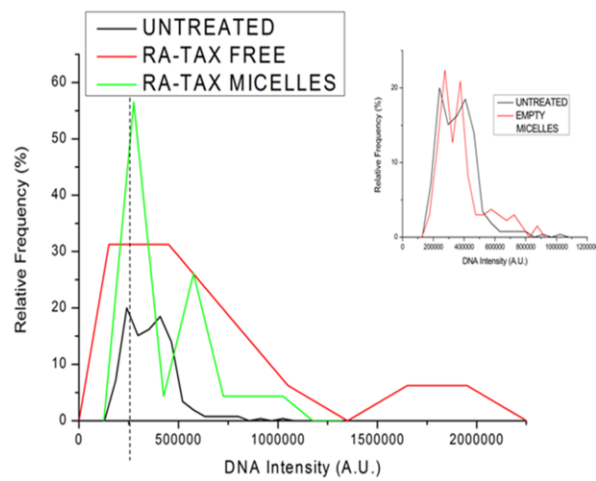
Figure 6.12. A) Treatments involving TAX causes about a 3-fold increase in nuclear area compared to untreated nuclei. While the presence of RA decreases the area slightly as compared to nuclei treated exclusively with TAX, the effects of TAX are still evident in images and DNA distribution. **B)** All drug treatments decrease levels of DNA (normalized to area), through different mechanisms. RA halts cell-cycle, while TAX prevents nuclei from splitting after division, both ultimately affecting DNA synthesis. **C)** DNA histogram of treated and untreated cells show polyploidy in surviving cells as well as a reduction in the replicating fraction. Post treatment with RA-TAX, most cells exhibit DNA intensity greater than 4N, signifying polyploidy. This effect is further enhanced with encapsulated drugs. Empty nanocarriers do not appreciably change this distribution (inset histogram).
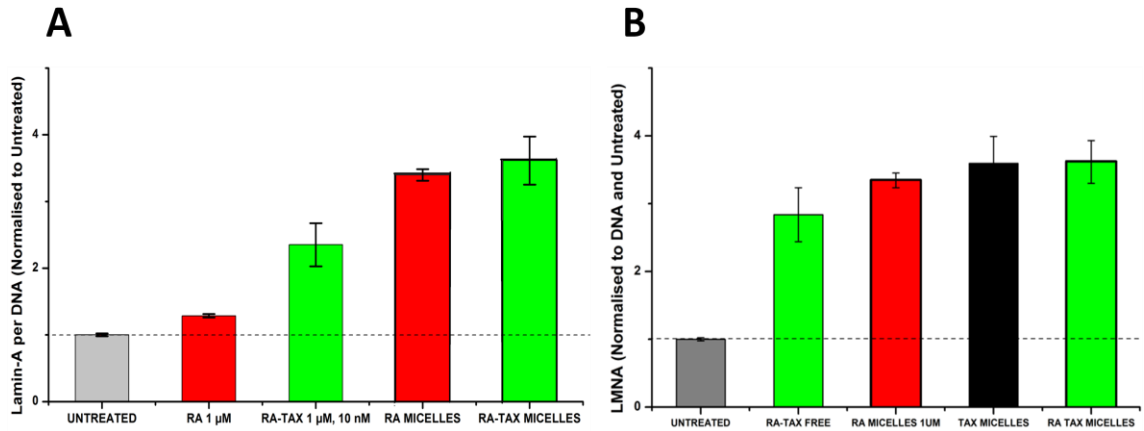
Figure 6.13. A) RA and TAX treated cells were found to have higher levels of lamin-A than untreated ones, suggesting differentiation. Lamin-A levels were higher for drugs delivered via nanocarriers, than for free drugs. **B)** As with RA, treatment with TAX or RA-TAX increased Lamin-A levels.
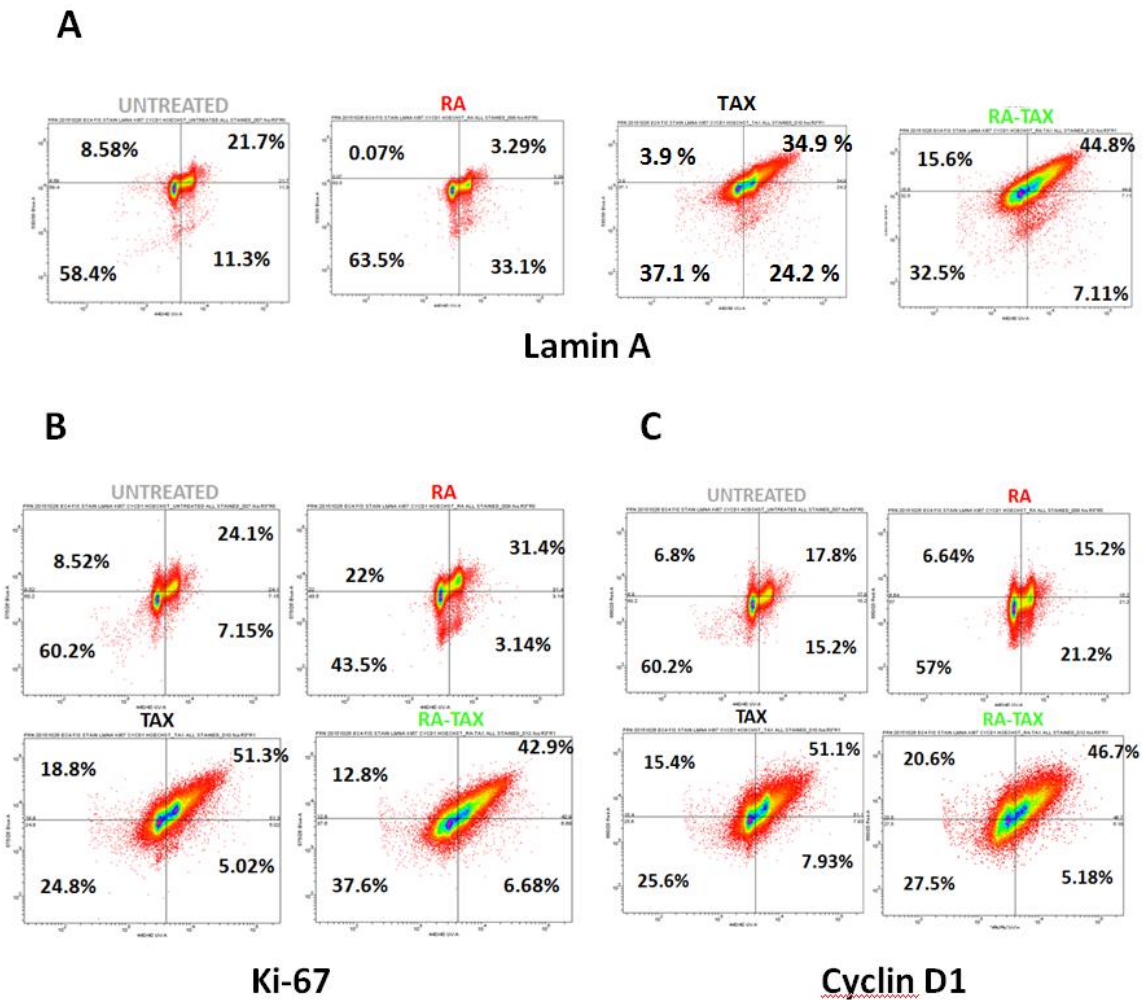
Figure 6.14. Flow cytometry scatter plots for **A)** Lamin A, **B)** Ki67 and **C)** Cyclin D1 on the y-axis and DNA (Hoechst) on the x-axis.
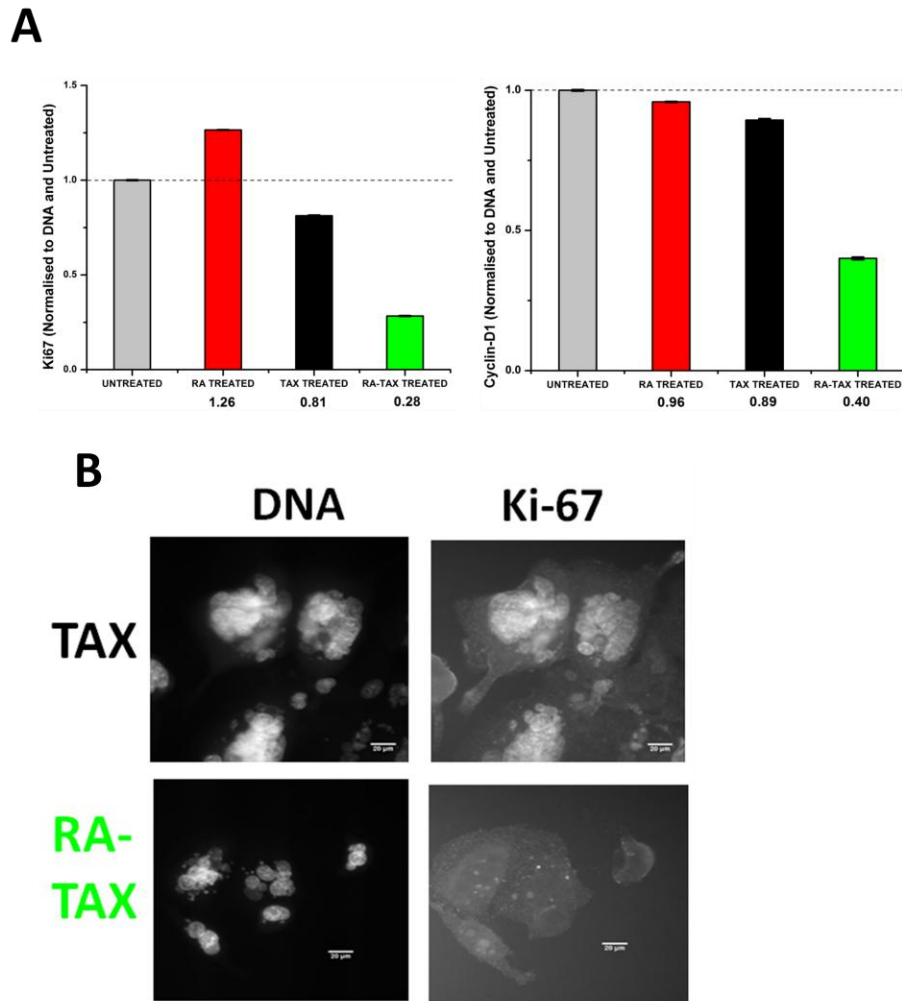
Figure 6.15 A) RA-TAX treated cells have lowest levels of Ki-67 (left) and Cyclin-D1 (right) than either TAX or RA alone treated cells. Cells treated with RA have lower Cyclin D1 as RA decreases cell proliferation. Hence the durability of RA-TAX combination might be explained by its inhibitory role on protein synthesis (via Ki67) and to a lesser extent, the regulation of cell cycle (CyclinD1). **B)** Images (40x magnification) of cells treated with TAX alone (top) and with RA-TAX combination (bottom). While Hoechst intensities are similar (images on the left), cells treated with TAX alone still

stain positive for Ki-67 (top right), while those treated with RA-TAX are null for the

same (bottom right).
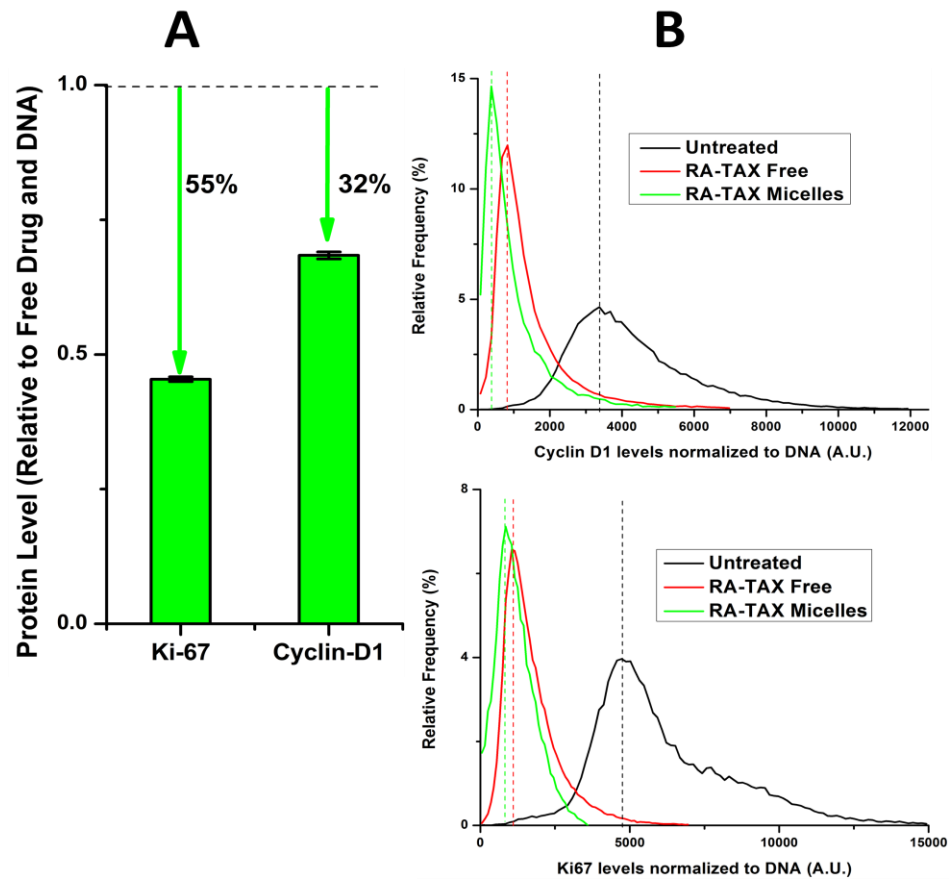
Figure 6.16 A) Delivery of drugs via worms has been proven to be superior to free drugs, and this mode further reduces levels of these two proteins, with Ki-67 levels being halved compared to free drug treated. **B)** Histogram of Ki67 and Cyclin D1 levels after treatment with various drugs loaded onto worms. The fraction of cells null for these proteins progressively increases from no treatment to free drug to micellar drug delivery. Lower the levels of these proteins, lower will be cell proliferation.
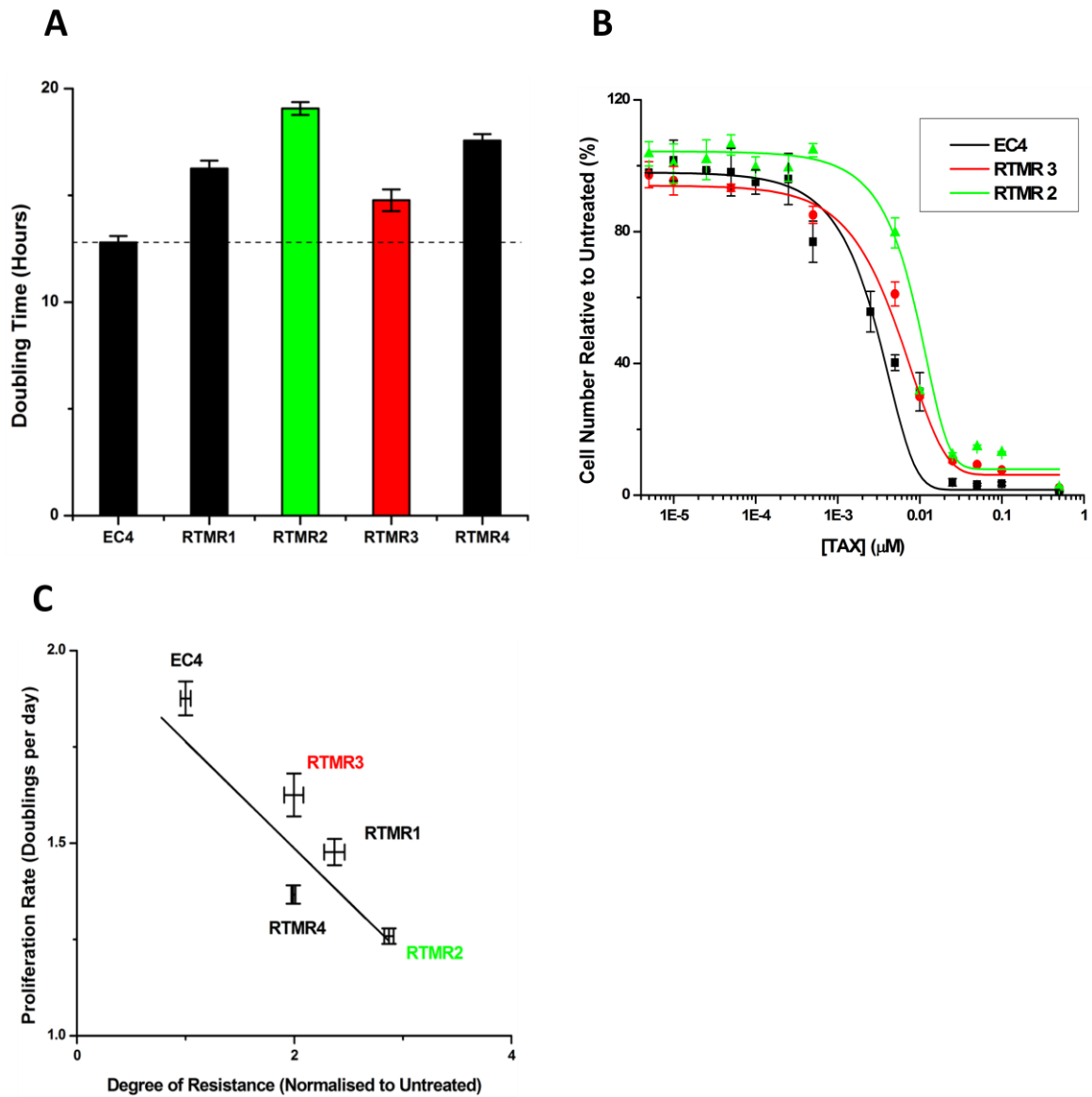
Figure 6.17. A) Quantification of doubling time of RA-TAX micelle resistant (RTMR)

EC4 cells. All RTMR cells proliferate slower than untreated EC4 cells**. B)** Quantification

of response of RTMR cells to RA-TAX treatment. As expected, RTMR cells have higher

IC50 than WT EC4 cells, and hence higher resistance to RA-TAX treatment. However,

true resistance to drug treatment was been acquired by the resistant colonies. **C)** Resistant

colonies arising in after RA-TAX worm treatment were expanded further. RA-TAX

Micelle Resistant (RTMR) EC4 cells proliferate slower than untreated EC4 cells, but

have higher resistance to RA-TAX treatment. Plotting the proliferation rate against the degree of resistance gives an inverse relation, supporting the hypothesis that acquisition of drug-resistance occurs at the cost of proliferation.
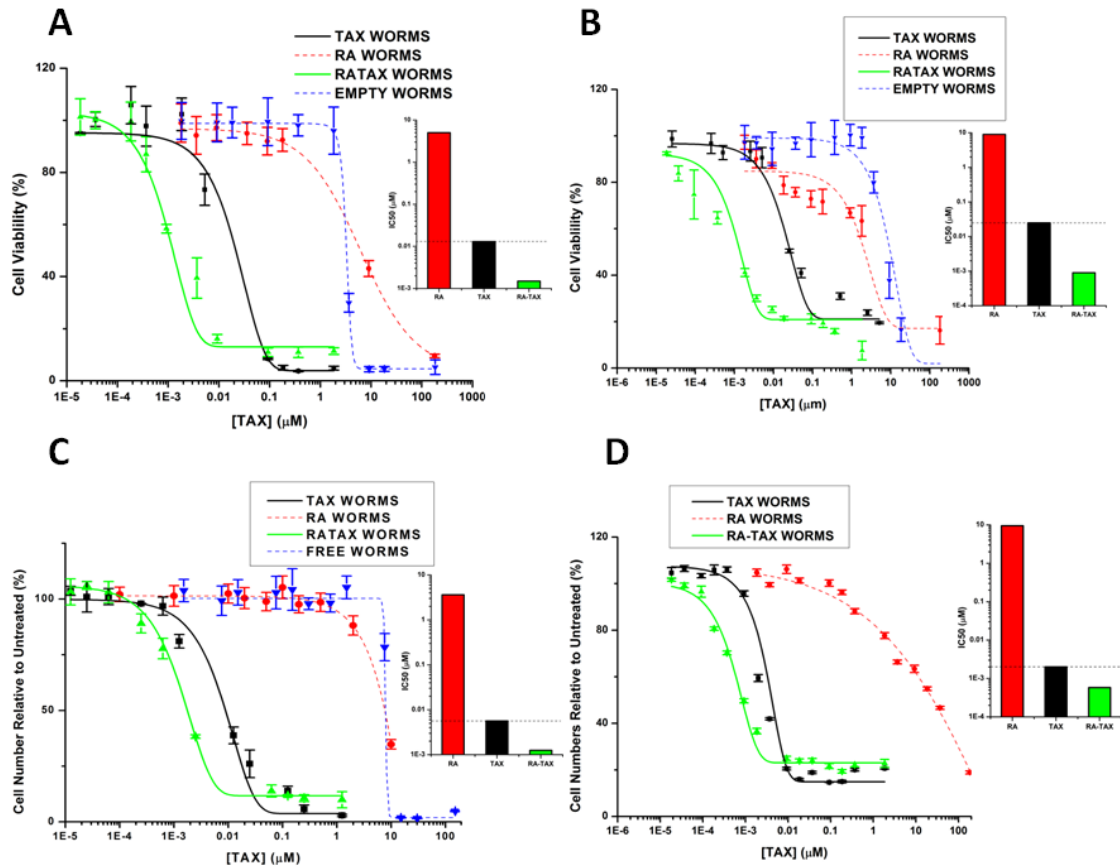
Figure 6.18 A) The efficacy of RA-TAX combo is not limited to the EC4 mouse liver cancer cell line. It is just as effective in huh7, which is a human liver cancer cell line. This is despite the fact that both RA and TAX are not as effective as they were with EC4 cells. **B), C), and D)** This combination was tested on A549s, U2OS, and RH30 which are human lung adenocarcinoma, osteosarcoma and rhabdomyosarcoma cell lines respectively. The dual drug treatment retained its efficacy despite varying responses to TAX and RA (as measured by IC50 values) across cell lines derived from different tissues of origin.
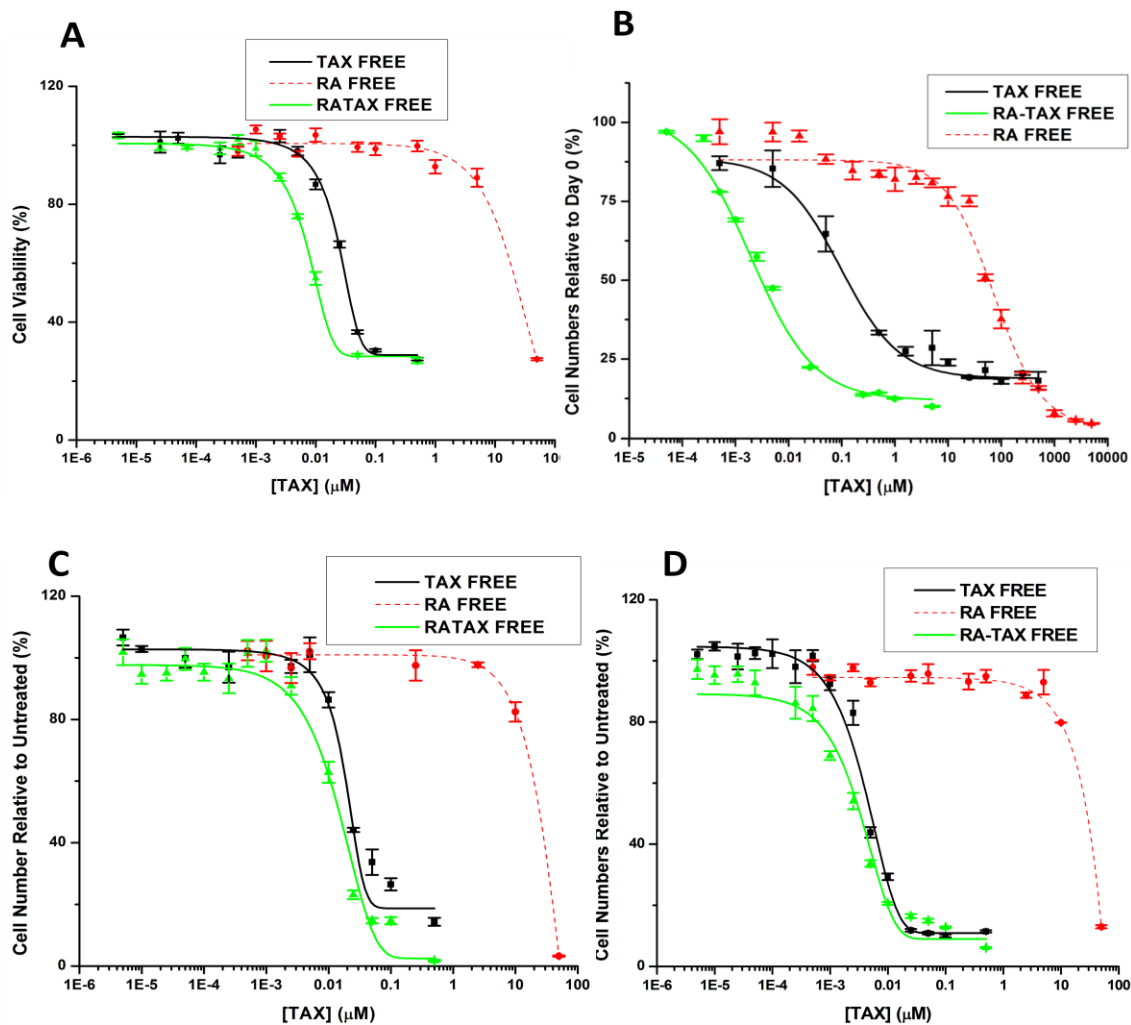
Figure 6.19: Dose response curves for free drug treatments with **A)** Huh7 (human hepatocellular carcinoma), **B)** A549 (human lung epithelial adenocarcinoma), **C)** U2OS (human osteosarcoma), and **D)** RH30 (human rhabdomyosarcoma) cell lines respectively. The dual drug treatment retains its efficacy despite varying responses to TAX and RA across different cell lines.
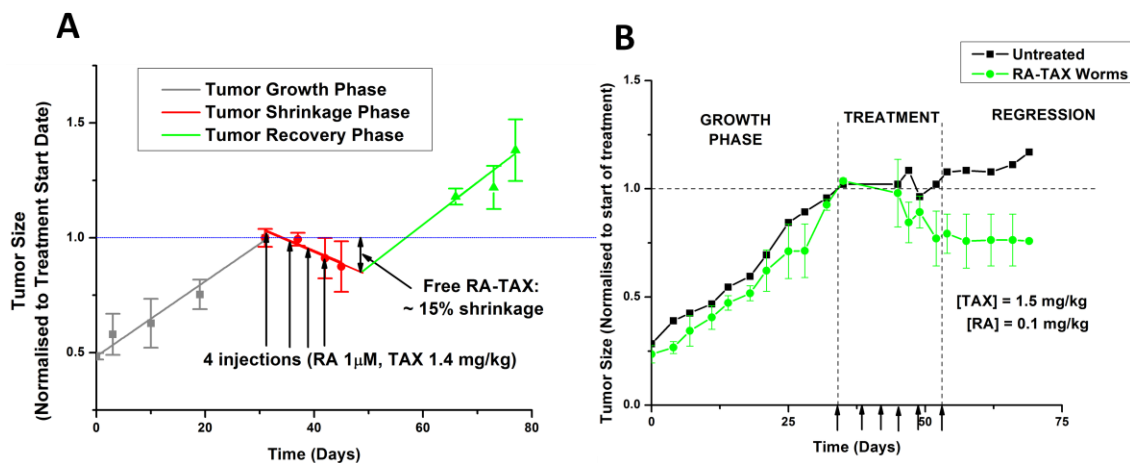
Figure 6.20 A) Free RA-TAX injections in nude mice with A549 xenografts led to a 15%

shrinkage in tumor size after 4 injections over the course of 11 days. Treatment was

started at day 31 and tumors shrank till day 49, after which the resumed an upward trend.

B) Six injections of RA-TAX loaded worms led to 25% shrinkage of A549 subcutaneous

tumors, and most importantly, the tumors did not resume an upward trend nearly 45 days

from the start of the treatment.
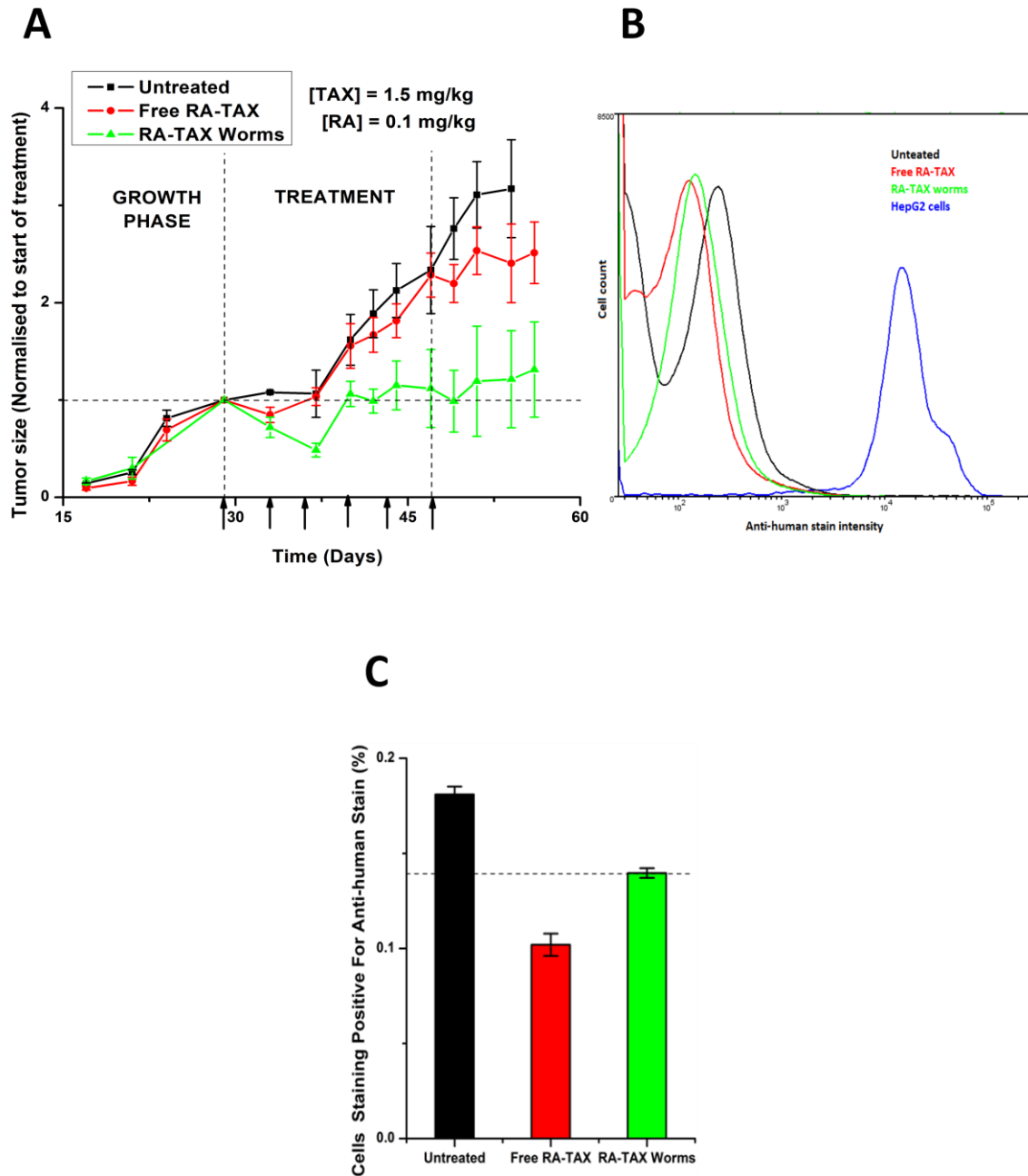
Figure 6.21 A) Injections in NOD-SCID mice with HepG2 subcutaneous tumors

suppressed the growth of tumors. In mice treated with RA-TAX worms, the tumors grew

by 30%, while untreated tumors more than tripled in size during the same time frame (3.2

times from the start of treatment). Unlike A549 xenografts, free RA-TAX produced

minimal retardation in tumor growth, with final size 2.5 times from the onset of

treatment. RA-TAX worms with increased drug dosage was tested on mice with subcutaneous and orthotopic liver A549 xenografts. **B)** Histogram of anti-human staining intensities of HepG2 tumors to detect HepG2 cells among mouse cells. HepG2 cells from culture (blue curve) elicited a much higher signal than cells from tumors. **C)** Quantification of Fig. 6.21 B shows that the proportion of HepG2 cells in tumors is very low (<0.2%). This number decreases further with drug treatment.
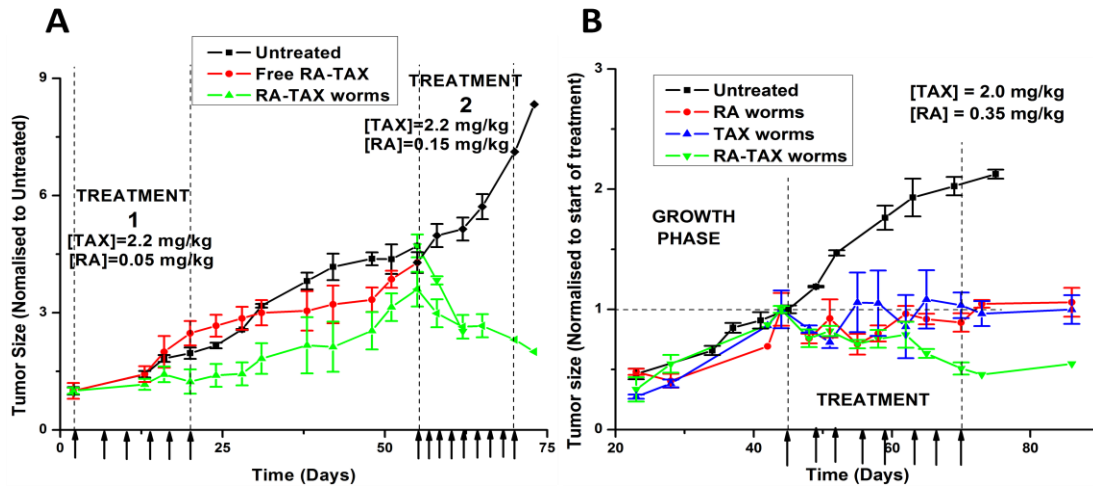
Figure 6.22 A) Lower dosage of RA failed to shrink tumors in A549 subcutaneous tumors, although it did retard its growth. Second treatment at higher RA concentration produced shrinkage in both treated groups (previously untreated and RA-TAX worms treated). Mice that had been injected with free RA-TAX previously were the untreated controls in the second round. **B)** RA-TAX worms shrunk subcutaneous A549 tumors by ~50%. Single drug controls arrest the growth of tumors 30 days from the start of the treatment. During the same time frame, untreated tumors more than double in size.
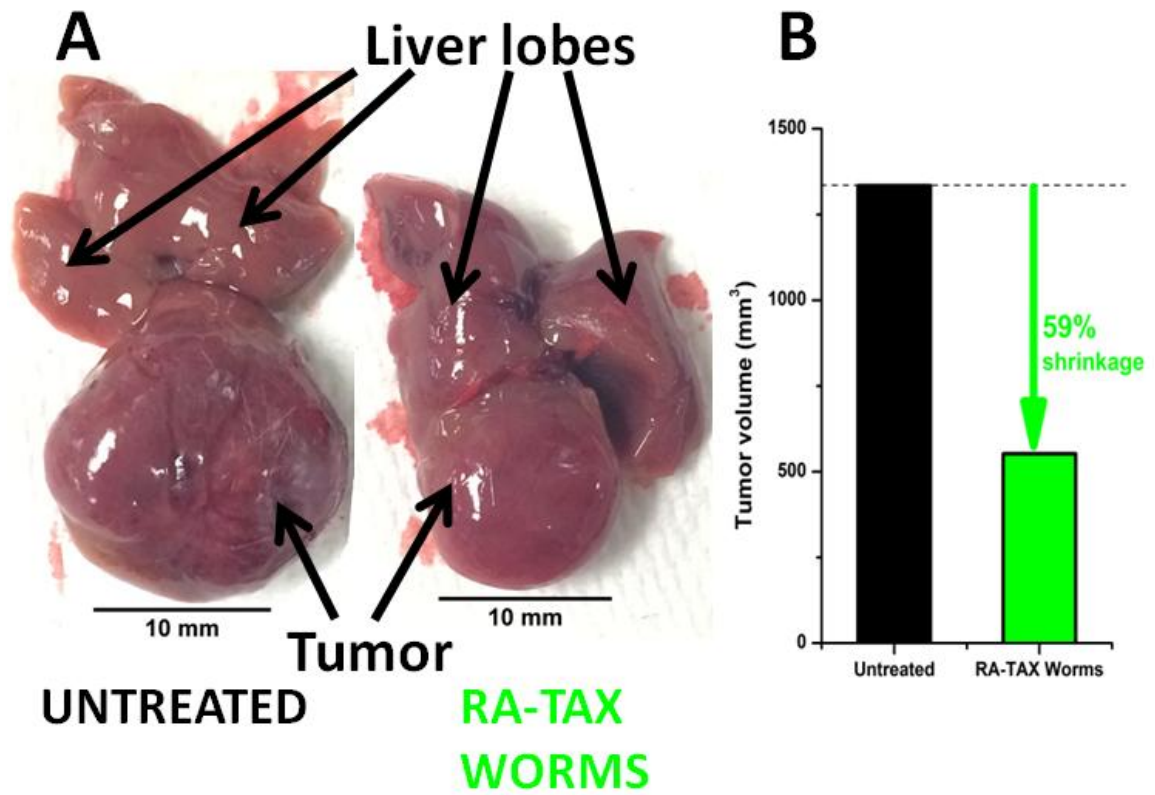
Figure 6.23. Orthotopic liver tumors established *in vivo* from HepG2 cells. RA-TAX

treated tumors are 65% smaller than untreated tumors as quantified in the bar graph.
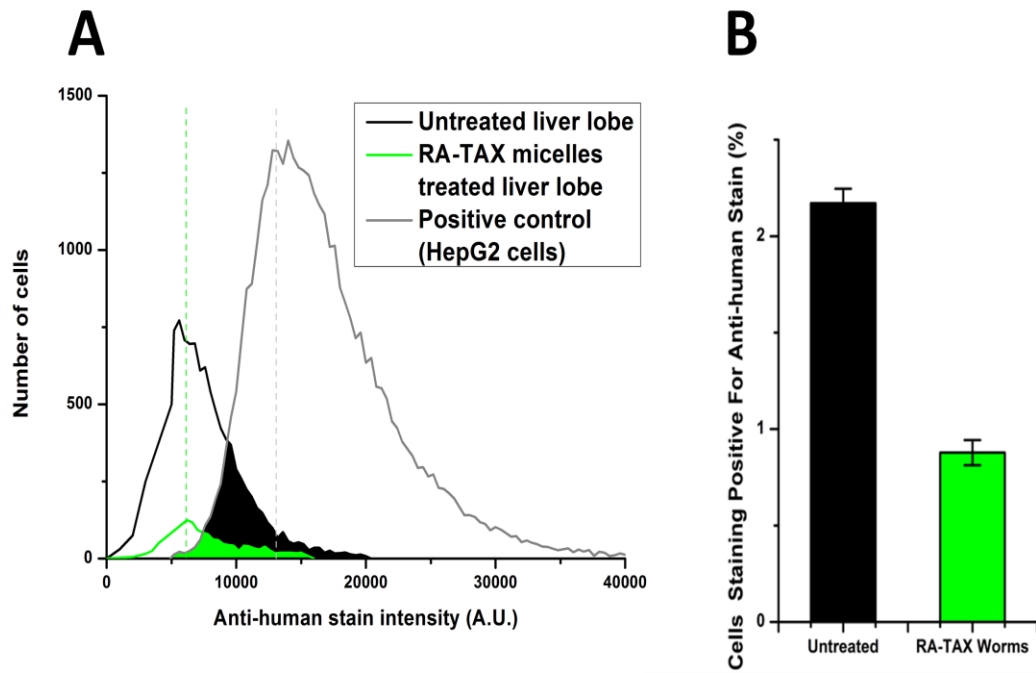
Figure 6.24. Liver lobe adjacent to that containing the tumor, were disaggregated and stained with Anti-human antibody to identify number of HepG2 cells metastasizing from orthotopic tumors. Untreated lobe shows a much larger peak of anti-human staining (black shaded region), indicating migrated cells, which is minimal in treated mice (green region). Quantification of cells staining positive is depicted in the bar graph.
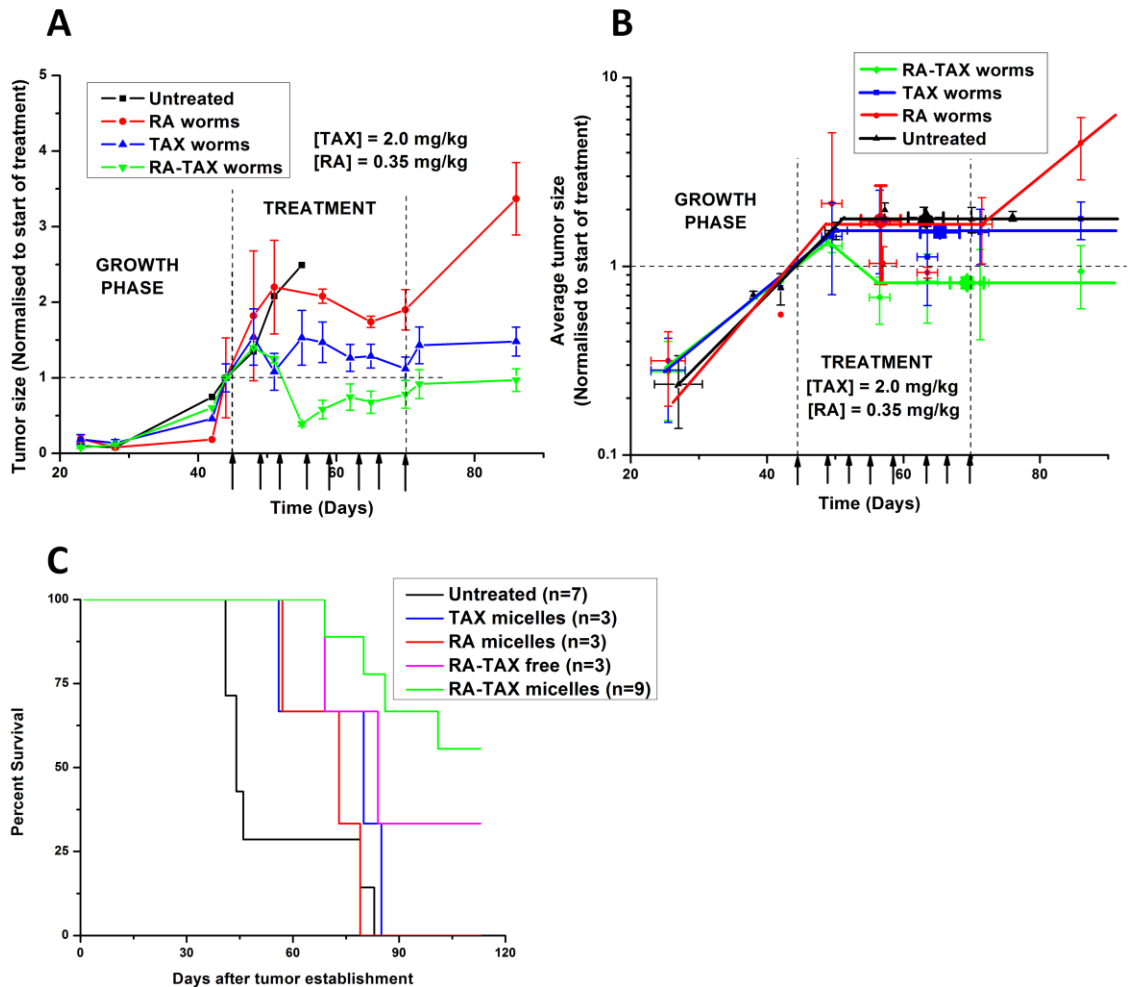
Figure 6.25 A) RA-TAX worms were efficacious with orthotopic A549 liver tumors.

They shrunk and arrested the growth of tumors, while single drugs failed to do both.

While TAX controlled the growth of tumors, those treated with RA continue to grow.

B) Quantification of total tumor burden in mice, bearing A549 subcutaneous and liver

tumors, with time. RA-TAX worms were the only treatment that shrunk tumors at

conclusion. TAX loaded worms produced a slight benefit compared to untreated, while

there was no difference between untreated and RA treated. **C)** Efficacy of RA-TAX

treatment leads to a survival benefit in mice, as depicted by the Kaplan Meier curve.

183
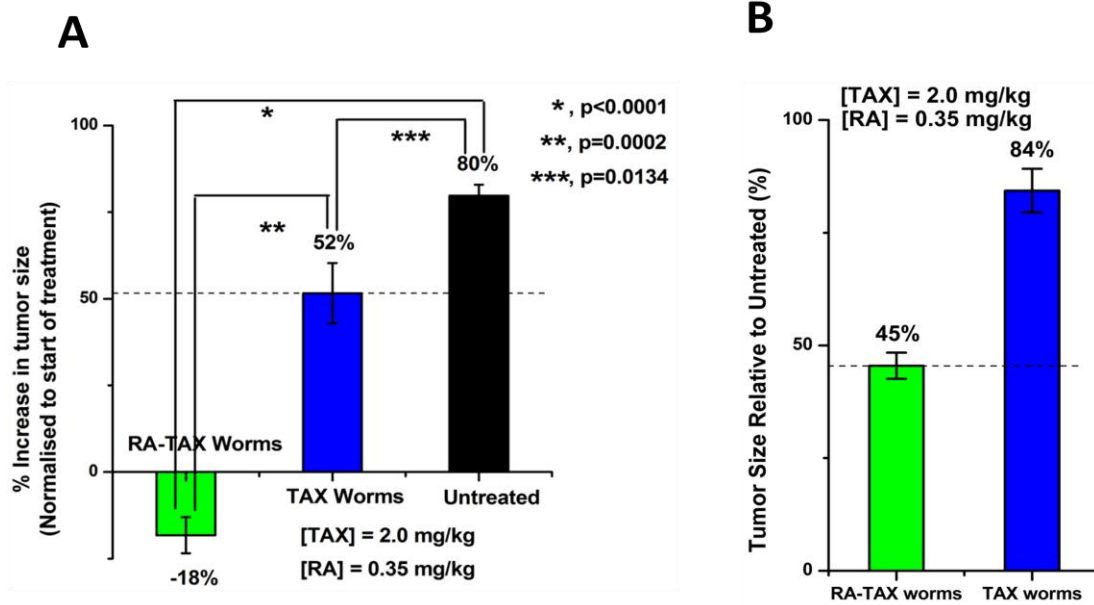
Figure 6.26. Quantification of total tumor size. RA-TAX worms produce the only shrinkage from start of treatment, and final size is less than half of the final untreated tumors.
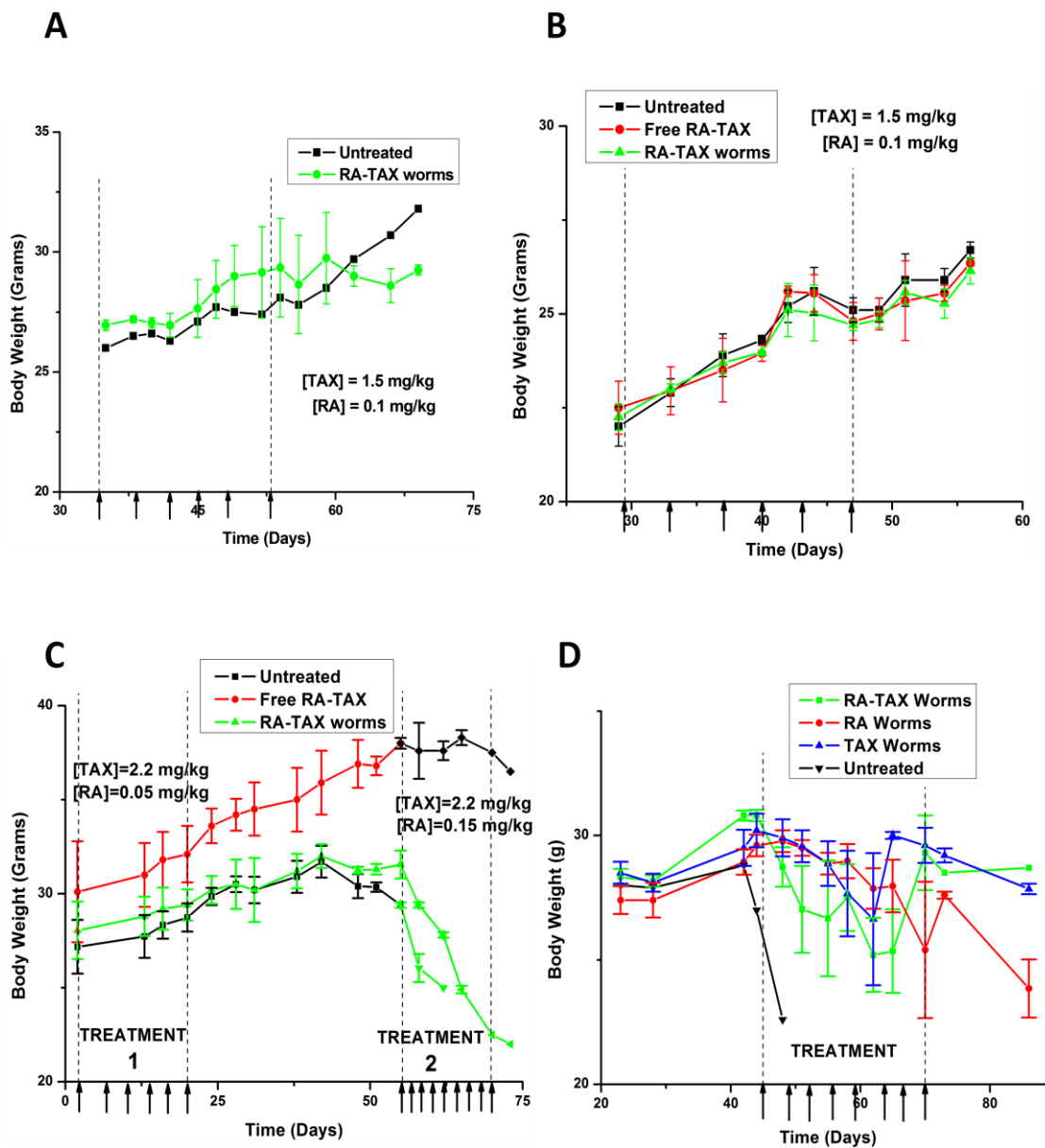
Figure 6.27. Mouse body weight data for *in vivo* treatments corresponding to **A)** Fig. 6.19 B **B)** Fig. 6.20 A **C)** Fig. 6.21 AF **D)** Fig. 6.21 B and Fig. 6.24

CHAPTER 7. CONCLUSION AND FUTURE DIRECTIONS

7.1. Summary

The shortcomings of current chemotherapy, highlighted in the first chapter, necessitate the use of nanocarriers. However, most nanocarriers are eliminated rapidly by phagocytes of the immune system and rarely last in circulation past three days. Flexible cylindrical micelles or filomicelles have been shown to circulate longer and load more drug, increasing the efficacy of the therapy overall.

First experimental part (chapter four) focuses on changing the core chemistry to incorporate aromatic groups in the polymer backbone, which leads to higher loading of an aromatic chemotherapeutic, paclitaxel. Despite the possibility of rigidifying interactions such as ring-stacking (as occurs in a DNA double helix), these aromatic-filomicelles are not rigid and readily deliver to cells. TAX-filomicelles maximized cell death and minimized toxicity as empty nano-carriers. These aromatic-filomicelles also maximized aneuploidy among surviving cells. Initial tests of *in vivo* treatment showed a continuous shrinkage with time at moderate TAX dosage. Overall, these filomicelles of TAX provide a more potent and potentially durable treatment *in vivo* as well as *in vitro*.

However, treatment with single drugs face a number of problems including the development of drug resistance and relapse, as well as the ineffectiveness of conventional

chemotherapeutics on CSCs. While combination of chemotherapeutics can help reduce resistance and relapse, they have minimal effect on CSCs. RA is an essential physiological molecule derived after multiple oxidations of vitamin A. Chapter five briefly highlights the anti- proliferative and differentiative effect of RA after incubation with EC4 cells. Higher concentrations of RA were more effective, and RA loaded onto worms was an order of magnitude more effective than free drug.

RA has been used in clinics for the treatment of APL. Combination of RA with arsenic trioxide induced complete remission in more than 80% of the patients, which highlights the strategy of differentiating cells irreversibly. In chapter six, a chemo-differentiative therapy was developed with focus on liver cancers. RA plays an important role in normal liver function as well as tumorigenesis, and was combined with Paclitaxel. This combination not only retains the potency of TAX, but improves on it. Most notably, cells exposed to RA-TAX combination had lower chances of proliferating post-treatment. They had all the hallmarks of TAX treatment such as increased cell size and DNA accumulation, and these effects were durable as well. This durability may be attributed to lower levels of Ki-67 and Cyclin D1, most importantly Ki67, which are key proliferation proteins. The durability of the treatment was translated to in vivo models, with tumor sizes staying constant almost a month after treatment. Subcutaneous tumors as well orthotopic liver tumors were shrunk, and in many cases was the only treatment that did so. This efficacy was despite using much lower doses of drugs compared to MTD.

Effects of single drugs are often transient, and nanocarriers have been proven to improve treatments. In this thesis, attempts have been made to improve nanocarrier-mediated chemotherapy. These efforts fall into two categories:

- Modification of nanocarriers to improve characteristics such as drug loading

- Addition of a differentiative drug to existing treatment in order to irreversibly differentiate surviving cells

The experiments utilize drugs that are currently in clinic, and demonstrate the irreversible synergy of killing cells while driving differentiation. By adding different components (such as RA) and utilizing nanocarriers, we have demonstrated a more durable treatment than current existing ones.

7.2. Future directions

While a dosage that produces tumor shrinkage in vivo was determined in Chapter 6, the optimal dosage has not been determined. This requires extensive testing in vivo. To better understand the pathway affected by the synergy between the two drugs, RNA-seq is an attractive option.

Another important question that remains to be investigated is the efficacy of this combination against drug resistant cell lines. Generation of drug-resistant cell lines and establishment of tumors in vivo provide an excellent platform for early testing.

Filomicelles have been shown to deliver to subcutaneous tumors and liver tumors. However, subcutaneous tumors are not orthotopic and delivery to livers is not surprising given that nanoparticles are cleared by phagocytes and end up in the liver and spleen. Tumors established in different parts (such as intraperitoneal tumors) are still to be tested, and it would be interesting to study delivery to those tumors.

While nanoparticles improve delivery to tumors, they can be made more selective by active targeting towards groups that are selectively upregulated in tumors. First chapter provides some examples of suitable groups such as folate, transferrins, and lectins. These groups are well-established targets in their class of tumors (breast and colon), and their overexpression has been taken advantage of by antibody-drug-conjugates and nanoparticles. The presence genetic diversity between cells might optimize their fitness and growth, but increased mutational growth also leads to more neoantigen that are displayed on the cell surface. Nanoparticles with groups on the surface that recognize and bind to these neoantigens can, in principle, bind exclusively to cancer cells and deliver the drugs. This would severely reduce the off-target effects commonly associated with chemotherapy.

Clearance by immune system (also discussed in chapter 1) is the other major barrier to nanoparticle delivery. While filomicelles circulate longer due to their flexibility, they do so by delaying their clearance and not completely avoiding them. Nanoparticles that

189

exhibit a form of 'self' signals that is also displayed by the endogenous cells in the body could help avoid this clearance. Proteins that signal 'self' such as CD47 have been the subject of attention in this regard. While the conjugation of entire protein might be too bulky for the nanoparticle surface, 'self' peptide which is the active part of CD47 that signals to the receptor has been identified computationally and synthesized. These have been attached to beads to prolong their circulation *in vivo* (Rodriguez et al., 2013). The display of this peptide to drug-loaded filomicelles would enable them to escape phagocytosis by macrophages and prolong their circulation, increasing the duration of treatment and its efficacy. Additionally, this would lead to lesser accumulation of the drug in the MPS organs (liver and spleen) and hence lesser off target effects, increasing the MTD. Combination of the above two strategies could lead to nanoparticles that circulate for very long periods *in vivo* (time scale of months), that accumulate sleectively in tumor cells and release all of their drugs in tumor cells. This is the ultimate goal of the nanoparticle field, and the means to achieve it is well within reach.

A better understanding of main aberrations in cancer cell signaling would help identify druggable candidates. This could include the bolstering of tumor suppressive pathways (such as the administration of retinoids to induce proliferation arrest and differentiation) or reduction of its inhibitors (like the reduction of MDM2, which targets p53 for degradation). Blocking hyperactive signaling (such as EGFR and other aberrant RTK signaling) is the other arm of this strategy. This could lead to the development of novel drugs that could partner the current successful drugs in combination therapies. The development of chemo-differentiative therapies can be furthered by using vitamin D

190

derivatives instead of retinoids. Both bind to their receptors and drive the transcription of their target genes. For example, p21 (involved in regulating cell cycle and differentiation, discussed in Chapter 5) is responsive to vitamin D derivatives due to the presence of Vitamin D response Elements in its promoter.

The development of effective combination therapies, which would then be loaded into the modified nanoparticles mentioned above, would constitute a massive improvement over current treatment. This would lead to higher efficacy, greatly increasing survivability and quality of life, while decreasing the financial burden.

REFERENCES

Ahmed, F., & Discher, D. E. (2004). Self-porating polymersomes of PEG–PLA and PEG–PCL: hydrolysis-triggered controlled release vesicles. *Journal of controlled release*, *96*(1), 37-53.

Ahmed, F., Pakunlu, R. I., Brannan, A., Bates, F., Minko, T., & Discher, D. E. (2006a). Biodegradable polymersomes loaded with both paclitaxel and doxorubicin permeate and shrink tumors, inducing apoptosis in proportion to accumulated drug. *Journal of Controlled Release*, *116*(2), 150-158.

Ahmed, F., Pakunlu, R. I., Srinivas, G., Brannan, A., Bates, F., Klein, M. L., ... & Discher, D. E. (2006b). Shrinkage of a rapidly growing tumor by drug-loaded polymersomes: pH-triggered release through copolymer degradation. *Molecular pharmaceutics*, *3*(3), 340-350.

Alexis, F., Pridgen, E., Molnar, L. K., & Farokhzad, O. C. (2008). Factors affecting the clearance and biodistribution of polymeric nanoparticles. *Molecular pharmaceutics*, *5*(4), 505-515.

Alkema, N. G., Wisman, G. B. A., van der Zee, A. G., van Vugt, M. A., & de Jong, S. (2016). Studying platinum sensitivity and resistance in high-grade serous ovarian cancer: different models for different questions. *Drug Resistance Updates*, *24*, 55-69.

Amini-Fazl, M. S., Mobedi, H., & Barzin, J. (2014).Investigation of aqueous stability of taxol in different release media. *Drug development and industrial pharmacy*, *40*(4), 519-526.

Andriole, G. L., Crawford, E. D., Grubb III, R. L., Buys, S. S., Chia, D., Church, T. R., ... & Weissfeld, J. L. (2009). Mortality results from a randomized prostate-cancer screening trial. *New England Journal of Medicine*, *360*(13), 1310-1319.

Aranda-Espinoza H, Bermudez H, Bates FS, Discher DE (2001) Electromechanical limits of polymersomes. Phys Rev Lett 87:208301.

ATCC Animal Cell Culture Guide 2014, CB-0813-03

Avis, I., Mathias, A., Unsworth, E. J., Miller, M. J., Cuttitta, F., Mulshine, J. L., & Jakowlew, S. B. (1995). Analysis of small cell lung cancer cell growth inhibition by 13-cis-retinoic acid: importance of bioavailability. *Cell growth & differentiation: the molecular biology journal of the American Association for Cancer Research*, *6*(5), 485-492.

Barenholz, Y. C. (2012). Doxil®—the first FDA-approved nano-drug: lessons learned. *Journal of controlled release*, *160*(2), 117-134.

Battaglia G, Ryan AJ (2005) Bilayers and interdigitation in block copolymer vesicles. J Am Chem Soc 127:8757-8764.

Battaglia G, Ryan AJ, Tomas S (2006) Polymeric vesicle permeability: a facile chemical assay. Langmuir 22:4910-4913.

Baumann, B. C., Kao, G. D., Mahmud, A., Harada, T., Swift, J., Chapman, C., ... & Dorsey, J. F. (2013). Enhancing the efficacy of drug-loaded nanocarriers against brain tumors by targeted radiation therapy. *Oncotarget*, *4*(1), 64-79.

Bermudez H, Brannan AK, Hammer DA, Bates FS, Discher DE (2002) Molecular weight dependence of polymersome membrane structure, elasticity, and stability. Macromolecules 35: 8203-8208.

Bermúdez H, Aranda-Espinoza H, Hammer DA, Discher DE (2003) Pore stability and dynamics in polymer membranes. Europhys Lett 64:550.

Bermudez H, Hammer DA, Discher DE (2004) Effect of bilayer thickness on membrane bending rigidity. Langmuir 20:540-543.

Blanazs, A., Armes, S. P., & Ryan, A. J. (2009). Self-assembled block copolymer aggregates: from micelles to vesicles and their biological applications. *Macromolecular rapid communications*, *30*(4-5), 267-277.

Blaner, W. S., O'Byrne, S. M., Wongsiriroj, N., Kluwe, J., D'Ambrosio, D. M., Jiang, H., ... & Libien, J. (2009). Hepatic stellate cell lipid droplets: a specialized lipid droplet for retinoid storage. *Biochimica et Biophysica Acta (BBA)-Molecular and Cell Biology of Lipids*, *1791*(6), 467-473.

Bokemeyer, C., Oechsle, K., Honecker, F., Mayer, F., Hartmann, J. T., Waller, C. F., ... & Kollmannsberger, C. (2008). Combination chemotherapy with gemcitabine, oxaliplatin, and paclitaxel in patients with cisplatin-refractory or multiply relapsed germ-

cell tumors: a study of the German Testicular Cancer Study Group. *Annals of oncology*, *19*(3), 448-453.

Bonnemain, B. (1998). Superparamagnetic agents in magnetic resonance imaging: physicochemical characteristics and clinical applications a review. *Journal of drug targeting*, *6*(3), 167-174.

Borchert U, Lipprandt U, Bilang M, Kimpfler A, Rank A, Peschka-Süss R, Schubert R, Lindner P, Förster, S (2006) pH-induced release from P2VP-PEO block copolymer vesicles. Langmuir 22:5843-5847.

Breitman, T. R., Selonick, S. E., & Collins, S. J. (1980). Induction of differentiation of the human promyelocytic leukemia cell line (HL-60) by retinoic acid. *Proceedings of the National Academy of Sciences*, *77*(5), 2936-2940.

Brigger, I., Dubernet, C., & Couvreur, P. (2002). Nanoparticles in cancer therapy and diagnosis. *Advanced drug delivery reviews*, *54*(5), 631-651.

Brooks, M. D., Burness, M. L., & Wicha, M. S. (2015). Therapeutic implications of cellular heterogeneity and plasticity in breast cancer. *Cell Stem Cell*, *17*(3), 260-271.

Brown, M. D., Schätzlein, A., Brownlie, A., Jack, V., Wang, W., Tetley, L., ... & Uchegbu, I. F. (2000). Preliminary characterization of novel amino acid based polymeric vesicles as gene and drug delivery agents. *Bioconjugate chemistry*, *11*(6), 880-891.

Buzdar, A. U., Valero, V., Ibrahim, N. K., Francis, D., Broglio, K. R., Theriault, R. L., ... & Sahin, A. A. (2007). Neoadjuvant therapy with paclitaxel followed by 5-fluorouracil, epirubicin, and cyclophosphamide chemotherapy and concurrent trastuzumab in human

epidermal growth factor receptor 2–positive operable breast cancer: an update of the initial randomized study population and data of additional patients treated with the same regimen. *Clinical Cancer Research*, *13*(1), 228-233.

Cai S, Vijayan K, Cheng D, Lima EM, Discher DE (2007) Micelles of different morphologies—advantages of worm-like filomicelles of PEO-PCL in paclitaxel delivery. Pharm Res 24:2099-2109.

Cerritelli S, Velluto D, Hubbell JA (2007) PEG-SS-PPS: reduction-sensitive disulfide block copolymer vesicles for intracellular drug delivery. Biomacromolecules 8:1966-1972.

Checot F, Lecommandoux S, Klok HA, Gnanou Y (2003) From supramolecular polymersomes to stimuli-responsive nano-capsules based on poly (diene-b-peptide) diblock copolymers. Eur Phys J E 10:25-35

Chemin M, Brun PM, Lecommandoux S, Sandre O, Le Meins JF (2012) Hybrid polymer/lipid vesicles: fine control of the lipid and polymer distribution in the binary membrane. Soft Matter 8:2867-2874.

Chen, W., Meng, F., Cheng, R., & Zhong, Z. (2010). pH-Sensitive degradable polymersomes for triggered release of anticancer drugs: a comparative study with micelles. *Journal of Controlled Release*, *142*(1), 40-46.

Cheng, G. Z., Chan, J., Wang, Q., Zhang, W., Sun, C. D., & Wang, L. H. (2007). Twist transcriptionally up-regulates AKT2 in breast cancer cells leading to increased migration, invasion, and resistance to paclitaxel. *Cancer research*, *67*(5), 1979-1987.

Chidambaram, M., Manavalan, R., & Kathiresan, K. (2011). Nanotherapeutics to overcome conventional cancer chemotherapy limitations. *Journal of pharmacy & pharmaceutical sciences*, *14*(1), 67-77.

Chiannilkulchai, N., Driouich, Z., Benoit, J. P., Parodi, A. L., & Couvreur, P. (1989). Doxorubicin-loaded nanoparticles: increased efficiency in murine hepatic metastases. *Selective cancer therapeutics*, *5*(1), 1-11.

Chiannilkulchai, N., Ammoury, N., Caillou, B., Devissaguet, J. P., & Couvreur, P. (1990). Hepatic tissue distribution of doxorubicin-loaded nanoparticles after iv administration in reticulosarcoma M 5076 metastasis-bearing mice. *Cancer chemotherapy and pharmacology*, *26*(2), 122-126.

Cho, K., Wang, X. U., Nie, S., & Shin, D. M. (2008). Therapeutic nanoparticles for drug delivery in cancer. *Clinical cancer research*, *14*(5), 1310-1316.

Christian, D. A., Cai, S., Garbuzenko, O. B., Harada, T., Zajac, A. L., Minko, T., & Discher, D. E. (2009a). Flexible filaments for in vivo imaging and delivery: persistent circulation of filomicelles opens the dosage window for sustained tumor shrinkage. *Molecular pharmaceutics*, *6*(5), 1343-1352.

Christian DA, Tian A, Ellenbroek WG, Levental I, Rajagopal K, Janmey PA, Liu AJ, Baumgart T, Discher DE (2009b) Spotted vesicles, striped micelles and Janus assemblies induced by ligand binding. Nat Mater 8:843-849.

Christian, D. A., Cai, S., Bowen, D. M., Kim, Y., Pajerowski, J. D., & Discher, D. E. (2009c). Polymersome carriers: from self-assembly to siRNA and protein therapeutics. *European Journal of Pharmaceutics and Biopharmaceutics*, *71*(3), 463-474

Christian DA, Garbuzenko OB, Minko T, Discher DE (2010) Polymer Vesicles with a Red Cell-like Surface Charge: Microvascular Imaging and in vivo Tracking with Near-Infrared Fluorescence. Macromol Rapid Commun 31:135-141.

Chua, T. C., Robertson, G., Liauw, W., Farrell, R., Yan, T. D., & Morris, D. L. (2009). Intraoperative hyperthermic intraperitoneal chemotherapy after cytoreductive surgery in ovarian cancer peritoneal carcinomatosis: systematic review of current results. *Journal of cancer research and clinical oncology*, *135*(12), 1637-1645.

Collins, S. J. (1987). The HL-60 promyelocytic leukemia cell line: proliferation, differentiation, and cellular oncogene expression. *Blood*, *70*(5), 1233-1244.

Connolly, R. M., Nguyen, N. K., & Sukumar, S. (2013). Molecular pathways: current role and future directions of the retinoic acid pathway in cancer prevention and treatment. *Clinical Cancer Research*, *19*(7), 1651-1659.

Cui, H., Chen, Z., Zhong, S., Wooley, K. L., & Pochan, D. J. (2007). Block copolymer assembly via kinetic control. *Science*, *317*(5838), 647-650.

Cunningham, J. J., Gatenby, R. A., & Brown, J. S. (2011). Evolutionary dynamics in cancer therapy. *Molecular pharmaceutics*, *8*(6), 2094-2100.

Dalhaimer, P., Engler, A. J., Parthasarathy, R., & Discher, D. E. (2004). Targeted worm micelles. *Biomacromolecules*, *5*(5), 1714-1719.

Deeken, J. F., & Löscher, W. (2007). The blood-brain barrier and cancer: transporters, treatment, and Trojan horses. *Clinical Cancer Research*, *13*(6), 1663-1674.

De Jong, W. H., & Borm, P. J. (2008). Drug delivery and nanoparticles: applications and hazards. *International journal of nanomedicine*, *3*(2), 133..

Demain, A. L., & Vaishnav, P. (2011). Natural products for cancer chemotherapy. *Microbial biotechnology*, *4*(6), 687-699.

Deng, G.-L., Zeng, S., & Shen, H. (2015). Chemotherapy and target therapy for hepatocellular carcinoma: New advances and challenges. *World Journal of Hepatology*, *7*(5), 787–798. http://doi.org/10.4254/wjh.v7.i5.787

De Ruyter, M. G., Lambert, W. E., & De Leenheer, A. (1979). Retinoic acid: an endogenous compound of human blood. Unequivocal demonstration of endogenous retinoic acid in normal physiological conditions. *Analytical biochemistry*, *98*(2), 402-409.

Dimova R, Seifert U, Pouligny B, Förster S, Döbereiner HG (2002) Hyperviscous diblock copolymer vesicles. Eur Phys J E 7:241-250.

Discher BM, Won YY, Ege DS, Lee JC, Bates FS, Discher DE, Hammer DA (1999) Polymersomes: tough vesicles made from diblock copolymers. Science 284:1143-1146.

Discher DE, Eisenberg A (2002) Polymer vesicles. Science 297:967-973.

Discher DE, Ortiz V, Srinivas G, Klein ML, Kim Y, Christian D, Cai S, Photos P, Ahmed F (2007) Emerging applications of polymersomes in delivery: from molecular dynamics to shrinkage of tumors. Prog Polym Sci 32:838-857.

Druker, B. J. (2002). STI571 (Gleevec™) as a paradigm for cancer therapy. *Trends in molecular medicine*, *8*(4), S14-S18.

Dvorak, H. F. (1989). Leaky tumor vessels: consequences for tumor stroma generation and for solid tumor therapy. *Progress in clinical and biological research*, *354*, 317-330.

El-Serag, H. B., Marrero, J. A., Rudolph, L., & Reddy, K. R. (2008). Diagnosis and treatment of hepatocellular carcinoma. *Gastroenterology*, *134*(6), 1752-1763.

Fang, J., Nakamura, H., & Maeda, H. (2011). The EPR effect: unique features of tumor blood vessels for drug delivery, factors involved, and limitations and augmentation of the effect. *Advanced drug delivery reviews*, *63*(3), 136-151.

Fattal, E., Vauthier, C., Aynie, I., Nakada, Y., Lambert, G., Malvy, C., & Couvreur, P. (1998). Biodegradable polyalkylcyanoacrylate nanoparticles for the delivery of oligonucleotides. *Journal of Controlled Release*, *53*(1), 137-143.

Feld, R., Sridhar, S. S., Shepherd, F. A., Mackay, J. A., & Evans, W. K. (2006). Use of the epidermal growth factor receptor inhibitors gefitinib and erlotinib in the treatment of non-small cell lung cancer: a systematic review. *Journal of Thoracic Oncology*, *1*(4), 367-376.

Ferlay, J., Autier, P., Boniol, M., Heanue, M., Colombet, M., & Boyle, P. (2007). Estimates of the cancer incidence and mortality in Europe in 2006. *Annals of oncology*, *18*(3), 581-592.

Ferrara, N., Hillan, K. J., Gerber, H. P., & Novotny, W. (2004). Discovery and development of bevacizumab, an anti-VEGF antibody for treating cancer. *Nature reviews Drug discovery*, *3*(5), 391-400.

Ferrara, N., & Kerbel, R. S. (2005). Angiogenesis as a therapeutic target. *Nature*, *438*(7070), 967-974.

Fidler, I. J. (2003). The pathogenesis of cancer metastasis: the'seed and soil'hypothesis revisited. *Nature Reviews Cancer*, *3*(6), 453-458.

Flaherty, K. T., Puzanov, I., Kim, K. B., Ribas, A., McArthur, G. A., Sosman, J. A., ... & Chapman, P. B. (2010). Inhibition of mutated, activated BRAF in metastatic melanoma. *New England Journal of Medicine*, *363*(9), 809-819.

Folkman, J. (1971). Tumor angiogenesis: therapeutic implications. *New england journal of medicine*, *285*(21), 1182-1186.

Folkman, J. (1995). Angiogenesis in cancer, vascular, rheumatoid and other disease. *Nature medicine*, *1*(1), 27-30.

Frei, E., & Canellos, G. P. (1980). Dose: a critical factor in cancer chemotherapy. *The American journal of medicine*, *69*(4), 585-594.

Frei E III, Eder JP. Combination Chemotherapy. In: Kufe DW, Pollock RE, Weichselbaum RR, et al., editors. Holland-Frei Cancer Medicine. 6th edition. Hamilton (ON): BC Decker; 2003. Available from:
https://www.ncbi.nlm.nih.gov/books/NBK13955/

Fukumura, D., & Jain, R. K. (1998). Role of nitric oxide in angiogenesis and microcirculation in tumors. *Cancer and Metastasis Reviews*, *17*(1), 77-89.

Gatenby, R. A., Brown, J., & Vincent, T. (2009). Lessons from applied ecology: cancer control using an evolutionary double bind. *Cancer research*, *69*(19), 7499-7502.

Geng, Y., & Discher, D. E. (2005). Hydrolytic degradation of poly (ethylene oxide)-block-polycaprolactone worm micelles. *Journal of the American Chemical Society*, *127*(37), 12780-12781.

Geng, Y., & Discher, D. E. (2006). Visualization of degradable worm micelle breakdown in relation to drug release. *Polymer*, *47*(7), 2519-2525.

Geng, Y. A. N., Dalhaimer, P., Cai, S., Tsai, R., Tewari, M., Minko, T., & Discher, D. E. (2007). Shape effects of filaments versus spherical particles in flow and drug delivery. *Nature nanotechnology*, *2*(4), 249-255.

Ghoroghchian, P. P., Li, G., Levine, D. H., Davis, K. P., Bates, F. S., Hammer, D. A., & Therien, M. J. (2006). Bioresorbable vesicles formed through spontaneous self-assembly of amphiphilic poly (ethylene oxide)-block-polycaprolactone. *Macromolecules*, *39*(5), 1673-1675.

Ginestier, C., Wicinski, J., Cervera, N., Monville, F., Finetti, P., Bertucci, F., ... & Charafe-Jauffret, E. (2009). Retinoid signaling regulates breast cancer stem cell differentiation. *Cell cycle*, *8*(20), 3297-3302.

Gordon, D. J., Resio, B., & Pellman, D. (2012). Causes and consequences of aneuploidy in cancer. *Nature Reviews Genetics*, *13*(3), 189-203.

Gradishar, W. J., Tjulandin, S., Davidson, N., Shaw, H., Desai, N., Bhar, P., ... & O'shaughnessy, J. (2005). Phase III trial of nanoparticle albumin-bound paclitaxel compared with polyethylated castor oil–based paclitaxel in women with breast cancer. *Journal of clinical oncology*, *23*(31), 7794-7803.

Greaves, M., & Maley, C. C. (2012). Clonal evolution in cancer. *Nature*, *481*(7381), 306-313.

Green, J. A., Kirwan, J. M., Tierney, J. F., Symonds, P., Fresco, L., Collingwood, M., & Williams, C. J. (2001). Survival and recurrence after concomitant chemotherapy and radiotherapy for cancer of the uterine cervix: a systematic review and meta-analysis. *The Lancet*, *358*(9284), 781-786.

Gref, R., Lück, M., Quellec, P., Marchand, M., Dellacherie, E., Harnisch, S., ... & Müller, R. H. (2000). 'Stealth'corona-core nanoparticles surface modified by polyethylene glycol (PEG): influences of the corona (PEG chain length and surface density) and of the core composition on phagocytic uptake and plasma protein adsorption. *Colloids and Surfaces B: Biointerfaces*, *18*(3), 301-313.

Griffin, A. M., Butow, P. N., Coates, A. S., Childs, A. M., Ellis, P. M., Dunn, S. M., & Tattersall, M. H. N. (1996). On the receiving end V: patient perceptions of the side effects of cancer chemotherapy in 1993. *Annals of oncology*, *7*(2), 189-195.

Groopman, J. E., & Itri, L. M. (1999). Chemotherapy-induced anemia in adults: incidence and treatment. *Journal of the National Cancer Institute*, *91*(19), 1616-1634.

Gruenbaum, Y., & Medalia, O. (2015). Lamins: the structure and protein complexes. *Current opinion in cell biology*, *32*, 7-12.

Hamley IW (2005). Nanoshells and nanotubes from block copolymers. Soft Matter 1:36-43.

Harada, T., Swift, J., Irianto, J., Shin, J. W., Spinler, K. R., Athirasala, A., ... & Discher, D. E. (2014). Nuclear lamin stiffness is a barrier to 3D migration, but softness can limit survival. *J Cell Biol*, jcb-201308029.

Hattinger, C. M., Vella, S., Tavanti, E., Fanelli, M., Picci, P., & Serra, M. (2016). Pharmacogenomics of second-line drugs used for treatment of unresponsive or relapsed osteosarcoma patients. *Pharmacogenomics*, *17*(18), 2097-2114.

Hofheinz, R. D., Gnad-Vogt, S. U., Beyer, U., & Hochhaus, A. (2005). Liposomal encapsulated anti-cancer drugs. *Anti-cancer drugs*, *16*(7), 691-707.

Hong, G. Y., Jeong, Y. I., Lee, S. J., Lee, E., Oh, J. S., & Lee, H. C. (2011). Combination of paclitaxel-and retinoic acid-incorporated nanoparticles for the treatment of CT-26 colon carcinoma. *Archives of pharmacal research*, *34*(3), 407-417.

Huang, J., Bi, Y., Zhu, G. H., He, Y., Su, Y., He, B. C., Yuxi Su, Bai-Cheng He, Yi Wang ... & Luo, Q. (2009). Retinoic acid signalling induces the differentiation of mouse fetal liver-derived hepatic progenitor cells. *Liver International*, *29*(10), 1569-1581.

Israelachvili JN (1991) Intermolecular and Surface Forces, 2nd Ed, London: Academic.

Itel F, Chami M, Najer A, Lörcher S, Wu D, Dinu IA, Meier W (2014) Molecular organization and dynamics in polymersome membranes: A lateral diffusion study. Macromolecules 47:7588-7596.

Iyer, A. K., Khaled, G., Fang, J., & Maeda, H. (2006). Exploiting the enhanced permeability and retention effect for tumor targeting. *Drug discovery today*, *11*(17), 812-818.

Jeong, I. K., Gao, G. H., Li, Y., Kang, S. W., & Lee, D. S. (2013). A Biodegradable Polymersome with pH-Tuning On-Off Membrane Based on Poly (β-amino ester) for Drug Delivery. *Macromolecular bioscience*, *13*(7), 946-953.

Jing, Y., Wang, L., Xia, L., Chen, G. Q., Chen, Z., Miller, W. H., & Waxman, S. (2001). Combined effect of all-trans retinoic acid and arsenic trioxide in acute promyelocytic leukemia cells in vitro and in vivo. *Blood*, *97*(1), 264-269.

Johnson, K. R., Wang, L., Miller, M. C., Willingham, M. C., & Fan, W. (1997). 5-Fluorouracil interferes with paclitaxel cytotoxicity against human solid tumor cells. *Clinical cancer research*, *3*(10), 1739-1745.

Jordan, M. A., Wendell, K., Gardiner, S., Derry, W. B., Copp, H., & Wilson, L. (1996). Mitotic block induced in HeLa cells by low concentrations of paclitaxel (Taxol) results in abnormal mitotic exit and apoptotic cell death. *Cancer research*, *56*(4), 816-825.

Juliano, R. L., Alahari, S., Yoo, H., Kole, R., & Cho, M. (1999). Antisense pharmacodynamics: critical issues in the transport and delivery of antisense oligonucleotides. *Pharmaceutical research*, *16*(4), 494-502.

Kaiser, M. H., & Ellenberg, S. S. (1985). Pancreatic cancer: adjuvant combined radiation and chemotherapy following curative resection. *Archives of surgery*, *120*(8), 899-903.

Kamath, K., Wilson, L., Cabral, F., & Jordan, M. A. (2005). βIII-tubulin induces paclitaxel resistance in association with reduced effects on microtubule dynamic instability. *Journal of Biological Chemistry*, *280*(13), 12902-12907.

Kano, Y., Akutsu, M., Tsunoda, S., Ando, J., Matsui, J., Suzuki, K., ... & Adachi, K. (1996). Schedule-dependent interaction between paclitaxel and 5-fluorouracil in human carcinoma cell lines in vitro. *British journal of cancer*, *74*(5), 704.

Karmakar, S., Banik, N. L., & Ray, S. K. (2008). Combination of all-trans retinoic acid and paclitaxel-induced differentiation and apoptosis in human glioblastoma U87MG xenografts in nude mice. *Cancer*, *112*(3), 596-607.

Kazunori K, Masayuki Y, Teruo O, Yasuhisa S (1993) Block copolymer micelles as vehicles for drug delivery. J Control Release 24:119-132.

Kim, Y. H., Shin, S. W., Kim, B. S., Kim, J. H., Kim, J. G., Mok, Y. J., ... & Kim, J. S. (1999). Paclitaxel, 5-fluorouracil, and cisplatin combination chemotherapy for the treatment of advanced gastric carcinoma. *cancer*, *85*(2), 295-301.

Kim, T. Y., Kim, D. W., Chung, J. Y., Shin, S. G., Kim, S. C., Heo, D. S., ... & Bang, Y. J. (2004). Phase I and pharmacokinetic study of Genexol-PM, a cremophor-free, polymeric micelle-formulated paclitaxel, in patients with advanced malignancies. *Clinical cancer research*, *10*(11), 3708-3716.

Kim Y, Dalhaimer P, Christian DA, Discher DE (2005) Polymeric worm micelles as nano-carriers for drug delivery. Nanotechnol 16:S484.

Kim S, Kim JH, Jeon O, Kwon IC, Park K (2009a) Engineered polymers for advanced drug delivery. Eur J Pharm Biopharm 71:420-430.

Kim Y, Tewari M, Pajerowski JD, Cai S, Sen S, Williams J, Sirsi S, Lutz G, Discher DE (2009b) Polymersome delivery of siRNA and antisense oligonucleotides. J Control Release 134:132-140.

Kim MS, Lee DS (2010) Biodegradable and pH-sensitive polymersome with tuning permeable membrane for drug delivery carrier. Chem Commun 46:4481-4483.

Kim, H. O., Kim, E., An, Y., Choi, J., Jang, E., Choi, E. B., ... & Suh, J. S. (2013). A biodegradable polymersome containing Bcl-xL siRNA and doxorubicin as a dual delivery vehicle for a synergistic anticancer effect. *Macromolecular bioscience*, *13*(6), 745-754.

Kim, S. C., Kim, C. K., Axe, D., Cook, A., Lee, M., Li, T., ... & Lee, Y. K. (2014). All-trans-retinoic acid ameliorates hepatic steatosis in mice by a novel transcriptional cascade. *Hepatology*, *59*(5), 1750-1760.

King, P. D., & Perry, M. C. (2001). Hepatotoxicity of chemotherapy. *The oncologist*, *6*(2), 162-176.

Kipp, J. E. (2004). The role of solid nanoparticle technology in the parenteral delivery of poorly water-soluble drugs. *International Journal of Pharmaceutics*, *284*(1), 109-122.

Kita-Tokarczyk, K., Grumelard, J., Haefele, T., & Meier, W. (2005). Block copolymer vesicles—using concepts from polymer chemistry to mimic biomembranes. *Polymer*, *46*(11), 3540-3563.

Klibanov AL, Maruyama K, Torchilin VP, Huang L (1990) Amphipathic polyethyleneglycols effectively prolong the circulation time of liposomes. FEBS Lett 268:235-237.

Komarova, N. L., & Wodarz, D. (2005). Drug resistance in cancer: principles of emergence and prevention. *Proceedings of the National Academy of Sciences of the United States of America*, *102*(27), 9714-9719.

Korobko, A. V., Jesse, W., & Van der Maarel, J. R. C. (2005). Encapsulation of DNA by cationic diblock copolymer vesicles. *Langmuir*, *21*(1), 34-42.

Korobko, A. V., Backendorf, C., & Van der Maarel, J. R. C. (2006). Plasmid DNA encapsulation within cationic diblock copolymer vesicles for gene delivery. *The Journal of Physical Chemistry B*, *110*(30), 14550-14556. Kwon GS, Okano T (1996) Polymeric micelles as new drug carriers. Adv Drug Deliv Rev 21:107-116.

Lasic DD, Papahadjopoulos D (1998) Medical applications of liposomes. Elsevier.

Lawson, N. D., & Berliner, N. (1999). Neutrophil maturation and the role of retinoic acid. *Experimental hematology*, *27*(9), 1355-1367

Leamon, C. P., & Reddy, J. A. (2004). Folate-targeted chemotherapy. *Advanced drug delivery reviews*, *56*(8), 1127-1141.

Lee, W. P. (1993). The role of reduced growth rate in the development of drug resistance of HOB1 lymphoma cells to vincristine. *Cancer letters*, *73*(2-3), 105-111.

Lee JCM, Bermudez H, Discher BM, Sheehan MA, Won YY, Bates FS, Discher DE (2001) Preparation, stability, and in vitro performance of vesicles made with diblock copolymers. Biotechnol Bioeng 73:135-145.

Lee JCM, Santore M, Bates FS, Discher DE (2002) From membranes to melts, rouse to reptation: diffusion in polymersome versus lipid bilayers. Macromolecules 35:323-326.

Lee, E. S., Na, K., & Bae, Y. H. (2003). Polymeric micelle for tumor pH and folate-mediated targeting. *Journal of Controlled Release*, *91*(1), 103-113.

Lee, E. S., Gao, Z., & Bae, Y. H. (2008). Recent progress in tumor pH targeting nanotechnology. *Journal of Controlled Release*, *132*(3), 164-170.

Lee, Y. A., Wallace, M. C., & Friedman, S. L. (2015). Pathobiology of liver fibrosis: a translational success story. *Gut*, *64*(5), 830-841.

Leid, M., Kastner, P., & Chambon, P. (1992). Multiplicity generates diversity in the retinoic acid signalling pathways. *Trends in biochemical sciences*, *17*(10), 427-433.

Le Meins JF, Sandre O, Lecommandoux S (2011) Recent trends in the tuning of polymersomes' membrane properties. Eur Phys J E 34:1-17.

Le Meins JF, Schatz C, Lecommandoux S, Sandre O (2013) Hybrid polymer/lipid vesicles: state of the art and future perspectives. Mater Today 16:397-402.

Leong KW, Brott BC, Langer R (1985) Bioerodible polyanhydrides as drug-carrier matrices. I: Characterization, degradation, and release characteristics. J Biomed Mat Res 19:941-955.

Li, C. (2002). Poly (L-glutamic acid)–anticancer drug conjugates. *Advanced drug delivery reviews*, *54*(5), 695-713.

Li YY, Cunin F, Link JR, Gao T, Betts RE, Reiver SH, Chin V, Bhatia SN, Sailor MJ (2003) Polymer replicas of photonic porous silicon for sensing and drug delivery applications. Science 299:2045-2047.

Li, X., Lewis, M. T., Huang, J., Gutierrez, C., Osborne, C. K., Wu, M. F., ... & Wong, H. (2008). Intrinsic resistance of tumorigenic breast cancer cells to chemotherapy. *Journal of the National Cancer Institute*, *100*(9), 672-679.

Liao DJ, Thankur A, Biliran H, Sarkar FH (2007). Perspectives on c-Myc, Cyclin D1, and their interaction in cancer formation, progression, and response to chemotherapy. *Critical Reviews in Oncogenesis, 13*(2), 93-158

Lim Soo, P., Luo, L., Maysinger, D., & Eisenberg, A. (2002). Incorporation and release of hydrophobic probes in biocompatible polycaprolactone-block-poly (ethylene oxide) micelles: implications for drug delivery. *Langmuir*, *18*(25), 9996-10004.

Lin, B. C., Hong, S. H., Krig, S., Yoh, S. M., & Privalsky, M. L. (1998). A conformational switch in nuclear hormone receptors is involved in coupling hormone binding to corepressor release. *Molecular and cellular biology*, *18*(12), 7603-7603.

Lippman, M. E., Cassidy, J., Wesley, M., & Young, R. C. (1984). A randomized attempt to increase the efficacy of cytotoxic chemotherapy in metastatic breast cancer by hormonal synchronization. *Journal of Clinical Oncology*, *2*(1), 28-36.

Liu, Y., Chen, H., Wang, J., Zhou, W., Sun, R., & Xia, M. (2015). Association of serum retinoic acid with hepatic steatosis and liver injury in nonalcoholic fatty liver disease. *The American journal of clinical nutrition*, *102*(1), 130-137.

Lodish H, Berk A, Zipursky SL, et al. Molecular Cell Biology. 4th edition. New York: W. H. Freeman; 2000. Section 15.1, Diffusion of Small Molecules across Phospholipid Bilayers.

Long, B. H., & Fairchild, C. R. (1994). Paclitaxel inhibits progression of mitotic cells to G1 phase by interference with spindle formation without affecting other microtubule functions during anaphase and telephase. *Cancer research*, *54*(16), 4355-4361.

LoPresti C, Lomas H, Massignani M, Smart T, Battaglia G (2009) Polymersomes: nature inspired nanometer sized compartments. J Mater Chem 19:3576-3590.

Loverde, S. M., Klein, M. L., & Discher, D. E. (2012). Nanoparticle Shape Improves Delivery: Rational Coarse Grain Molecular Dynamics (rCG-MD) of Taxol in Worm-Like PEG-PCL Micelles. *Advanced materials*, *24*(28), 3823-3830

Maeda, H., Takeshita, J., & Kanamaru, R. (1979). A lipophilic derivative of neocarzinostatin a polymer conjugation of an antitumor protein antibiotic. *Chemical Biology & Drug Design*, *14*(2), 81-87.

Maeda, H. (2001). The enhanced permeability and retention (EPR) effect in tumor vasculature: the key role of tumor-selective macromolecular drug targeting. *Advances in enzyme regulation*, *41*(1), 189-207.

Maeda, H., Greish, K., & Fang, J. (2006). The EPR effect and polymeric drugs: a paradigm shift for cancer chemotherapy in the 21st century. *Polymer therapeutics II*, 103-121.

Maeda, H. (2012). Macromolecular therapeutics in cancer treatment: the EPR effect and beyond. *Journal of Controlled Release*, *164*(2), 138-144.

Malik, N., Evagorou, E. G., & Duncan, R. (1999). Dendrimer-platinate: a novel approach to cancer chemotherapy. *Anti-cancer drugs*, *10*(8), 767-776.

Manchester, M., & Singh, P. (2006). Virus-based nanoparticles (VNPs): platform technologies for diagnostic imaging. *Advanced drug delivery reviews*, *58*(14), 1505-1522.

Mansour, A. M., Drevs, J., Esser, N., Hamada, F. M., Badary, O. A., Unger, C., ... & Kratz, F. (2003). A new approach for the treatment of malignant melanoma: enhanced antitumor efficacy of an albumin-binding doxorubicin prodrug that is cleaved by matrix metalloproteinase 2. *Cancer research*, *63*(14), 4062-4066.

Mark, M., Ghyselinck, N. B., & Chambon, P. (2006). Function of retinoid nuclear receptors: lessons from genetic and pharmacological dissections of the retinoic acid signaling pathway during mouse embryogenesis. *Annu. Rev. Pharmacol. Toxicol.*, *46*, 451-480.

Marshall, E. (2011). Cancer research and the $90 billion metaphor.

Marusyk, A., & Polyak, K. (2010). Tumor heterogeneity: causes and consequences. *Biochimica et Biophysica Acta (BBA)-Reviews on Cancer*, *1805*(1), 105-117.

Marzo, I., & Naval, J. (2013). Antimitotic drugs in cancer chemotherapy: promises and pitfalls. *Biochemical pharmacology*, *86*(6), 703-710.

Matsumura, Y., & Maeda, H. (1986). A new concept for macromolecular therapeutics in cancer chemotherapy: mechanism of tumoritropic accumulation of proteins and the antitumor agent smancs. *Cancer research*, *46*(12 Part 1), 6387-6392.

Mayer, L. D., Bally, M. B., & Cullis, P. R. (1986). Uptake of adriamycin into large unilamellar vesicles in response to a pH gradient. *Biochimica Et Biophysica Acta (BBA)-Biomembranes*, *857*(1), 123-126.

Mellman, I., Coukos, G., & Dranoff, G. (2011). Cancer immunotherapy comes of age. *Nature*, *480*(7378), 480-489.

Meng F, Zhong Z, Feijen J (2009) Stimuli-responsive polymersomes for programmed drug delivery. Biomacromolecules 10:197-209.

Messager L, Gaitzsch J, Chierico L, Battaglia G (2014) Novel aspects of encapsulation and delivery using polymersomes. Curr Opin Pharmacol 18:104-111.

Middleton JC, Tipton AJ (2000) Synthetic biodegradable polymers as orthopedic devices. Biomaterials 21:2335-2346.

Minko, T. (2004). Drug targeting to the colon with lectins and neoglycoconjugates. *Advanced drug delivery reviews*, *56*(4), 491-509.

Miyata, K., Christie, R. J., & Kataoka, K. (2011). Polymeric micelles for nano-scale drug delivery. *Reactive and Functional Polymers*, *71*(3), 227-234.

Murad, A. M., Petroianu, A., Guimaraes, R. C., Aragao, B. C., Cabral, L. O., & Scalabrini-Neto, A. O. (1999). Phase II trial of the combination of paclitaxel and 5-fluorouracil in the treatment of advanced gastric cancer: a novel, safe, and effective regimen. *American journal of clinical oncology*, *22*(6), 580.

Moghimi, S. M., Hunter, A. C., & Murray, J. C. (2001). Long-circulating and target-specific nanoparticles: theory to practice. *Pharmacological reviews*, *53*(2), 283-318.

Moghimi, S. M., Hunter, A. C., & Murray, J. C. (2005). Nanomedicine: current status and future prospects. *The FASEB journal*, *19*(3), 311-330.

Molavi, O., Ma, Z., Mahmud, A., Alshamsan, A., Samuel, J., Lai, R., ... & Lavasanifar, A. (2008). Polymeric micelles for the solubilization and delivery of STAT3 inhibitor cucurbitacins in solid tumors. *International journal of pharmaceutics*, *347*(1), 118-127.

Nair, P. R., Karthick, S. A., Spinler, K. R., Vakili, M. R., Lavasanifar, A., & Discher, D. E. (2016). Filomicelles from aromatic diblock copolymers increase paclitaxel-induced tumor cell death and aneuploidy compared with aliphatic copolymers. *Nanomedicine*, *11*(12), 1551-1569.

Napoli A, Boerakker MJ, Tirelli N, Nolte RJ, Sommerdijk NA, Hubbell JA (2004) Glucose-oxidase based self-destructing polymeric vesicles. Langmuir 20:3487-3491.

Nasr, R., Guillemin, M. C., Ferhi, O., Soilihi, H., Peres, L., Berthier, C., ... & Vitoux, D. (2008). Eradication of acute promyelocytic leukemia-initiating cells through PML-RARA degradation. *Nature medicine*, *14*(12), 1333-1342.

Nie, T., Zhao, Y., Xie, Z., & Wu, C. (2003). Micellar Formation of Poly (caprolactone-b lock-ethylene oxide-b lock-caprolactone) and Its Enzymatic Biodegradation in Aqueous Dispersion. *Macromolecules*, *36*(23), 8825-8829.

Nikolic, V., Savic, I., Savic, I., Nikolic, L., Stankovic, M., &Marinkovic, V. (2011). Paclitaxel as an anticancer agent: isolation, activity, synthesis and stability. *Open Medicine*, *6*(5), 527-536.

Obaya, A. J., Kotenko, I., Cole, M. D., & Sedivy, J. M. (2002). The Proto-oncogene c-myc Acts through the Cyclin-dependent Kinase (Cdk) Inhibitor p27Kip1to Facilitate the Activation of Cdk4/6 and Early G1Phase Progression. *Journal of Biological Chemistry*, *277*(34), 31263-31269.

Oltra, N. S., Swift, J., Mahmud, A., Rajagopal, K., Loverde, S. M., & Discher, D. E. (2013). Filomicelles in nanomedicine–from flexible, fragmentable, and ligand-targetable drug carrier designs to combination therapy for brain tumors. *Journal of Materials Chemistry B*, *1*(39), 5177-5185.

Oltra, N. S., Nair, P., & Discher, D. E. (2014). From stealthy polymersomes and filomicelles to "self" peptide-nanoparticles for cancer therapy. *Annual review of chemical and biomolecular engineering*, *5*, 281-299.

Onaca O, Enea R, Hughes DW, Meier W (2009) Stimuli-Responsive Polymersomes as Nanocarriers for Drug and Gene Delivery. Macromol Biosci 9:129-139.

Orlando, P. A., Gatenby, R. A., & Brown, J. S. (2012). Cancer treatment as a game: integrating evolutionary game theory into the optimal control of chemotherapy. *Physical biology*, *9*(6), 065007.

Ortiz V, Nielsen SO, Discher DE, Klein ML, Lipowsky R, Shillcock J (2005) Dissipative particle dynamics simulations of polymersomes. J Phys Chem B 109:17708-17714.

Pantano DA, Moore PB, Klein ML, Discher DE (2011) Raft registration across bilayers in a molecularly detailed model. Soft Matter 7:8182-8191.

Pardoll, D. M. (2012). The blockade of immune checkpoints in cancer immunotherapy. *Nature Reviews Cancer*, *12*(4), 252-264.

Pastorin, G., Wu, W., Wieckowski, S., Briand, J. P., Kostarelos, K., Prato, M., & Bianco, A. (2006). Double functionalisation of carbon nanotubes for multimodal drug delivery. *Chemical communications*, (11), 1182-1184.

Pelicano, H., Martin, D. S., Xu, R. A., & Huang, P. (2006). Glycolysis inhibition for anticancer treatment. *Oncogene*, *25*(34), 4633-4646.

Penn, I., & Starzl, T. E. (1973, March). Immunosuppression and cancer. In *Transplantation proceedings* (Vol. 5, No. 1, p. 943). NIH Public Access.

Peters EAJF (2004). Elimination of time step effects in DPD. Europhys Lett 66:311.

Photos PJ, Bacakova L, Discher BM, Bates FS, Discher DE (2003). Polymer vesicles in vivo: correlations with PEG molecular weight. J Control Release 90:323-334.

Pinkel, D. (1958). The use of body surface area as a criterion of drug dosage in cancer chemotherapy. *Cancer Research*, *18*(7), 853-856.

Pratt, M. C., Niu, M. Y., & Renart, L. I. (2006). Regulation of survivin by retinoic acid and its role in paclitaxel-mediated cytotoxicity in MCF-7 breast cancer cells. *Apoptosis*, *11*(4), 589-605.

Qu, A., Jiang, C., Cai, Y., Kim, J. H., Tanaka, N., Ward, J. M., ... & Gonzalez, F. J. (2014). Role of Myc in hepatocellular proliferation and hepatocarcinogenesis. *Journal of hepatology*, *60*(2), 331-338. Cdk4/6 and Early G1Phase Progression. *Journal of Biological Chemistry*, *277*(34), 31263-31269.

Rajagopal K, Mahmud A, Christian DA, Pajerowski JD, Brown AE, Loverde SM, Discher DE (2010) Curvature-coupled hydration of semicrystalline polymer amphiphiles yields flexible worm micelles but favors rigid vesicles: polycaprolactone-based block copolymers. Macromolecules 43:9736-9746.

Restifo, N. P., Dudley, M. E., & Rosenberg, S. A. (2012). Adoptive immunotherapy for cancer: harnessing the T cell response. *Nature Reviews Immunology*, *12*(4), 269-281.

Richheimer, S. L., Tinnermeier, D. M., & Timmons, D. W. (1992). High-performance liquid chromatographic assay of taxol. *Analytical chemistry*, *64*(20), 2323-2326.

Ries, F., & Klastersky, J. (1986). Nephrotoxicity induced by cancer chemotherapy with special emphasis on cisplatin toxicity. *American Journal of Kidney Diseases*, *8*(5), 368-379.

Ries, L. A., Harkins, D., Krapcho, M., Mariotto, A., Miller, B. A., Feuer, E. J., ... & Hayat, M. (2006). SEER cancer statistics review, 1975-2003.

Robert, C., Soria, J. C., Spatz, A., Le Cesne, A., Malka, D., Pautier, P., ... & Armand, J. P. (2005). Cutaneous side-effects of kinase inhibitors and blocking antibodies. *The lancet oncology*, *6*(7), 491-500.

Rodriguez, P. L., Harada, T., Christian, D. A., Pantano, D. A., Tsai, R. K., & Discher, D. E. (2013). Minimal" Self" peptides that inhibit phagocytic clearance and enhance delivery of nanoparticles. *Science*, *339*(6122), 971-975.

Rosenberg, S. A., Yang, J. C., & Restifo, N. P. (2004). Cancer immunotherapy: moving beyond current vaccines. *Nature medicine*, *10*(9), 909-915.

Sahoo, S. K., & Labhasetwar, V. (2005). Enhanced antiproliferative activity of transferrin-conjugated paclitaxel-loaded nanoparticles is mediated via sustained intracellular drug retention. *Molecular pharmaceutics*, *2*(5), 373-383.

Sawa, T., Wu, J., Akaike, T., & Maeda, H. (2000). Tumor-targeting chemotherapy by a xanthine oxidase-polymer conjugate that generates oxygen-free radicals in tumor tissue. *Cancer research*, *60*(3), 666-671.

Schmaljohann D (2006) Thermo-and pH-responsive polymers in drug delivery. Adv Drug Deliv Rev 58:1655-1670.

Schröder, F. H., Hugosson, J., Roobol, M. J., Tammela, T. L., Ciatto, S., Nelen, V., ... & Denis, L. J. (2009). Screening and prostate-cancer mortality in a randomized European study. *N Engl j Med*, *2009*(360), 1320-1328.

Sell, S. (2004). Stem cell origin of cancer and differentiation therapy. *Critical reviews in oncology/hematology*, *51*(1), 1-28.

Seki, T., Fang, J., & Maeda, H. (2009). Tumor-targeted macromolecular drug delivery based on the enhanced permeability and retention effect in solid tumor. In *Pharmaceutical Perspectives of Cancer Therapeutics* (pp. 93-120). Springer US.

Semple SC, Chonn A, Cullis PR (1998) Interactions of liposomes and lipid-based carrier systems with blood proteins: relation to clearance behavior in vivo. Adv Drug Deliv Rev 32:3-17.

Shimi, T., Kittisopikul, M., Tran, J., Goldman, A. E., Adam, S. A., Zheng, Y., ... & Goldman, R. D. (2015). Structural organization of nuclear lamins A, C, B1, and B2 revealed by superresolution microscopy. *Molecular biology of the cell*, *26*(22), 4075-4086.

Shirabe, K., Shimada, M., Gion, T., Hasegawa, H., Takenaka, K., Utsunomiya, T., & Sugimachi, K. (1999). Postoperative liver failure after major hepatic resection for hepatocellular carcinoma in the modern era with special reference to remnant liver volume. *Journal of the American College of Surgeons*, *188*(3), 304-309.

Shiota, G. (2005). Loss of function of retinoic acid in liver leads to steatohepatitis and liver tumor: a NASH animal model. *Hepatology research*, *33*(2), 155-160.

Shuvaev, V. V., Ilies, M. A., Simone, E., Zaitsev, S., Kim, Y., Cai, S., ... & Muzykantov, V. R. (2011). Endothelial targeting of antibody-decorated polymeric filomicelles. *ACS nano*, *5*(9), 6991-6999.

Siegel, R. L., Miller, K. D., & Jemal, A. (2015). Cancer statistics, 2015. *CA: a cancer journal for clinicians*, *65*(1), 5-29.

Siegel, R. L., Miller, K. D. and Jemal, A. (2017), Cancer statistics, 2017. CA: A Cancer Journal for Clinicians, 67: 7–30. doi:10.3322/caac.21387

Simbre, V. C., Duffy, S. A., Dadlani, G. H., Miller, T. L., & Lipshultz, S. E. (2005). Cardiotoxicity of cancer chemotherapy. *Pediatric Drugs*, *7*(3), 187-202.

Simmonds, P. C., Primrose, J. N., Colquitt, J. L., Garden, O. J., Poston, G. J., & Rees, M. (2006). Surgical resection of hepatic metastases from colorectal cancer: a systematic review of published studies. *British journal of cancer*, *94*(7), 982-999.

Smart T, Lomas H, Massignani M, Flores-Merino MV, Perez LR, Battaglia G (2008). Block copolymer nanostructures. Nano Today 3:38-46.

Soignet, S. L., Maslak, P., Wang, Z. G., Jhanwar, S., Calleja, E., Dardashti, L. J., ... & Pandolfi, P. P. (1998). Complete remission after treatment of acute promyelocytic leukemia with arsenic trioxide. *New England Journal of Medicine*, *339*(19), 1341-1348.

Srinivas G, Shelley JC, Nielsen SO, Discher DE, Klein ML (2004a). Simulation of diblock copolymer self-assembly, using a coarse-grain model. J Phys Chem B 108:8153-8160.

Srinivas G, Discher DE, Klein ML (2004b). Self-assembly and properties of diblock copolymers by coarse-grain molecular dynamics. Nat Mater 3:638-644.

Srinivas G, Klein ML (2004). Coarse-grain molecular dynamics simulations of diblock copolymer surfactants interacting with a lipid bilayer. Mol Phys 102:883-889.

Srinivas G, Discher DE, Klein ML (2005). Key roles for chain flexibility in block copolymer membranes that contain pores or make tubes. Nano Lett 5:2343-2349.

Stella, B., Arpicco, S., Peracchia, M. T., Desmaële, D., Hoebeke, J., Renoir, M., ... & Couvreur, P. (2000). Design of folic acid-conjugated nanoparticles for drug targeting. *Journal of pharmaceutical sciences*, *89*(11), 1452-1464.

Stolnik, S. S. D. S., Illum, L., & Davis, S. S. (1995). Long circulating microparticulate drug carriers. *Advanced Drug Delivery Reviews*, *16*(2), 195-214.

Storm, G., Belliot, S. O., Daemen, T., & Lasic, D. D. (1995). Surface modification of nanoparticles to oppose uptake by the mononuclear phagocyte system. *Advanced drug delivery reviews*, *17*(1), 31-48.

Surnar, B., Sharma, K., & Jayakannan, M. (2015). Core–shell polymer nanoparticles for prevention of GSH drug detoxification and cisplatin delivery to breast cancer cells. *Nanoscale*, *7*(42), 17964-17979.

Suzuki, M., Hori, K., Abe, I., Saito, S., & Sato, H. (1981). A new approach to cancer chemotherapy: selective enhancement of tumor blood flow with angiotensin II. *Journal of the National Cancer institute*, *67*(3), 663-669.

Suzuki, M., Takahashi, T., & Sato, T. (1987). Medial regression and its functional significance in tumor-supplying host arteries. A morphometric study of hepatic arteries in human livers with hepatocellular carcinoma. *Cancer*, *59*(3), 444-450.

Svenson, S., & Tomalia, D. A. (2012). Dendrimers in biomedical applications—reflections on the field. *Advanced drug delivery reviews*, *64*, 102-115.

Swift, J., Ivanovska, I. L., Buxboim, A., Harada, T., Dingal, P. D. P., Pinter, J., ... & Rehfeldt, F. (2013). Nuclear lamin-A scales with tissue stiffness and enhances matrix-directed differentiation. *Science*, *341*(6149), 1240104.

Tallman, M. S., Andersen, J. W., Schiffer, C. A., Appelbaum, F. R., Feusner, J. H., Ogden, A., ... & Wiernik, P. H. (1997). All-trans-retinoic acid in acute promyelocytic leukemia. *New England Journal of Medicine*, *337*(15), 1021-1028.

Theodosiou, M., Laudet, V., & Schubert, M. (2010). From carrot to clinic: an overview of the retinoic acid signaling pathway. *Cellular and molecular life sciences*, *67*(9), 1423-1445.

Tian, J., & Stella, V. J. (2008). Degradation of paclitaxel and related compounds in aqueous solutions II: Nonepimerization degradation under neutral to basic pH conditions. *Journal of pharmaceutical sciences*, *97*(8), 3100-3108.

Torchilin, V. (2011). Tumor delivery of macromolecular drugs based on the EPR effect. *Advanced drug delivery reviews*, *63*(3), 131-135.

Trédan, O., Galmarini, C. M., Patel, K., & Tannock, I. F. (2007). Drug resistance and the solid tumor microenvironment. *Journal of the National Cancer Institute*, *99*(19), 1441-1454.

Trotti, A., Bellm, L. A., Epstein, J. B., Frame, D., Fuchs, H. J., Gwede, C. K., ... & Zilberberg, M. D. (2003). Mucositis incidence, severity and associated outcomes in patients with head and neck cancer receiving radiotherapy with or without chemotherapy: a systematic literature review. *Radiotherapy and oncology*, *66*(3), 253-262.

Ulmschneider, M. B., & Sansom, M. S. (2001). Amino acid distributions in integral membrane protein structures. *Biochimica et Biophysica Acta (BBA)-Biomembranes*, *1512*(1), 1-14.

Varkouhi, A. K., Scholte, M., Storm, G., & Haisma, H. J. (2011). Endosomal escape pathways for delivery of biologicals. *Journal of Controlled Release*, *151*(3), 220-228.

Vasey, P. A., Kaye, S. B., Morrison, R., Twelves, C., Wilson, P., Duncan, R., ... & Burtles, S. (1999). Phase I clinical and pharmacokinetic study of PK1 [N-(2-hydroxypropyl) methacrylamide copolymer doxorubicin]: first member of a new class of chemotherapeutic agents—drug-polymer conjugates. *Clinical Cancer Research*, *5*(1), 83-94.

Vasir, J. K., & Labhasetwar, V. (2008). Quantification of the force of nanoparticle-cell membrane interactions and its influence on intracellular trafficking of nanoparticles. *Biomaterials*, *29*(31), 4244-4252.

Vega-Villa, K. R., Takemoto, J. K., Yáñez, J. A., Remsberg, C. M., Forrest, M. L., & Davies, N. M. (2008). Clinical toxicities of nanocarrier systems. *Advanced Drug Delivery Reviews*, *60*(8), 929-938.

Vicent, M. J., Ringsdorf, H., & Duncan, R. (2009). Polymer therapeutics: clinical applications and challenges for development. *Advanced Drug Delivery Reviews*, *61*(13), 1117-1120.

Vines, T., & Faunce, T. A. (2009). Assessing the safety and cost-effectiveness of early nanodrugs.

Virmani, A. K., Rathi, A., Zöchbauer-Müller, S., Sacchi, N., Fukuyama, Y., Bryant, D., ... & Minna, J. D. (2000). Promoter methylation and silencing of the retinoic acid receptor-β gene in lung carcinomas. *Journal of the National Cancer Institute*, *92*(16), 1303-1307.

Vriezema DM, Garcia PM, Sancho Oltra N, Hatzakis NS, Kuiper SM, Nolte RJ, Rowan AE, van Hest J (2007) Positional assembly of enzymes in polymersome nanoreactors for cascade reactions. Angew Chem 119:7522-7526.

Wall, M. E., & Wani, M. C. (1995). Paclitaxel: from discovery to clinic.

Wall, M. E. (1998). Camptothecin and taxol: discovery to clinic. *Medicinal research reviews*, *18*(5), 299-314.

Wang, A. Z., Langer, R., & Farokhzad, O. C. (2012). Nanoparticle delivery of cancer drugs. *Annual review of medicine*, *63*, 185-198.

Wang, J., Mao, W., Lock, L. L., Tang, J., Sui, M., Sun, W., ... & Shen, Y. (2015). The role of micelle size in tumor accumulation, penetration, and treatment. *ACS nano*, *9*(7), 7195-7206.

Warren PB (1998) Dissipative particle dynamics. Curr Opin Colloid Interface Sci 3:620-624.

Weis, K., Rambaud, S., Lavau, C., Jansen, J., Carvalho, T., Carmo-Fonseca, M., ... & Dejean, A. (1994). Retinoic acid regulates aberrant nuclear localization of PML-RARα in acute promyelocytic leukemia cells. *Cell*, *76*(2), 345-356.

Wilson, W. H., Teruya-Feldstein, J., Fest, T., Harris, C., Steinberg, S. M., Jaffe, E. S., & Raffeld, M. (1997). Relationship of p53, bcl-2, and tumor proliferation to clinical drug resistance in non-Hodgkin's lymphomas. *Blood*, *89*(2), 601-609.

Woodle MC (1993) Surface-modified liposomes: assessment and characterization for increased stability and prolonged blood circulation. Chem Phys Lipids 64:249-262.

Wu, H., Zhang, G., Minton, J. E., Ross, C. R., & Blecha, F. (2000). Regulation of Cathelicidin Gene Expression: Induction by Lipopolysaccharide, Interleukin-6, Retinoic Acid, andSalmonella enterica Serovar Typhimurium Infection. *Infection and immunity*, *68*(10), 5552-5558.

Xiong, X. B., Mahmud, A., Uludağ, H., & Lavasanifar, A. (2008). Multifunctional polymeric micelles for enhanced intracellular delivery of doxorubicin to metastatic cancer cells. *Pharmaceutical research*, *25*(11), 2555-2566.

Xu, L., Pirollo, K. F., Tang, W. H., Rait, A., & Chang, E. H. (1999). Transferrin-liposome-mediated systemic p53 gene therapy in combination with radiation results in regression of human head and neck cancer xenografts. *Human gene therapy*, *10*(18), 2941-2952.

Xu JP, Ji J, Chen WD, Shen JC (2005) Novel biomimetic polymersomes as polymer therapeutics for drug delivery. J Control Release 107:502-512.

Yatvin, M. B., Kreutz, W., Horwitz, B. A., & Shinitzky, M. (1980). pH-sensitive liposomes: possible clinical implications. *Science*, *210*(4475), 1253-1255.

Yoshimura, T., Yokoyama, H., Fujii, S., Takayama, F., Oikawa, K., & Kamada, H. (1996). In vivo EPR detection and imaging of endogenous nitric oxide in lipopolysaccharide-treated mice. *Nature biotechnology*, *14*(8), 992-994.

Zhang, X., Burt, H. M., Hoff, D. V., Dexter, D., Mangold, G., Degen, D., ... & Hunter, W. L. (1997). An investigation of the antitumour activity and biodistribution of polymeric micellar paclitaxel. *Cancer chemotherapy and pharmacology*, *40*(1), 81-86.

Zhang, Y., Guan, D. X., Shi, J., Gao, H., Li, J. J., Zhao, J. S., ... & Xue, J. (2013). All-trans retinoic acid potentiates the chemotherapeutic effect of cisplatin by inducing differentiation of tumor initiating cells in liver cancer. *Journal of hepatology*, *59*(6), 1255-1263.

Zhu, W. Y., Jones, C. S., Kiss, A., Matsukuma, K., Amin, S., & De Luca, L. M. (1997). Retinoic acid inhibition of cell cycle progression in MCF-7 human breast cancer cells. *Experimental cell research*, *234*(2), 293-299.

Zitvogel, L., Apetoh, L., Ghiringhelli, F., & Kroemer, G. (2008). Immunological aspects of cancer chemotherapy. *Nature reviews immunology*, *8*(1), 59-73.

Zolot, R. S., Basu, S., & Million, R. P. (2013). Antibody–drug conjugates. *Nature Reviews Drug Discovery*, *12*(4), 259-260.